Impact of permafrost dynamics on Arctic groundwater flow systems with application to the evolution of spring and lake taliks

A thesis submitted to the School of Environmental Sciences of the University of East Anglia in partial fulfilment of the requirements for the degree of Doctor of Philosophy

By Johanna Michaela Scheidegger

December 2013

Abstract

Groundwater flow in permafrost is restricted to unfrozen zones, known as taliks. There is an interaction between groundwater flow and heat flow, because the permafrost distribution determines the occurrence of groundwater, but groundwater also contributes to advective heat transport influencing the distribution of permafrost. However, the advective heat flow component is small where the hydraulic gradient is low, or where recharge is limited. Conversely, where recharge is not driven by precipitation, as for example found under a wet based glacier, groundwater fluxes can be more significant. This thesis aims to improve understanding of the impacts of permafrost dynamics on Arctic groundwater flow systems for past and predicted climate change. Numerical modelling of coupled heat and fluid flow including phase change of water/ice is used to study different environments; lakes in a periglacial environment, and lakes and springs in a proglacial terrain. Results show that the transient effects of heat storage can influence the present day distribution of permafrost. This is especially pronounced underneath surface water bodies, where there are cases for which under a steady state scenario no through talik is expected, but there are through taliks under a transient scenario. In addition, heat advection by groundwater flow can influence the permafrost distribution by permafrost erosion and aggregation. The magnitude of heat advection is driven by topographically driven groundwater flow and the release of groundwater from elastic storage. The latter is significant in previously glaciated areas that have undergone a large change in hydraulic head over time. In partially frozen ground, the choice of the permafrost-permeability-reduction function is crucial to quantify groundwater flow and advective heat flow. The occurrence of through taliks is influenced by the regional scale groundwater flow, but taliks also influence the regional scale hydrogeologic system by reversal of the general groundwater flow direction.

Acknowledgements

I would like to thank Victor Bense for his supervision, guidance and inspiration throughout this PhD. It has been a pleasure working with you! Also thanks to Kevin Hiscock for discussions during supervisory meetings.

I would also like to thank the School of Environmental Sciences who funded this project. I particularly enjoyed the attendance of conferences at EGU in Vienna, and IAH in Niagara Falls, for which the School of Environmental Sciences has provided support. I was also able to attend a summer school about 'Principles and application of flow and transport modelling in the subsurface' at the University of Liège, for which I was awarded funding by the School of Environmental Sciences. In addition, I like to thank the University of Oslo for providing a stipend to attend a Permafrost modelling course at the University of Oslo and a field excursion in Southern Norway.

Whenever I tell people about my work, they ask whether I have been to the Arctic. Now, I can now say 'yes, to Greenland', thanks to the School of Environmental Sciences who provided financial support for this trip. Also special thanks Tom and Emily who kindly came along to 'Tundra Madness', and the GAP project for logistic support and borrowing of their equipment. Also thanks to the technicians at UEA, who helped with logistical support. This trip has inspired me for developing models that are part of this thesis.

In addition to my supervisor, there are numerous people who helped me with proofreading my thesis; thank you Rob who read the entire thesis during these three years, Mel, who provided a very valuable last minute proofreading service after having submitted herself a week before me, Tom, who has read a couple of chapters throughout the process, and Mel who read several sections! Thank you all!

Also special thanks to my friends at UEA, especially Jennie, Katie, Maria, Mel, Mel, and Tom, who supported me morally throughout this process, and we shared many happy moments! Also, I would like to thank the Norwich Mountaineering and Climbing Club, and the University Orchestra who gave me a good distraction from my work.

Many thanks to my family, who were always here for me! My parents who have always supported my education and have awakened already in early years my interest in science! Thanks for your encouragement and support throughout this process! Also many thanks to Rob for being here for me and your endless support!

Contents

List of tables

List of figures

Chapter 1

Introduction

This chapter provides a literature review of the current state of permafrost hydrogeology and explains the general principles of permafrost and hydrogeology in cold environments. Observed hydrological changes that may be related to a hydrogeological response to climate change are outlined. Examples of numerical modelling of permafrost hydrology that aim to explain these hydrological changes are presented, leading to open questions in hydrogeological modelling in permafrost covered regions. Finally, an outline of the thesis is presented.

1.1 Permafrost

1.1.1 Definition of permafrost

The definition of permafrost is solely based on temperature; permafrost is defined as soil, unconsolidated deposits, and bedrock, in which temperatures below 0°C exist for two years or more (*Williams*, 1970).

As the definition of permafrost is solemnly temperature dependent, the occurrence of permafrost does not determine whether liquid water is present. Hence, there are two sets of definition of cold ground; based on temperature (Figure 1.1, left) and state of liquid water (Figure 1.1, right). Permafrost, or perennially cryotic ground, is defined as ground with temperature at or below 0°C, regardless of whether its water is in liquid or frozen state. In contrast, perennially frozen ground refers to the ground where most of the soil water is frozen (*Woo*, 2012).

The active layer that overlays the perennially frozen ground is subject to seasonal freeze and thaw conditions, and is deeper than the seasonally cryotic zone laying above the permafrost table, due to the freezing point

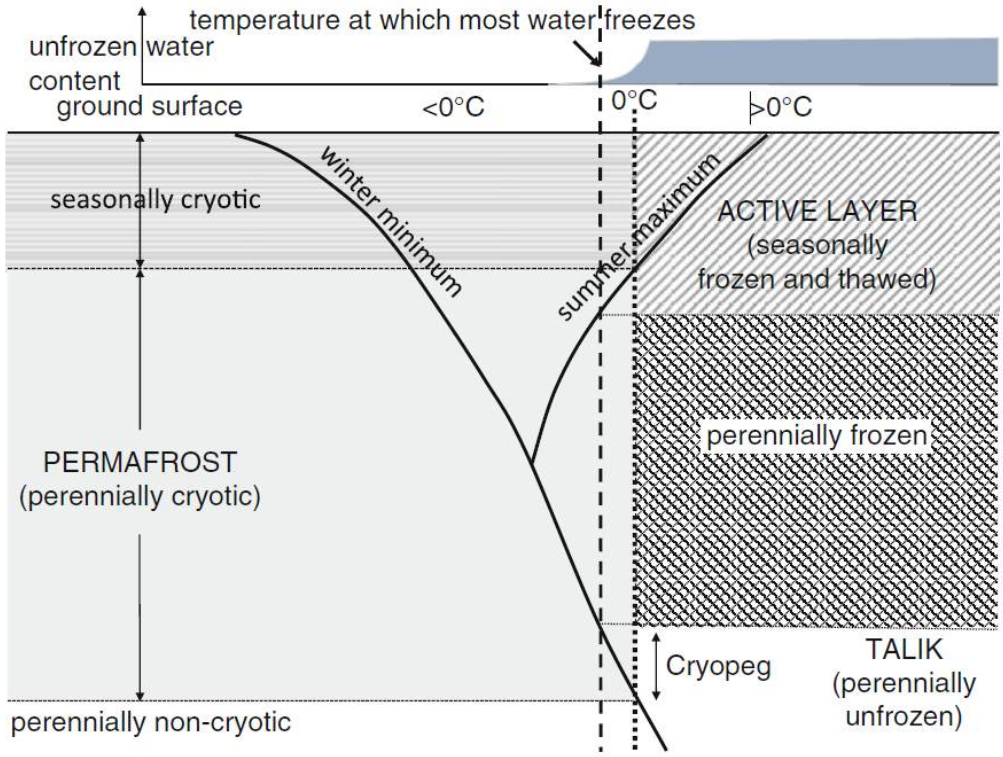

Figure 1.1: Definition of permafrost and associated features based on intersections between 0°C line and annual maximum and minimum ground temperature profiles. Frozen zone is defined on the basis of intersections of the annual maximum temperature profile with the temperature of ice nucleation which is usually ¡0°C and varies with soil type. Image from *Woo* (2012).

depression. In discontinuous, or relict permafrost areas, the active layer and the perennially frozen layer may be separated by an unfrozen zone; an intrapermafrost talik (*Williams and Smith*, 1989; *French*, 2007; *Woo*, 2012).

The lower boundary of the permafrost is referred to as the permafrost base and its depth is determined by the geothermal gradient and the mean annual ground surface temperature. The cryopeg is the difference between the depth of the permafrost base and the base of the perennially frozen zone, which has a temperature below 0°C but with water remaining unfrozen (*Williams and Smith*, 1989; *French*, 2007; *Woo*, 2012).

The thermal regime of permafrost is different from that of unfrozen soil due to the influence of latent heat and a change of thermal conductivity. When water freezes, latent heat of fusion is released and ground temperatures remain initially around 0°C. This effect is called "zero curtain" (*Williams and Smith*, 1989; *French*, 2007). The thermal conductivity of frozen soil is larger than that of unfrozen soil, because the thermal conductivity of ice is approximately four times higher than that of water. Therefore, heat

penetrates frozen soil faster than unfrozen soil (*Williams and Smith*, 1989; *French*, 2007).

1.1.2 Distribution of permafrost

Permafrost covers 25% of the northern hemisphere (Figure 1.2) and is classified into continuous (90-100%), discontinuous (50 - 90%), sporadic (10 - 50%) and isolated (<10%) permafrost coverage (*Walsh*, 2005; *French*, 2007). In the continuous zone, permafrost is present at all locations except under surface water bodies. In the discontinuous zone, the extent to which permafrost is perforated by unfrozen zones depends largely on local conditions, such as aspect of topography, micro climate, vegetation and snow cover, which influence the ground surface temperature. In the sporadic or isolated zone, permafrost is restricted to islands, often occurring under organic rich sediments. Permafrost thickness ranges from less than one meter in sporadic or isolated permafrost to 1500 m in the continuous permafrost zone (*Williams and Smith*, 1989; *French*, 2007).

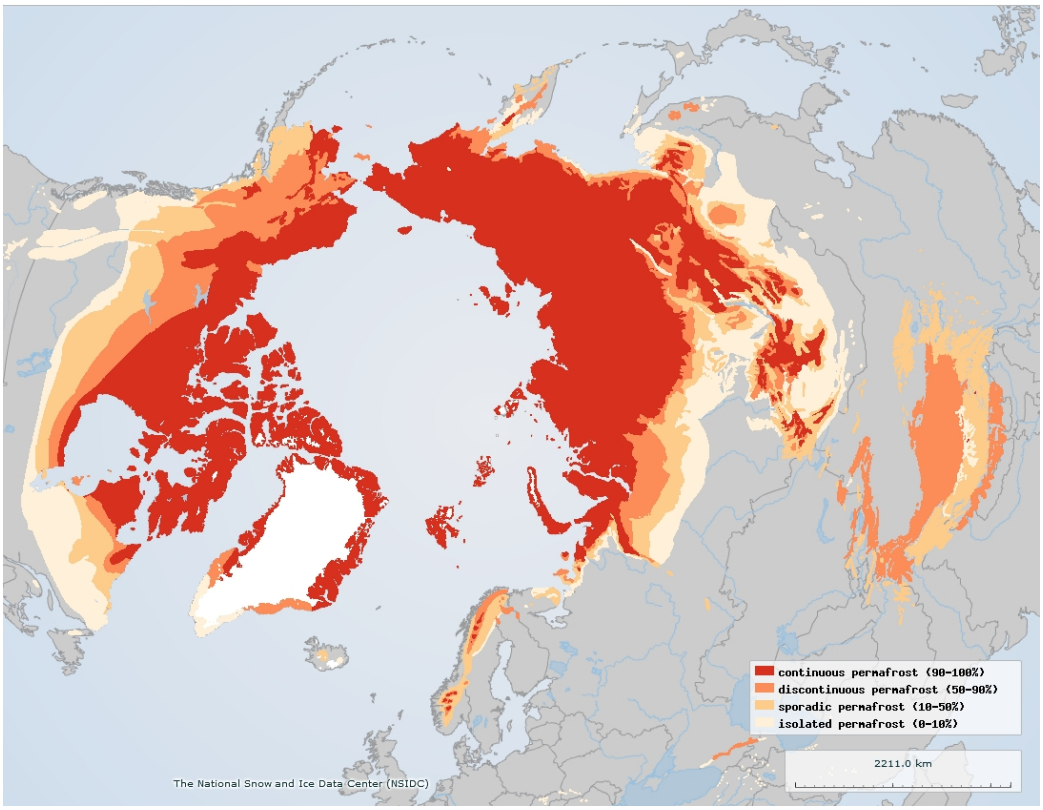

Figure 1.2: Permafrost distribution and zonation in the northern hemisphere (*Arctic Portal*, 2013).

1.2 Hydrogeology in permafrost areas

Permafrost acts as an impermeable barrier, because the pore spaces are generally filled with ice within the zone of saturation. The ice- and water-saturation in permafrost is important for the groundwater movement, because the hydraulic conductivity in frozen media decreases over the freezing interval by several orders of magnitudes (e.g. *Kleinberg and Griffin*, 2005). However, as the definition of permafrost is only temperature dependent, liquid water content can occur at temperatures <0°C due to the depression of the freezing point (*Williams and Smith*, 1989). The freezing point depression has two causes; a high solute content will shift the freezing point to subzero temperatures, and capillary and adsorptive forces can attract liquid water to the soil pores. As there is a distribution of pore size, freezing occurs over a temperature range where water and ice coexist. Generally, water in larger pores freezes before water in smaller pores, and smaller pores thaw before ice thaws in larger pores (*Ireson et al.*, 2013). The impermeability of permafrost makes recharge and discharge of water to and from the aquifers beneath permafrost to the unfrozen zones that perforate the permafrost (*Williams*, 1970; *French*, 2007). There is a complex interaction between permafrost occurrence and groundwater movement due to transient storage effects of heat flow and fluid flow. This will be elaborated on throughout this thesis.

1.2.1 Groundwater movement in permafrost

Generally, groundwater movement in permafrost covered regions follows the same physical principles as in permafrost free areas. For fully saturated fluid flow in porous media, groundwater movement is described with Darcy's Law, which is described in more detail in Chapter 2. However, groundwater flow in permafrost covered areas is restricted to unfrozen zones, also called taliks (Figure 1.3). Taliks can be found as supra-permafrost taliks, intra-permafrost taliks and sub-permafrost taliks (*Sloan and Van Everdingen*, 1988; *Woo*, 2012).

Supra-permafrost groundwater occurs in the active layer, which is seasonally unfrozen (Figure 1.3). In addition, supra-permafrost taliks can be found under surface water bodies, which insulate the ground from the air temperatures. For supra-permafrost groundwater, the permafrost acts as a confining lower boundary of the aquifer. Supra-permafrost aquifers can also be found under recently drained lakes, underneath relict river channels, or be found in regions where the thaw depth in summer is larger than the freezing depth

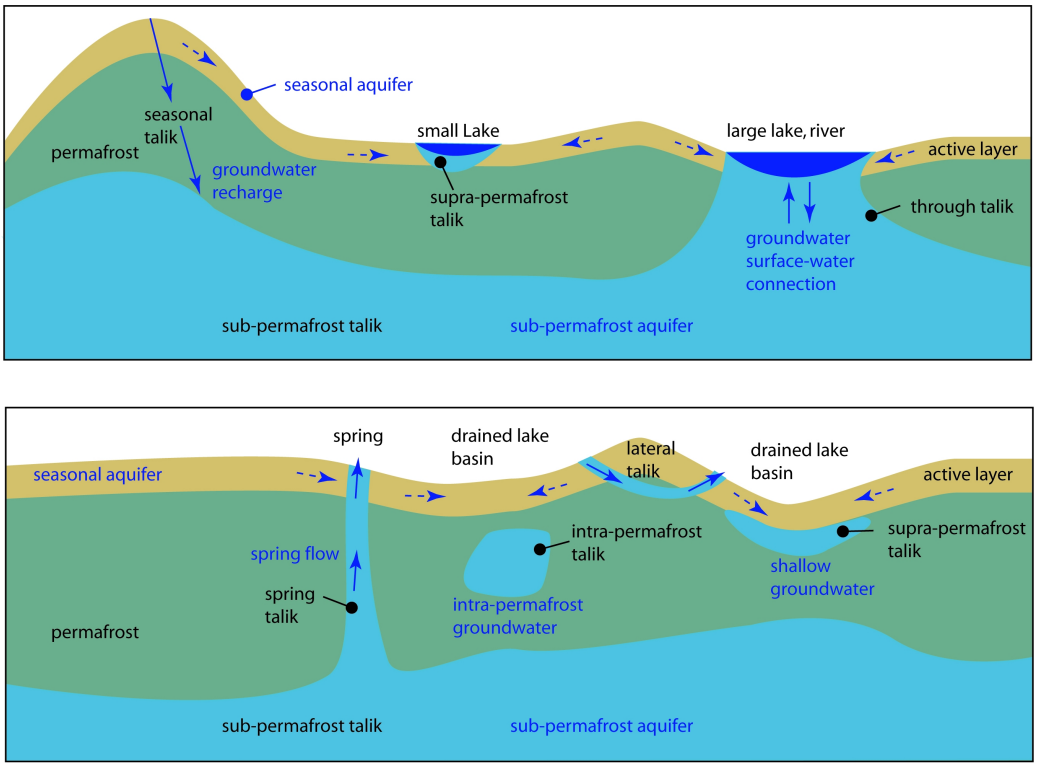

Figure 1.3: Taliks found under lakes, springs, and drained lake basins, modified after *Sloan and Van Everdingen* (1988).

in winter. Seasonal frost advancing from the surface also forms an upper confining boundary, which can develop 'quick' conditions and result in the formation of seasonal frost mounds and icings (*Sloan and Van Everdingen*, 1988; *Woo*, 2012).

Intra-permafrost groundwater is groundwater within the permafrost (Figure 1.3). Intra-permafrost taliks are not subject to seasonal freezing, but respond to long term temperature changes and can be hydrothermal with T>0°C or hydrochemical with T<0°C (*Sloan and Van Everdingen*, 1988). Intra-permafrost taliks can also be found underneath drained lake basins or ancient river channels, where a supra-permafrost talik freezes from the top. These taliks are of transient nature, and their size decreases over time. When water pressures are high under drained lakes, an ice cored frost mound, or pingo can develop (*Sloan and Van Everdingen*, 1988).

Open, or through taliks (Figure 1.3), can be found under surface water bodies whose size and lake bottom temperature is sufficient to insulate the ground from the air temperatures and allow the talik to penetrate the entire depth of the permafrost (*Burn*, 2005). A through talik provides a connection of sub-permafrost groundwater with surface water (*Sloan and Van Everdingen*, 1988). For example, a connection of sub-permafrost groundwater can

be observed along permeable fault zones, as observed at the Troll hot spring system at Bockfiorden, Spitzbergen (*Haldorsen et al.*, 2010), or along karstified carbonates as found in springs near Ny Alesund in Svalbard (*Haldorsen and Heim*, 1999), or in salt layers as suggested on Axel Heiberg Island in the Canadian Arctic (*Andersen et al.*, 2002).

Lateral intra-permafrost groundwater can be found in high-permeability deposits and remain unfrozen due to the heat content of moving water (Figure 1.3). Water flow within the permafrost occurs through subsurface voids or taliks and must provide enough energy to prevent freezing. When the water flow is through a saturated stratum, water flow must be constantly maintained (*Moorman*, 2003).

Sub-permafrost groundwater is found beneath the permafrost (Figure 1.3). The confining permafrost layer results in artesian pressure of the sub-permafrost groundwater (*Sloan and Van Everdingen*, 1988).

1.2.2 Groundwater recharge

Groundwater recharge in permafrost covered areas is generally very low due to limited rainfall in Arctic regions combined with a confining permafrost layer, resulting in most of the precipitation running off as surface water (*Woo*, 2012). The presence of numerous lakes and ponds in the Arctic demonstrates that infiltration and recharge is restricted (*Sloan and Van Everdingen*, 1988). Groundwater is recharged from infiltration of rainfall, snow melt, glacial melt water, or from surface water bodies. Water reaches aquifers at depth only through unfrozen taliks that perforate the permafrost, such as those beneath streams, lakes, and slopes of low hills. Supra-permafrost water migrates laterally on the slope of the permafrost table until it discharges at the surface or reaches an unfrozen zone. If supra-permafrost water reaches the unfrozen zone at a level that is above the level of the water beneath the permafrost, it moves downward as intra-permafrost water until it reaches the water level of the sub-permafrost aquifer (*Williams*, 1970; *French*, 2007; *Sloan and Van Everdingen*, 1988).

1.2.2.1 Recharge by precipitation

Groundwater recharge from precipitation can occur from adjacent non permafrost covered uplands or through supra- and intra-permafrost connections. In continuous permafrost, recharge is restricted but can be enhanced through fractures and solution conduits (*Woo*, 2012; *Utting et al.*, 2012). Large openings for infiltration of water, such as open fractures and joints in sedimentary

rock; solution conduits in soluble sedimentary rock; and in areas of thick sequences of coarse grained sediments are least affected by the presence of permafrost (*Sloan and Van Everdingen*, 1988). In addition, recharge can fluctuate seasonally, as the reduction in permeability of the frozen soil during winter impedes the groundwater recharge, but during spring snow melt and thaw period, recharge fluxes are largest (*Ireson et al.*, 2013). An example of seasonally varying recharge is presented by *Ireson et al.* (2013) and shows that the water table rises rapidly during spring melt, and that the persistence of the 0.1°C isotherm indicates that the soil is not completely thawed during recharge and occurs through partially frozen ground.

In a study by *Utting et al.* (2012) groundwater recharge is stated to occur in summer through the active layer. The organic soil, where the frozen organic soil layer is the only limiting parameter for recharge, is underlain by highly fractured or karstified bedrock. Groundwater is able to move through the fractures and the karstified limestone, which has a permafrost thickness of 90 m (*Utting et al.*, 2012).

In crystalline rock, the continuity of fractures with depth is more restricted than in sedimentary strata, limiting recharge to a larger extent, and is very restricted in areas covered with thick sequences of medium- to fine grained unconsolidated deposits (*Sloan and Van Everdingen*, 1988).

1.2.2.2 Recharge through surface water bodies

Lakes and rivers that are underlain by a talik, can recharge or discharge groundwater into the aquifer (*Woo*, 2012). In the High Arctic, surface water bodies have been stated as a groundwater recharge area for spring systems (*Andersen et al.*, 2002; *Moorman et al.*, 2003).

1.2.2.3 Glacially recharged groundwater

Sub-glacial recharged groundwater is another source of recharge. *Boulton et al.* (1993) propose that groundwater recharges from meltwater into underlying aquifers, and questioned the consensus on impermeable glacier beds.

Sub-glacial water can either originate from in situ melt, or drain from the surface to the ice base, through crevasses, moulins or incision of englacial drainage structures (*Zwally et al.*, 2002). Frictional heating between the glacier and the substratum or through ice movement can result in a substantial amount of meltwater at the base of thermal parts of the glacier (*Boulton et al.*, 1993; *Piotrowski*, 2006). Under wet-based or thermal ice, the glacier bed is unfrozen and a talik may survive beneath High Arctic glaciers

(*Irvine-Fynn et al.*, 2011). If a glacier or an ice sheet rests on a wet-based permeable bed, a part of the sub-glacial meltwater will enter the bed and be evacuated as groundwater flow (*Piotrowski*, 2006). Karstified limestones and dolomites underlying glaciers enables water to flow through relatively wide channels into aquifers (*Haldorsen and Heim*, 1999). In crystalline bedrock, fracture systems, which are often in association with fault zones, provide the permeability required for a substantial sub-glacial recharge.

Groundwater flow under an ice sheet is governed by the same physical rules as in confined aquifers outside the glaciated areas, where the total groundwater flow is determined by the product of the hydraulic gradient, the cross-sectional area, and the hydraulic conductivity (*Domenico and Schwarz*, 1998). However, there are two major differences: first the flow is driven by the hydraulic gradient imposed by ice overburden, and second, some groundwater may be advected within the sediment, if it deforms in response to glacier stress (*Piotrowski*, 2006). The hydraulic head distribution under a wet-based ice sheet runs approximately parallel to the ice surface corresponding to the water pressure. Because of the density difference between ice and water, the maximal ice overburden pressure is the ice thickness by a factor of 0.9, and *Piotrowski* (1997) estimate the potentiometric head from paleo-porewater pressures as a factor of 0.72 of the ice thickness, which is inferred from the stress characteristics of the fine-grained sediments. Given the high flow velocities and hydraulic heads, groundwater can penetrate deep into the sub-glacial sediments and rocks. Because of the typical layered structure of till, the flow pattern is highly anisotropic with preferential flow horizontal in the aquifer and vertical in the aquitard (*Piotrowski*, 2006).

Groundwater flow under polythermal glaciers and ice sheets will be affected by the distribution of frozen ground in ice-marginal areas and central parts of ice sheets where basal freezing may occur due to advection of cold ice. Pressurized groundwater will be forced under the permafrost, and the confined drainage system will terminate outside the permafrost zone or at taliks under rivers and lakes *Piotrowski* (2006). At the glacier margin, pressurised, often artesian groundwater can cause hydrofracturing of sediment and rocks. This may occur to a depth of about 400 m, and the zone affected by hydrofracturing can extend many tens of kilometres into the ice foreland (*Boulton and Caban*, 1995). However, in this thesis, we will only consider the hydraulic head distribution driven by the ice sheet thickness, as the modelling of glaciotectonics is beyond the scope of this project.

In extreme arid permafrost, as found in the Dry Valley in Antarctica,

meltwater from glaciers and snow patches is the only source of runoff and groundwater recharge (*Gooseff et al.*, 2013). Groundwater there is found near snow patches or surface water bodies.

1.2.3 Groundwater discharge

Groundwater is discharged in topographically low places, as in valleys or along the coast. In winter, discharge areas can be identified by icings, or aufeis fields. Icings are masses of surface ice up to 6 m thick that are formed by freezing of successive thin sheets of water seeping from the ground. Discharge of sub-permafrost water is generally perennial and occurs through fractures and faults in bedrock, cavernous zones in limestone, large openings in volcanic rocks, and permeable unconsolidated deposit. Supra-permafrost springs normally cease flowing in winter when the water becomes frozen (*Williams*, 1970; *French*, 2007; *Sloan and Van Everdingen*, 1988).

Groundwater seeps occur across a poorly defined area whose size changes depending on the groundwater discharge. Seeps are often supported by supra-permafrost groundwater and seepage occurs where the water table intersects with the topography. Groundwater discharge can be intermittent and stop when the active layer is frozen (*Woo*, 2012).

In this thesis, the focus is on sub-permafrost groundwater discharge, however, in this introduction, supra-permafrost groundwater discharge is also mentioned.

1.2.3.1 Groundwater discharge in rivers

Baseflow is the proportion of streamflow that is fed by groundwater. Where baseflow is fed from supra-permafrost groundwater the groundwater may freeze above the ground in winter as an icing. When the river is underlain by a intra-permafrost or sub-permafrost talik, baseflow continues during winter (*Woo*, 2012).

Groundwater discharge into rivers can be determined through hydrochemical analysis of the river water. For example, *O'Donnell et al.* (2012) find that the dissolved organic matter (DOM) variability in catchments of the Yukon river basin appears to be driven partly by the spatial variation in supra-permafrost and sub-permafrost groundwater contributions to streamflow. In addition, the composition and concentration of dissolved organic carbon (DOC) changes seasonally for the six largest Arctic rivers (*Amon et al.*, 2012). Moreover, the analysis of uranium isotopes has been suggested

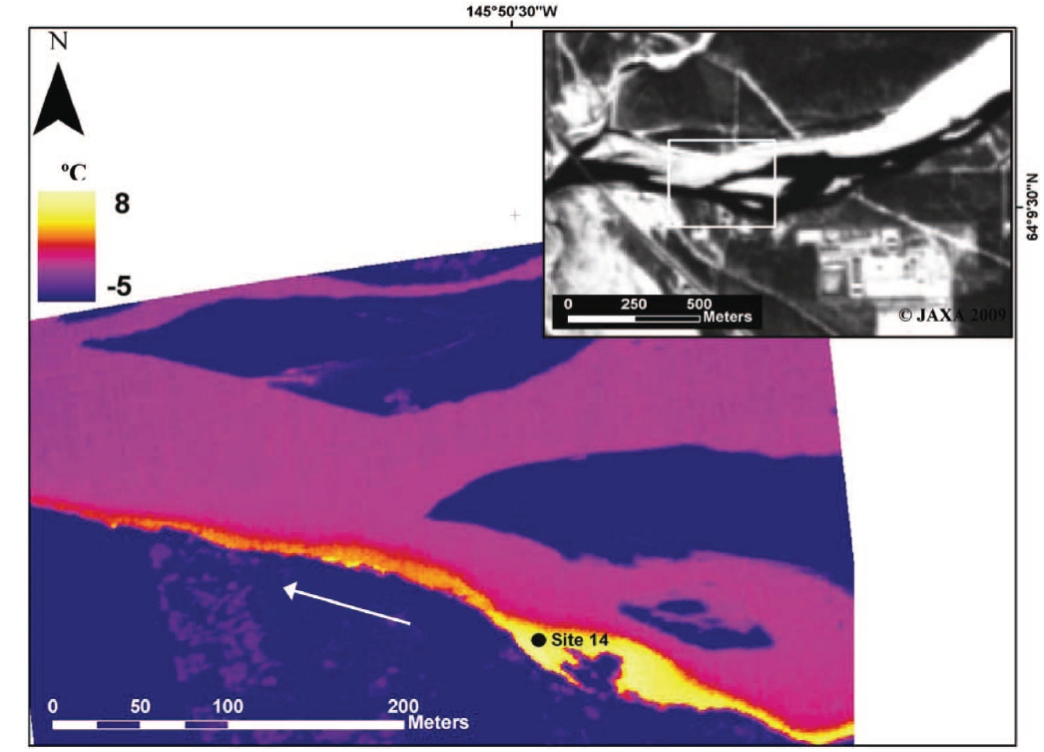

Figure 1.4: Forward-looking infrared showing warm groundwater influx (yellow shaded area) compared with the cooler surface water (pink shaded area). Image from *Wirth et al.* (2012).

to identify the water sources to rivers in the Yukon Basin, and to detect recent flow changes by the analysis of time series (*Kraemer and Brabets*, 2012).

Another method to determine groundwater discharge into rivers is to use infrared images. For example, *Wirth et al.* (2012) use forward-looking infrared radiometer images to determine a groundwater source into the Tanana River, Alaska. In winter the groundwater is several degrees warmer than the river water (Figure 1.4).

The groundwater component into rivers can also be determined by the analysis of cold-season flow behaviour, as the presence of permafrost should be a first order control on the groundwater component into streamflow (*Watson et al.*, 2013). Analysis of cold season flow behaviour in subarctic river basins of Siberia has shown three different types of cold season flow recession. First, a fast recession and cessation of flow has been observed in some basins in continuous permafrost, which suggests no groundwater component into these rivers. The second group shows little, but continuous cold season flow in continuous permafrost, which proposes the existence of taliks feeding groundwater to the streamflow. The third group in non-continuous permafrost shows perennial cold season flow, but little flow recession and high

discharge, which suggest a large groundwater component to the stream. This analysis of stream flow surmises that permafrost extent and, abundance and interconnection of taliks, have a dominant control enhancing groundwater recharge and discharge (*Watson et al.*, 2013).

1.2.3.2 Groundwater discharge into lakes

Groundwater discharge into lakes can occur when a sub-permafrost aquifer, an intra-permafrost aquifer, or a supra-permafrost aquifer is connected to a lake. Supra-permafrost groundwater discharge may be seasonal and generally, groundwater recharge is limited. For a sub-permafrost groundwater source, the lake needs to be underlain by a through talik, a talik penetrating the entire depth of the permafrost. When surface insulation of the lake is sufficient, a through talik can develop, connecting the lake with a sub-permafrost aquifer (*Sloan and Van Everdingen*, 1988; *Woo*, 2012).

A through talik under a lake develops when ground beneath lakes is warmer than the surrounding permafrost, because the lake bottom temperatures do not fall below 0°C unless the lake freezes through. For example, *Burn* (2002) show that water temperatures over 2°C were measured at the end of the winter in lakes where the pool is 4 m or more deep, whereas in shallower water the temperatures are close to 0°C. Therefore, a mean annual lake bottom temperature of $\sim$ 2°C for lakes less than 4 m deep is proposed, and for deeper lakes close to 4°C (*Burn*, 2002).

Evidence of a through talik under lakes has been found with electromagnetic imaging of the Yukon river basin, shown in Figure 1.5 (*Minsley et al.*, 2012). However, direct evidence of groundwater discharge into these lakes is sparse. Measuring groundwater discharge into lakes is difficult, as Arctic lakes are ice covered over the winter. Employing seepage meters and piezometers is logistically difficult and therefore, relatively little is know about groundwater discharge into polar lakes (*Dugan et al.*, 2012). One example can be found in a tundra pond in Vendom Fiord on Ellesmere Island, Canadian High Arctic (*Marsh and Woo*, 1977), where water balance measurements suggests a groundwater source to maintain the measured water levels.

Evidence of groundwater discharge into lakes can be found with geochemical tracers and *Dugan et al.* (2012) use dissolved radon-222, that has entered the aqueous solution during water-rock interaction, and thus can be used as an indirect tracer for groundwater discharge.

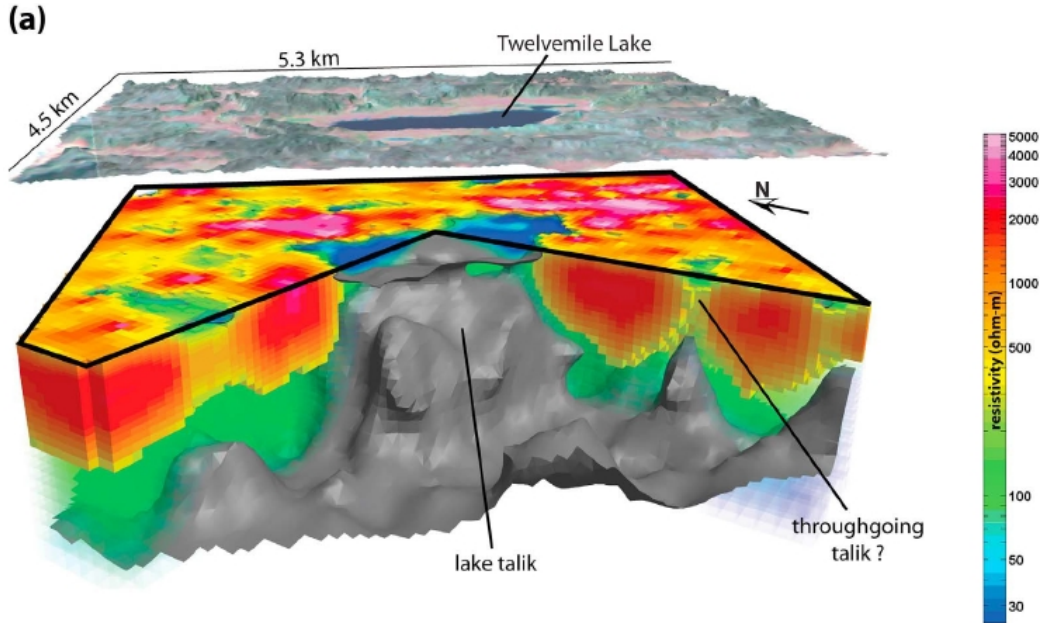

Figure 1.5: Three-dimensional cut-out view of the resistivity model of Twelvemile Lake. The grey iso-surfaces are interpreted to indicate the base of permafrost in the subsurface. Image from *Minsley et al.* (2012).

Another tracer for groundwater flow in surface water is heat, as the temperature of the groundwater has a different temperature to the surface water. Examples of heat used as a tracer is with distributed temperature sensing (DTS), that can measure temperatures at a high spatial and temporal interval (*Selker et al.*, 2006; *Sebok et al.*, 2013). Satellite infrared imaging (AVNIR-2 on ALOS) can also be used to spatially determine different surface water temperatures (*Wirth et al.*, 2012) or thermal photos using a FLIR system or different temperatures of frozen groundwater seeps (*Pandey et al.*, 2013).

1.2.3.3 Groundwater discharge into the ocean

Groundwater flow to the Arctic Ocean is considered to be orders of magnitudes lower than river discharge, but is very important during winter, when other sources of discharge are substantially reduced (*Walsh*, 2005). For example, submarine discharge into the Arctic seas from the European Russian territory is estimated at 1.73 km^3 a^{-1} (*Zektser and Dzyuba*, 2010).

DeFoor et al. (2011) relate geochemical anomalies in continental shelf sediments of south-eastern Greenland to ice sheet-derived submarine groundwater discharge. Their modelling results indicate that the magnitude of this submarine groundwater discharge fluctuates during glacial-interglacial cycles and is highest during glacial conditions. Moreover, their model shows that

a large part of the sub-glacial groundwater is discharged on land (*DeFoor et al.*, 2011).

1.2.3.4 Springs in permafrost areas

Springs are discrete discharge points of groundwater and are fed by either supra-permafrost groundwater, or sub-permafrost groundwater. Springs that are fed by supra-permafrost groundwater may be intermittent or perennial, as the groundwater recharge is not continuous (*Sloan and Van Everdingen*, 1988). When the spring is recharged from a sub-permafrost groundwater source, the spring flow is continuous. This section will focus on springs discharging groundwater from a sub-permafrost groundwater source.

A glacial influence for the development of springs has been found by *Yoshikawa et al.* (2007), who propose a relationship between springs, or aufeis distribution and glacial limits at Brooks Range, Alaska, and the development of hydraulic pathways during past periods of glaciation when thermal glaciers contributed for groundwater recharge. *Yoshikawa et al.* (2007) state that the current distribution of springs and aufeis is a relict feature of the periglacial groundwater systems. In Spitzbergen, a glacial recharge has also been suggested at Troll springs whose water is a composition of glacial meltwater and hot thermal brine as water chemistry and stable isotopes infer (*Lauritzen and Bottrell*, 1994). In addition, on Ellesmere Island, Canadian High Arctic, supra-glacial sulfur springs have also been found to be recharged by glacial meltwater, as suggested by isotopic analysis (*Grasby et al.*, 2003). These will be discussed in more detail in Chapter 5.

A recharge from surface water bodies for spring water has also been suggested. One example is found on Axel Heiberg Island, where the recharge is postulated from sub-glacial meltwater from a lake nearby and the flowpath occurs through permeable salt layers and diapirs through the permafrost aquitard (*Andersen et al.*, 2002, 2008). Furthermore, on Bylot Island in the vicinity of Fountain and Stagnation Glacier, a spring, approximately 50 m from the glacier terminus was observed which stopped at the same time as the drainage of a proglacial lake *Moorman et al.* (2003).

Kane et al. (2013) hypothesise that the analysis of hydrochemistry and flow rate of numerous springs in the continuous permafrost zone in the North Slope of Alaska proposes that their recharge occurs on the South side of the Brooks range in areas of karstified limestone. This would suggests that the recharged groundwater crosses the topographic divide and discharges through fault zones as springs and icings.

A groundwater-surface water connection can also occur under drained lakes, often forming a massive ice cored hill which is associated with long-term frost heave of the terrain surface (*French*, 2007; *Grosse and Jones*, 2011). Hydrostatic pingos form under the surface of a drained lake that is underlain by saturated sand. At the initial stage, there is a deep pool with a talik underneath it. When the lake drains rapidly, permafrost aggregates downwards through the talik, expelling the water within the talik sediments. Water is forced up to the near surface at the thinnest part of the permafrost and refreezes, forming an ice dome. Hydrostatic pingos typically occur in regions with continuous permafrost (*French*, 2007; *Gurney*, 1998). Hydraulic pingos develop where intra-permafrost or sub-permafrost groundwater emerges to the surface under artesian pressure (*French*, 2007; *Gurney*, 1998).

1.2.3.5 Shallow groundwater flow connected to surface water bodies

Shallow groundwater in a seasonally unfrozen active layer can connect the water budget of surrounding slopes or topographically lower areas with the the water balance of the surface water body. Furthermore, groundwater transport in the active layer influences the thermal regime of the ground (*Woo*, 2012).

Woo (2006) investigates the hydrological connectivity and seasonal storage change of tundra ponds, located within ice wedge-polygons on Ellesmere Island. Water level measurements suggest a seasonal subsurface flow between ponds and adjacent slopes.

1.3 Influence of climate change on surface and subsurface hydrology in permafrost

Recent warming in the Arctic has presented a consistent pattern of environmental change; sea ice extent and multi-year ice has decreased, the snow covered area has diminished in Eurasia and North America, an increase in river discharge has been measured over much of the Arctic, glaciers and ice sheets have had a negative mass balance, and permafrost temperature over most of the subarctic has increased by 2 to 3°C over the past few decades (*Walsh*, 2005). Changes in river baseflow, lake numbers and area, spring discharge and water storage have been observed (e.g. *Smith et al.*, 2005, 2007;

Haldorsen et al., 2010; *Muskett and Romanovsky*, 2011).

1.3.1 Response of permafrost to climate change

Climate change in the Arctic has resulted in a Pan-Arctic increase in permafrost temperatures for the last two to three decades. Generally, warming rates are slower for permafrost close to 0°C, especially for ice-rich permafrost in which latent heat effects dominate the ground thermal regime, than for colder permafrost, where the temperature regime is warming more rapidly (*Romanovsky et al.*, 2010a). This global pattern is confirmed in North America, where the rates of warming have been variable, but are generally greater north of the tree line, than in the southern, discontinuous zone permafrost zone, where the latent heat effects dominate the thermal regime (*Smith et al.*, 2010). In Russia, permafrost has been warming typically from 0.5°C to 2°C at the depth of zero annual amplitude, and thawing is most profound within the discontinuous permafrost zone, but has also been observed in the continuous zone. This results in a northwards displacement of the boundary between the continuous and the discontinuous permafrost zones (*Romanovsky et al.*, 2010b).

Permafrost is expected to respond to climate change by a reduction in area, a shift between the zones of continuous, discontinuous and sporadic permafrost, and an increase of the active layer (*Walsh*, 2005). Simulations of future permafrost distribution predict a substantial decline in near-surface permafrost during the next century (*Lawrence et al.*, 2012). This change in permafrost thickness, temperature and extent may have a profound influence in the surface and subsurface hydrogeology, which will be discussed throughout this thesis.

1.3.2 Changes of groundwater input to lakes

As mentioned above, groundwater discharge into lakes is difficult to quantify, and therefore a direct observation and quantification of hydrogeological changes is problematic. Nevertheless, changes in lake size and number can potentially be part of a changing groundwater source or sink, but it may also be part of a natural thermokarst cycle, that is not necessarily driven by climate change, or be part of changing net water input (*Yoshikawa and Hinzman*, 2003; *Jepsen et al.*, 2013; *Wellman et al.*, 2013).

Lake morphology has undergone different processes in permafrost regions.

Shrinking ponds in thin permafrost areas in Alaska (*Yoshikawa and Hinzman*, 2003) and Siberia (*Smith et al.*, 2005) have been observed, which is associated with lateral or vertical drainage through taliks, or complete lake drainage through ice wedges (*Wang et al.*, 2012). This surface drainage of thermokarst lakes (catastrophic drainage) has been suggested through ice wedges to occur in a period of one day (*Mackay*, 1998). *Marsh et al.* (2009) observed lake drainage pattern and found a decrease in lake drainage in the Western Canadian Arctic and hypothesise this change is related to a warming climate, however the causes are unknown. The authors suggest that lake drainage is influenced by a combination of a deep active layer and a high lake level. In addition, an increase in lake numbers in continuous zones in Siberia has been observed due to thermokarst processes (*Smith et al.*, 2005), or lake expansion in Siberia (*Walter et al.*, 2006). These changes in lake morphology can be part of a natural thermokarst cycle.

Thermokarst lakes mostly are initiated by natural events such as climate change, forest fires or ponding of surface water (*Burn and Smith*, 1990). Climate change may lead to thermokarst development by altering the surface energy balance and increasing ground temperatures. The Holocene climatic optimum in NW Canada has been associated with thermokarst development. More recent formation of thermokarst lakes has been associated with climate change since the Little Ice Age. Forest fires alter the energy balance and deepen the active layer thickness (*Burn and Smith*, 1990). Thermokarst develops where an increase in the depth of thaw results in the melting of shallow ground ice and the formation of a depression. Once initiated, thermokarst lakes enlarge due to thawing of the underlying ice. When the lake bottom temperature remains above 0°C, the thawing of the underlying permafrost is continuous and year round (*Burn and Smith*, 1990). In addition to thaw, thermomechanical erosion can be another process enlarging thermokarst lakes as wind driven waves and currents accelerate lake expansion (*Wang et al.*, 2012). A thermokarst lake cycle is terminated by lake drainage by bank overflow, ice wedge erosion, or lake breaching by stream meandering (*Wang et al.*, 2012), or by through talik formation drainage to an aquifer (*Yoshikawa and Hinzman*, 2003).

The influence of climate change on thaw lakes can also be caused by increasing lake bottom temperatures and formation of through taliks. *Burn* (2002) estimates that the thermal regime for deep pools may be dominated by a longer and warmer summer season, whereas the impact on the terraces

would be greatest in winter with deeper snow cover and higher air temperatures warming the lake bottom. *Burn* (2005) estimates that on Richards Island, 25% of over 1220 lakes are underlain by through taliks and that with climate change, another 20% of lakes will develop through taliks.

However, lake dynamics is not necessarily driven by through talik formation alone, but is a combination of different processes. *Jepsen et al.* (2013) suggest that a combination of changes in shallow lateral groundwater flow to the lake, and increased loss of lake water as downward groundwater flow through an open talik to a permeable sub-permafrost aquifer, or reduced snow meltwater inputs are the main contributors to lake dynamics in the Yukon Flats.

1.3.3 Changing river flow characteristics

Analysis of river discharge characteristics has shown an increase of discharge to the Arctic Ocean, rising minimum daily flows, an increase in winter baseflow or an increase in groundwater to stream discharge (*McClelland et al.*, 2006; *Smith et al.*, 2007; *Walvoord and Striegl*, 2007; *St Jacques and Sauchyn*, 2009; *Overeem and Syvitski*, 2010; *Brutsaert and Hiyama*, 2012; *Sjöberg et al.*, 2013). The causes of these changes are non-uniform and complex and some of them are attributed to changes in permafrost thickness and extent (*St Jacques and Sauchyn*, 2009), decrease of seasonal soil freezing (*Smith et al.*, 2007), changes in atmospheric circulation patterns (*Overeem and Syvitski*, 2010) or shift from above ground to below ground water storage (*St Jacques and Sauchyn*, 2009). Some examples are outlined below.

Analysing river discharge time series has given a varied pattern of change over the last decades of which some have been related to permafrost thaw and increasing groundwater flow (*McClelland et al.*, 2006). For example, discharge to the Arctic Ocean increased by 5.6 km^3a^{-1} during 1964-2000, for which the six largest Eurasian Arctic rivers accounted for 87% of the change in discharge from Eurasia to the Arctic Ocean. However, expressed relative to size, discharge from the ten smaller Eurasian Arctic rivers changed at a rate that was similar to that observed for the six largest Eurasian Arctic rivers. Precipitation estimates for Eurasia do not consistently show increases that would explain the increasing river discharge, but there are alternative mechanisms such as changes in permafrost and fires that may link warming with the observed increases in Eurasian Arctic river discharge (*McClelland et al.*, 2006).

Overeem and Syvitski (2010) analysed the stream flow characteristics of 19

large rivers over the entire Arctic region and their results suggest a consistent pattern of increase in annual discharge of 9.8% over the last 30 years. The authors find an increase in melt month discharge and a decrease in peak month discharge, and attribute the considerable change in the melt month to a shift in snowmelt in the drainage basin. The changes observed are consistent, but not entirely uniform, as individual rivers respond to different atmospheric circulation changes (*Overeem and Syvitski*, 2010).

Furthermore, *Smith et al.* (2007) observe rising minimum daily flows in northern Eurasian rivers in Russia from 1936-1999 and 1958-1989 and minimum flow increases in summer and winter in permafrost and non-permafrost area is found. The authors suggest that decreased seasonal freezing of soils caused by warmer winter and/or deeper snowpack, might promote such activity in both permafrost and non permafrost environments.

In addition, *St Jacques and Sauchyn* (2009) found an increase in winter baseflow and mean annual streamflow in the Northwest Territories, Canada. In winter, the surface runoff is negligible due to freezing conditions, and all discharge into rivers is from baseflow. It was observed that 20 of 23 long-term records showed a significant upward trend in winter baseflow over the full period of record, and 9 of 23 showed a significant increasing annual flow. The increase in baseflow, probably from soil water and groundwater inputs into rivers, could be due to permafrost thawing (*St Jacques and Sauchyn*, 2009). This is supported by shrinking and draining lakes in Alaska and Siberia (e.g. *Yoshikawa and Hinzman*, 2003; *Smith et al.*, 2005). The finding of increased winter flow, and presumably groundwater flow throughout much of the regions predicts a rising role of groundwater processes in the high-altitude water cycle under global warming. *St Jacques and Sauchyn* (2009) therefore, conclude that above-ground water storage shifts to below ground water storage with an increased soil infiltration, unsaturated zone storage and groundwater movement in permafrost regions.

Furthermore, *Walvoord and Striegl* (2007) found an increased groundwater to stream discharge from permafrost thawing in the Yukon River basin. Most streamflow records in the Yukon river basin demonstrate a significant increases in groundwater flow and a minimal change in annual flow. *Walvoord and Striegl* (2007) interpret that the observed trends are due mainly to enhanced groundwater input to streams, as increased winter flow throughout the Yukon river basin in the absence of evidence for precipitation increases. Also, increased winter precipitation would result in a thicker snow layer to better insulate the ground below, perhaps delaying annual freezing

of the active layer and/or enhancing thawing of permafrost ice, and not directly result in greater discharge. Western Arctic summer temperatures have increased faster than annual temperatures from 1980-2000, resulting in permafrost warming. Permafrost thawing deepens the active layer and allows for increased infiltration, which would cause increased groundwater contribution to annual flow (*Walvoord and Striegl*, 2007).

Brutsaert and Hiyama (2012) also hypothesise that changes in baseflow are related to permafrost dynamics. The authors find that base flow in a river is fed by groundwater seepage from upstream shallow aquifers in the basin, and that permafrost thawing and permafrost growth directly affect the groundwater storage amount and mobility, controlling the seepage to the river flow from shallow aquifers.

Sjöberg et al. (2013) find that baseflow in northern Sweden has increased significantly in nine basins, and in seven basins changes in recession characteristics are consistent with degradation of permafrost. The increase in minimum flow in winter is associated with an altered flow connectivity of the aquifer system with permafrost thaw, and the change in recession flow during summer responds to a warming of the active layer.

In contrast, there seems also to be relations of stream flow with non-permafrost related changes as comparison of streamflow characteristics with the Pacific Decadal Oscillation between 1944 to 2005 demonstrates that some of the change in streamflow characteristics can be attributed to the modes of the Pacific Decadal Oscillation (*Brabets and Walvoord*, 2009).

It has been hypothesised that future warming will change the Arctic hydrological system from a surface water dominated system to a groundwater dominated system (*St Jacques and Sauchyn*, 2009). This hydrogeological change is predicted to increase mineral-rich groundwater flow to stream flow, which will result in an increase in major ions, phosphate and silicate export (*Frey and McClelland*, 2009). Furthermore, permafrost driven changes in groundwater discharge into rivers has been hypothesized to alter the flux of dissolved organic carbon (DOC) in rivers (*O'Donnell et al.*, 2012). Over the past 30 years, the discharge normalized flux of DOC has decreased during summer and autumn in the Yukon river basin, which has been attributed to increases in active layer thickness, depth of subsurface flows, and water residence time (*Walvoord and Striegl*, 2007; *O'Donnell et al.*, 2012). In addition, permafrost thaw is likely to increase the transport of dissolved solids (*Frey et al.*, 2007), as comparison between permafrost covered an non-permafrost watersheds in the Kara Region suggests.

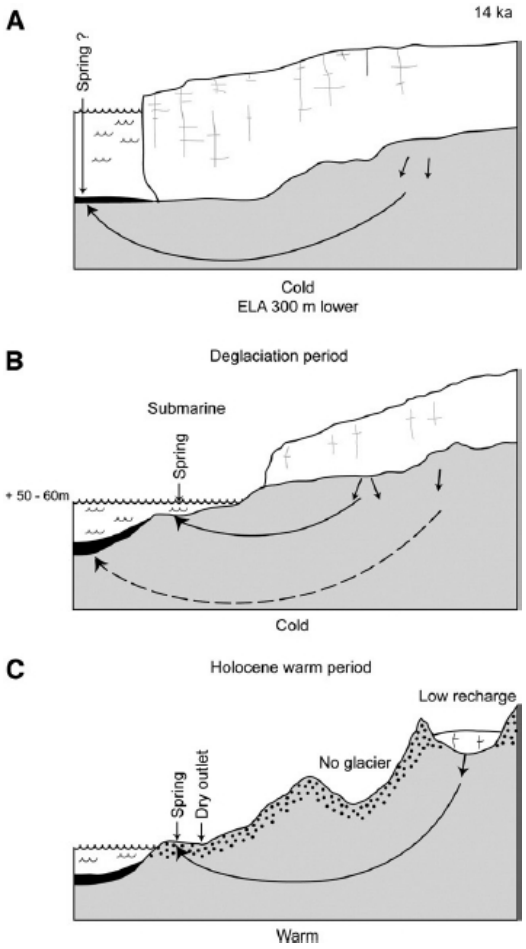

Figure 1.6: Conceptual model of the groundwater flow system in Svalbard. The dashed line indicate the permafrost zone. (A) Full glaciation with groundwater discharge in the fjord. (B) Groundwater discharge in shallow submarine position during the deglaciation phase. (C) More restricted spring systems during the Holocene optimum. Figure from *Haldorsen et al.* (2010).

1.3.4 Changing spring flow characteristics

Because springs that emerge through thick permafrost cannot be explained with a thermal talik as found under lakes, these systems may be transient and might have formed under past climatic conditions (e.g. *Haldorsen et al.*, 2010; *Grasby et al.*, 2012).

Haldorsen et al. (2010) derive a conceptual model for the development of the Troll hot springs over a full glacial cycle (Figure 1.6) and suggest the formation of these springs to be submarine. Glacio-isostatic rebound results in uplift and the springs become terrestrial. The springs are fed by a subglacial meltwater source from wet-based parts of the glacier. During an interglacial, the springs become surrounded by permafrost. Only groundwater springs and conduits related to glaciers that remain warm-based during the whole interglacial will persist into the next glaciation (*Haldorsen et al.*, 2010). The

heat transfer from groundwater, being dependent upon water temperatures and water fluxes controls whether the spring will remain open in the future. With climate change, glaciers may become cold based and the recharge may decrease resulting in a freezing of the springs (*Haldorsen and Heim*, 1999).

A more recent change in spring discharge has been observed from Ester spring, found in a coal mine near Ny Alesund, Svalbard, with a reduction by 50% of groundwater discharge during the 20th century (*Haldorsen and Heim*, 1999). The recharge is also suggested to originate from a glacial source, percolating through karstified limestones and dolomites. The authors relate this decrease in discharge to a higher melting rate of glacial ice during the first half of the 20th century, which increased the water balance of the catchment (*Haldorsen and Heim*, 1999).

In addition, climate change might also result in the formation of new hydrostatic pingos in some regions due to increased occurrence of thermokarst lake drainage. *Mackay* (1998) describes the rapid growth of pingos after lake drainage on Tukoyaktuk Peninsula (*Grosse and Jones*, 2011). Pingos have also been observed to migrate, as observed along a railway in the northern Tibetan Plateau, and have damaged the railway and bridges *Wu et al.* (2005). The migrating pingos are suggested to be the result of coupling of active fault movement, thermal groundwater, fine-grained surface deposits, seasonal changes and human activity in the areas of permafrost of the northern Tibetan Plateau *Wu et al.* (2005).

1.3.5 Water storage changes in the Arctic

It has recently become possible to measure inter-annual water mass variations in the Arctic with the Gravity Recovery And Climate Experiment (GRACE) satellite data, launched in 2002 (*Frappart et al.*, 2011). On a global scale, GRACE measures variations in the gravity field corresponding to the total change of mass from multiple sources. In terrestrial regions, mass changes include those from snow, soil and vegetation moisture, lake storage, groundice, runoff and groundwater storage (*Muskett and Romanovsky*, 2011). Results show an increase in water storage in the Siberian permafrost regions, whereas in Alaska, an increase in the Alaska coastal plain and a decrease in the Yukon watershed are observed (*Muskett and Romanovsky*, 2009, 2011; *Frappart et al.*, 2011). *Muskett and Romanovsky* (2011) link the increase of groundwater storage in the continuous permafrost zone with the formation of new closed- and open taliks under thaw lakes. In contrast, the decrease of groundwater storage in the discontinuous permafrost zones is linked to

new open taliks and a reduction of permafrost extent and a decrease of thaw lakes. This is supported by the observation of increased surface water bodies in the continuous zone and a decrease of bogs, ponds and lakes in the discontinuous zone. Furthermore, the authors conclude that these changes have the potential to reduce groundwater residence-time by storage depletion in the discontinuous permafrost zone, and conversely increase groundwater residence time by groundwater recharge through the newly formed taliks (*Muskett and Romanovsky*, 2011).

1.4 Modelling of groundwater flow in permafrost areas

Because there is a dearth of observational studies in order to fully understand hydrogeological changes in a dynamic permafrost environment, modelling serves as the primary means to help understand these systems. In addition, hydrogeological response of climate change and permafrost dynamics are difficult to predict, and empirical or numerical modelling provides a useful tool to make first order predictions.

There are many modelling challenges for predicting hydrologic response with permafrost degradation which have been reviewed by *Painter et al.* (2013). Challenges included are as follows: First, coupling of thermal and hydrologic processes including thermal conduction, advective heat transport in flowing water, water movement due to liquid pressure gradients, vapour diffusion and partitioning among ice, liquid and vapour phases. Second, modelling of surface energy balances that include contributions from convective heat flux between the surface and flowing air, latent heat from evapotranspiration, net radiative flux, conduction to and from the soil, heat convected by moving water and energy associated with the melting of the snow pack. Third, a a deforming topography caused by permafrost thawing and associated with the evolution of surface topography and streams networks that are coupled to subsurface hydrologic systems is another challenge. Fourth, the evolution of surface flows on impermeable frozen soil and their coupling to the subsurface hydrology is another gap in knowledge (*Painter et al.*, 2013). Coupling of a permafrost model with another process improves a permafrost model and allows one to identify the relative importance of a second process. In this thesis, the focus lies on numerical models coupling heat and fully saturated fluid flow including phase change, in order to model hydrogeological changes related to permafrost dynamics or permafrost dynamics related

to hydrogeological changes. For further work, additional processes could be added stepwise, and the model of groundwater flow in permafrost could be expanded with a surface energy balance, a deforming topography, or surface flows, however this would go beyond the scope of this thesis. More about the theoretical background, and about numerical modelling and governing equations can be found in Chapter 2.

Models of coupled heat and fluid flow provide a good first order estimate whether a surface water body is underlain by a talik, whether one will develop with climate change, and whether this talik is capable of providing a passway for groundwater flow to or from that surface water body.

There are different levels of complexity, how taliks and or groundwater flow in permafrost can be modelled. The most simple case is by modelling just one process, either heat transport or fluid flow. For example, when modelling a talik under a surface water body, some studies consider heat transport only (e.g. *Ling*, 2003; *Ling and Zhang*, 2004; *Taylor et al.*, 2008). In contrast, a hydrogeological model where the characterisation of an impermeable permafrost layer results from a conduction only model and is thus decoupled from the fluid flow model has been developed by *Bosson et al.* (2012). This can provide a powerful tool to represent large scale and long-term processes, although the interaction of heat and fluid flow is not considered.

With consideration of permafrost dynamics influencing the hydrogeological regime or vice versa, models of coupled heat and fully saturated fluid flow have been developed and applied to local to regional scale settings. FlexPDE (*Bense and Person*, 2008; *Bense et al.*, 2009, 2012; *Scheidegger et al.*, 2012; *Scheidegger and Bense*, 2014), SUTRA-ICE (*McKenzie et al.*, 2007; *Ge et al.*, 2011; *McKenzie and Voss*, 2013; *Wellman et al.*, 2013), Cast3M (*Grenier et al.*, 2013) or ARCHY (*Rowland et al.*, 2011) are applied to model fully saturated conditions and applied to local and region scale settings for time-scales of years to Millennia.

Increasing in complexity, a full three-phase, non-isothermal water dynamics model (MarsFlo) in frozen porous media has been developed by *Painter* (2011) and applied by *Painter* (2011); *Frampton et al.* (2011, 2013) and *Sjöberg et al.* (2013) to simulate permafrost on a seepage face, or on Mars. This model can be applied to fully saturated as well as the unsaturated media. This type of model describes more realistically water dynamics with variable saturation in the active layer than a one component model (e.g. *McKenzie et al.*, 2007; *Bense and Person*, 2008; *Bense et al.*, 2009; *Ge et al.*, 2011; *Rowland et al.*, 2011; *Bense et al.*, 2012; *Scheidegger et al.*, 2012; *Grenier et al.*,

2013; *Vidstrand et al.*, 2012; *McKenzie and Voss*, 2013; *Wellman et al.*, 2013), however, the representation of the three phases of solid, liquid and gaseous is more computationally demanding. Further multiphase-multicomponent models have been developed by *White* (1995); *White and Oostrom* (2006).

Developed from the MarsFlo model, PFLOTRAN is a non-isothermal, single-component (water), three-phase model that treats air as an inactive component. PFLOTRAN enables large scale models for applications on Earth, which compares well to results from MarsFlo (*Karra et al.*, 2014).

1.4.1 Modelling of lake dynamics

Permafrost dynamics under lakes have initially been modelled with heat conduction only models. Scenarios such as lake expansion, lake formation, lake drainage and lake warming have been considered.

1.4.1.1 Heat conduction only models

Ling (2003) simulates permafrost thermal regime and talik development under shallow thaw lakes on the Alaskan Arctic Coastal Plain using a heat transfer model with phase change. The author finds that shallow thaw lakes are a significant heat source to permafrost, and that taliks form under thaw lakes with a long-term mean lake bottom temperature greater than 0°C. Furthermore, the author suggests that talik development rates are very high for several years after thaw lake formation and decrease gradually with time. In addition, no taliks form when the mean lake bottom temperature is less than 0°C.

Talik freeze-up and permafrost response under drained thaw lakes on the Alaskan Arctic Coastal Plain has been modelled by *Ling and Zhang* (2004), who propose that when a thaw lake under a talik drains, the exposed lake bottom is subject to the same cold climate as the surrounding tundra. Periglacial features begin to develop and, the soft lake bottom sediments harden from water loss caused by drainage, evaporation and freeze-thaw consolidation. Their model results demonstrate that the talik will freeze up within approximately a century and that that the downward talik freeze-up is much faster than the upward freeze-up. In addition, the release of latent heat during the freeze process is suggested to retard the penetration of the freezing front from the talik table and talik base. The authors suggest that the interaction between climate change and thaw lake drainage is still not clear, owing to the complex interactions between climate, permafrost and hydrology (*Ling and Zhang*, 2004).

Modelling of the subsurface permafrost regime under newly formed lakes has shown that thermal taliks quickly develop beneath all lakes, however the thermal regime is strongly dependent on lithology (*Taylor et al.*, 2008). The authors demonstrate that in sands, sediments beneath the taliks remained almost entirely ice-bonded from the onset of the Holocene to the present time, whereas in fine grained clays and silts, elevated zones of unfrozen water content that eventually extended to the base of the permafrost develop. This is stated to be caused by the smoother freezing function of clayey silt compared to sand (*Taylor et al.*, 2008).

Lake expansion occurs due to conduction of heat from warm lake water into adjacent permafrost, subsidence of icy permafrost on thawing and movement of thawed sediment from lake margins by mass wasting (*Plug and West*, 2009). This has been modelled by combining thermal processes and mass wasting, and is the first model to include geomorphic processes with heat conduction (*Plug and West*, 2009).

1.4.1.2 Heat conduction and advection models

None of the case studies presented in Section 1.4.1.1, included advective heat transport of moving groundwater. *Rowland et al.* (2011) model a temperature field under thermokarst lakes where groundwater flow is imposed across the model domain, and study the influence of advective heat transport on permafrost degradation. The authors find that the presence of sub-permafrost groundwater flow substantially reduces the thickness of permafrost and increases the rate of localized permafrost degradation compared to a heat conduction only model. However, the authors do not explain how the high hydraulic head gradient can be explained in their model (*Rowland et al.*, 2011).

Grenier et al. (2013) couple heat and fluid flow, and model the impact of advective heat flow from and into a river plain under a glaciation scenario. They find that the evolution of the talik underneath a river / surface water body is primarily determined by the size of the river. However, advective heat flow is an important correction to this and for groundwater flow from plain to river. Heat advection leads to reduced closure times while for the river to plain case, the closure times are delayed and closure happens at larger depths (*Grenier et al.*, 2013).

The most extensive study about modelling of talik dynamics under lakes has been carried out by *Wellman et al.* (2013), who simulate the talik evolution of a newly formed lake above thick permafrost with coupled heat and

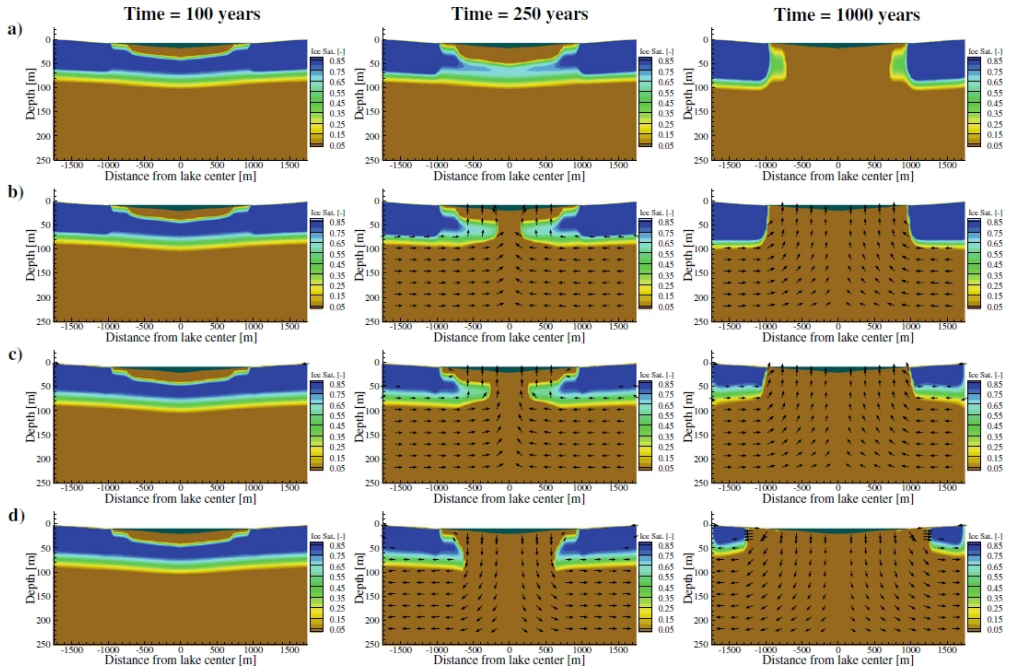

Figure 1.7: Lake talik models by *Wellman et al.* (2013). Cross section of 2D cylindrical model showing states of lake talik formation, ice saturation, and groundwater movement where a 12 m lake forms over a continuous permafrost layer. Figure columns distinguish early, middle and late-time conditions at 100, 250 and 1000 years from the time of lake formation. Figure rows differentiate four scenarios: a) current climate with no flow, b) current climate with a gaining lake, c) warmer climate with a gaining lake and d) warmer climate with a losing lake. Image is taken from *Wellman et al.* (2013).

fluid flow, where sub-permafrost as well as supra-permafrost groundwater is included (Figure 1.7). Three hydrologic scenarios are considered, hydrostatic conditions, a gaining lake and a losing lake, and two different climate scenarios for a gaining lake. The authors state that warm water entering the subsurface from surface water enhances permafrost degradation; in contrast, a lake gaining groundwater has a less pronounced acceleration of permafrost degradation compared with the losing lake. In addition, supra-permafrost groundwater flow is considered and is found to be low for the gaining or losing lakes, however for the hydrostatic lake, supra-permafrost flow is the dominant groundwater contribution into the lake. Generally, *Wellman et al.* (2013) note that advective heat transport from groundwater can be equally as important controls on the evolution of permafrost thaw as climate and lake size.

1.4.2 Modelling of groundwater contribution to rivers discharge

In order to study the base flow component to river discharge under a scenario of permafrost degradation due warming climate, several numerical modelling studies have been carried out. *Bense et al.* (2009) use coupled heat and fluid flow to model an idealised river basin and its response to warming surface temperatures. Their modelling results suggest that lowering of the permafrost table will establish a shallow groundwater flow system and when the permafrost disappears completely, deeper flow paths are established. In addition, the response of permafrost occurrence to surface temperature increase lags by several hundred years, and thus the hydrologic response of climate change is delayed. Further, the authors suggest a nonlinear increase in total groundwater discharge to streams with permafrost degradation, and a later stage acceleration of discharge when the residual permafrost is removed (*Bense et al.*, 2009).

Ge et al. (2011) study groundwater flow in the active layer over a seasonal cycle and find that groundwater flow is hampered from November to April, changing heat flow from conductive-advective over the summer to conductive only over the winter. Furthermore, the authors find that the fraction of advective heat flow is 5%, but under warming scenarios can reach 28% – 40%. The authors conclude that with increased warming, the active layer increases in thickness and that there will be more groundwater flow in the active layer, and therefore increased groundwater discharge to rivers. However, the authors point out that this is only valid if there is enough groundwater available to replenish the shallow groundwater system that undergoes increased discharge (*Ge et al.*, 2011).

Bense et al. (2012) model permafrost thaw in an idealised topographically driven flow system after *Tóth* (1963) with imposed surface water bodies at topographic low places, using different permafrost scenarios. One example is presented in Figure 1.8 and shows the permafrost degradation and groundwater flow development for a scenario with an intra-permafrost talik as the initial conditions and surface warming to positive temperatures modelled over time. Their modelling results suggest that the hydraulic head increases with permafrost thaw, resulting in groundwater uptake into elastic storage. This increased groundwater recharge is suggested to result in modified groundwater recharge and discharge trends, that result in a delay of increased groundwater fluxes to surface water bodies by several decades to centuries. In addition *Bense et al.* (2012) note that in an idealized Tóthian

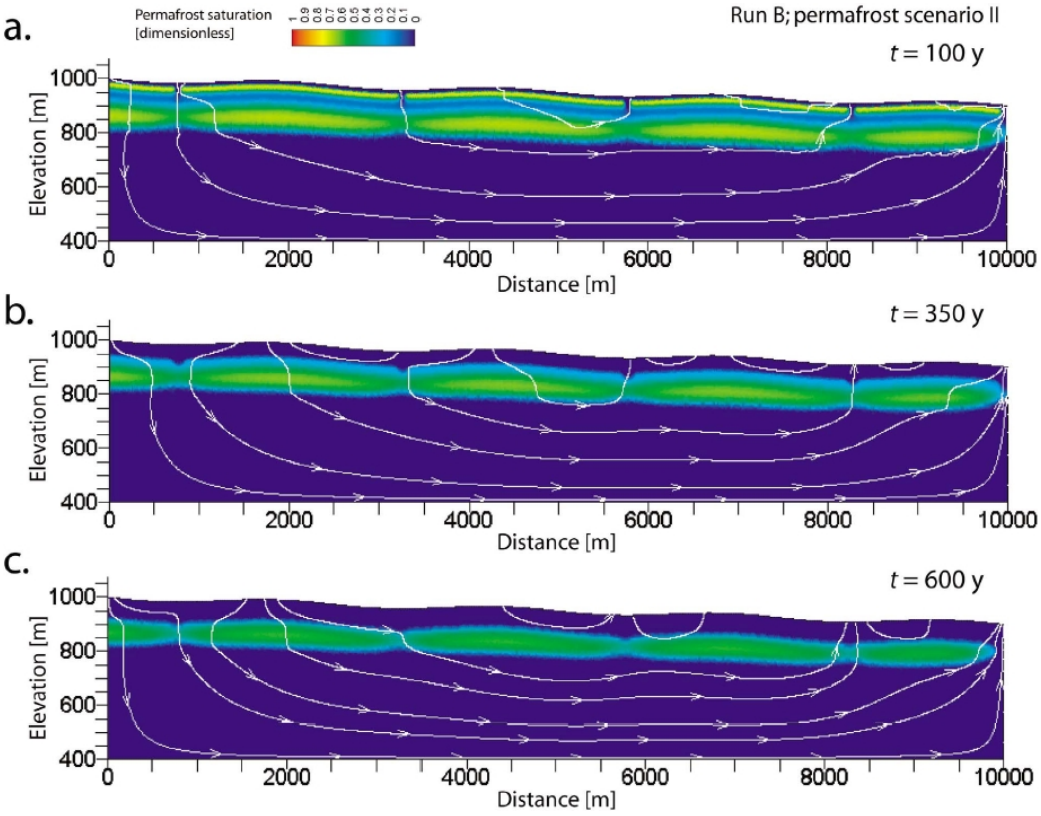

Figure 1.8: Regional scale groundwater flow development in a typical lowland landscape with taliks underneath rivers for a scenario in which there is a near-surface permafrost layer, underlain by a talik and followed by partially frozen ground, by *Bense et al.* (2012). The figure presents permafrost saturation and flow lines for a) 100 years, b) 350 years and c) 600 years of model simulation.

basin, as modelled in this study, recharge in a thawing permafrost environment is not sufficient for advective heat flow to be significant and have an impact on permafrost degradation. However, the authors point out that advective heat flow impacts transient taliks, where the recharge is not limited by effective rainfall, where flow is strongly focused, or where geothermal heat flow anomalies occur. Not limited by the amount of liquid precipitation are wet-based parts of a glacier or ice sheet or surface water bodies (*Bense et al.*, 2012).

Similar to *Bense et al.* (2012), *McKenzie and Voss* (2013) model permafrost thaw in a nested groundwater flow system under a climate warming scenario, however find that advective heat flow can accelerate permafrost thaw due to supra-permafrost groundwater movement compared to the conduction only model. Once an advective passway has developed, water can migrate through the subsurface and expand the existing talik network. In addition, they suggest that for a model including heat advection, thaw is largest

on hilltops where warm water recharges and relatively warm recharge is directed toward permafrost bodies, but in contrast, permafrost is thinnest for a conduction only model below valley bottoms where the initial permafrost distribution was thinnest. The effect of surface water bodies on thaw rate of permafrost has found to be largest when there are several lakes and a regional groundwater network can develop, however the authors state that the primary thaw mechanism is heat advection in the downward flow below hilltops. The authors conclude that advective heat flow has the potential to thaw a permafrost layer of several hundred meters within only some hundred years, as groundwater flow around permafrost bodies can greatly increase the rate of thaw (*McKenzie and Voss*, 2013).

This large impact of advective heat flow in permafrost degradation suggested by *McKenzie and Voss* (2013) stands in contrast with the findings from *Bense et al.* (2012) who suggest that for advective heat flow to accelerate permafrost degradation, effective rainfall in Arctic regions is not sufficient. The large permafrost degradation in recharge areas modelled by *McKenzie and Voss* (2013) leads to higher recharge (higher hydraulic head gradient and higher permeabilities) but potentially also different freezing functions and functions of hydraulic conductivity decrease over the freezing process, enabling groundwater movement in ground with higher ice saturation than for the model by *Bense et al.* (2012). The influence of the function of hydraulic conductivity decrease over the freezing process will be discussed in more detail in Chapter 4.

1.4.3 Shallow groundwater flow

Modelling of shallow groundwater flow in the active layer or interapermafrost taliks can be carried out in two ways; either with fully saturated flow (*Bense et al.*, 2009; *Ge et al.*, 2011; *Bense et al.*, 2012; *McKenzie and Voss*, 2013) or with multicomponent multiphase flow, where gas transport is added to transport of the liquid phase (*Painter*, 2011; *Frampton et al.*, 2011, 2013). The latter is computationally more expensive, but enables the study of water flow in the unsaturated zone.

Frampton et al. (2013) find that under a warming scenario, seepage flow will get reduced in temporal variability. Therefore, the authors infer, that a decreased inter-annual or seasonal variability in seepage flow may be an indicator of permafrost degradation and that changes in mean annual flow may take longer to respond. In addition, their model suggests that the largest changes can be observed by the magnitude of the minimum flow, whereas the

the peak annual flow does not change to such an extent. Furthermore, this study finds that there is an initial increase of seepage flow, but that once the saturated ice region has vanished, all liquid water content stored in the system gets released and the system reaches a new steady state, even if surface temperatures continue to increase (*Frampton et al.*, 2013).

1.4.4 Previously glaciated regions

Continental scale glaciations can have a large impact on the regional hydrogeology with enhanced infiltration of sub-glacial meltwater, and lithospheric flexure (e.g. *Iverson and Person*, 2012; *McIntosh et al.*, 2012; *Neuzil*, 2012). An extensive review of ice-sheet hydrogeologic interactions has been carried out by *Person* (2012) who point out uncertainties in modelled processes, boundary conditions and model parameters. The author highlights that there is no theoretical basis for coupling ice sheet and subsurface hydrogeologic models, but geomorphologic data sets suggest feedbacks between ice sheet dynamics and hydrogeologic processes. Nevertheless, there are models that incorporate permafrost dynamics and prescribed glacial geometry, as discussed below.

A continental scale groundwater model during a glacial cycle, considering sub-glacial infiltration, density-dependent groundwater flow, permafrost evolution, isostasy, sea level changes and ice loading has developed and used for the Canadian landscape during the Wisconsinian glaciation (*Lemieux et al.*, 2008a,b,c). The authors surmise that much of the infiltration of subglacial meltwater occurs during ice sheet advance and that during ice sheet retreat, groundwater mainly discharges on the surface, in both the subglacial and periglacial environments.

Bense and Person (2008) simulate the transient impact of ice sheet advance and retreat for a intercratonic sedimentary basin, including hydrodynamics in sedimentary basins that consider mechanical loading, lithospheric flexure, permafrost formation and thawing, and the emplacement of dense brines with fresh glacial meltwater (Figure 1.9). The authors conclude that present day fluid patterns within formerly glaciated regions may not have reached a steady state yet and is still responding to the last glaciation 10 ka BP. Furthermore, the authors find that near surface permafrost strongly impacts the distribution of hydraulic heads and associated fluid patterns (*Bense and Person*, 2008).

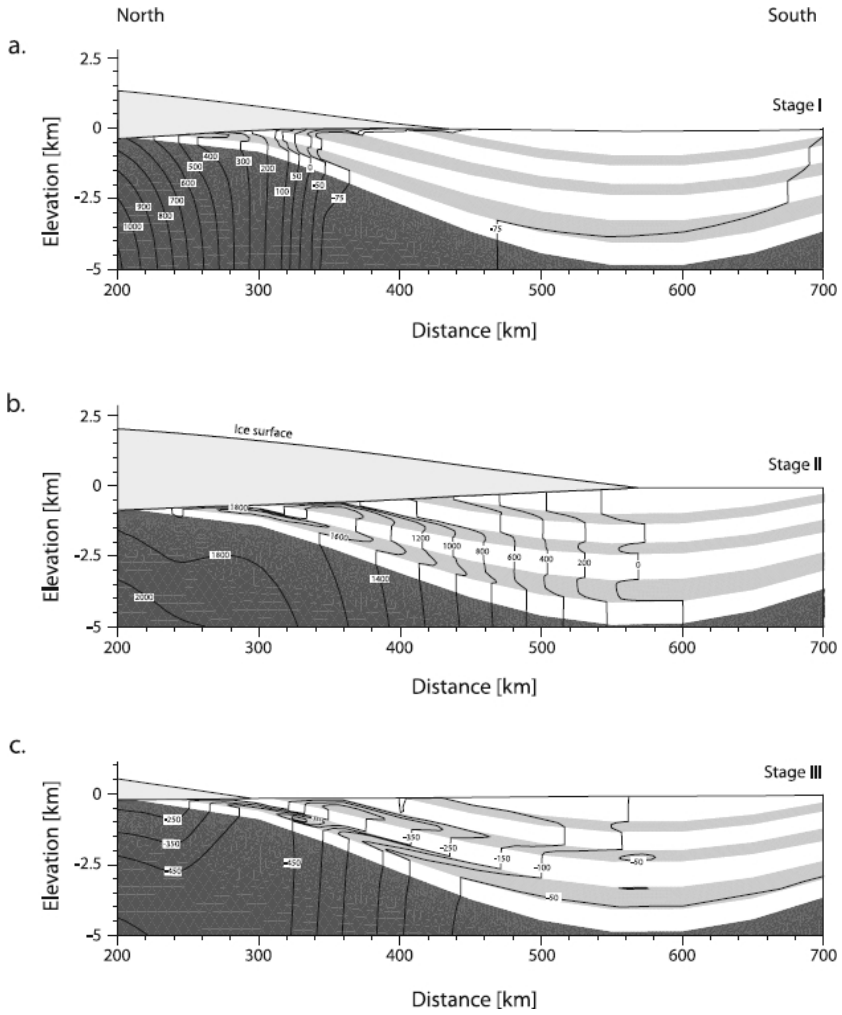

Figure 1.9: Glacial recharged groundwater in an intercratonic sedimentary basin by *Bense and Person* (2008). Graph presents the hydraulic head patterns during ice sheet advance (Stage I at 25 ka B.P.), during the LGM (Stage II at 17.5 ka B.P.) and during ice sheet retreat (Stage III at 12.5 ka. B.P.).

1.5 Aims and Objectives

In order to understand the processes driving the observed Arctic hydrologic changes, a conceptual framework describing and modelling the underlying processes of permafrost hydrogeology is needed. At the start of this project in 2010, very few studies in modelling hydrological changes with permafrost dynamics existed (*McKenzie et al.*, 2007; *Bense and Person*, 2008; *Bense et al.*, 2009), and there was (and still is) large uncertainty about how the hydrogeologic regime may respond to past and present climate change and permafrost dynamics in the Arctic.

Overall aim: The principal aim of this thesis is to improve understanding of the impacts of permafrost dynamics on Arctic groundwater flow systems

with climatic change and vice versa.

Overall approach: There is a dearth of field data, and the hydrogeologic response and permafrost dynamics are difficult to predict with changing climatic conditions from empirical studies alone. This thesis addresses the principal aim by investigating different generic settings described with conceptual models of potential groundwater-surface water connections by the means of numerical modelling of coupled heat and fluid flow including phase changes of ice/water. These conceptual models are a great abstraction and simplification of the reality, but allow us to understand the relevant processes and carry out research of the first principles of permafrost hydrogeology. The conceptual models are then numerically simulated with coupling heat and fluid flow developed by *Bense and Person* (2008) and *Bense et al.* (2009), using different input parameters and boundary conditions for each case study. All other processes influencing permafrost hydrology under a changing climate, as outlined above and reviewed by *Painter et al.* (2013), are not considered. This is beyond the scope of this thesis and coupling heat and fluid flow including phase change in a regional scale setting is already computationally demanding. The aims and objectives of the different case studies are outlined below.

Objective 1: In order to study the influence of climate change on the evolution of potentially new groundwater surface water connections under lakes, the temperature at a lake bottom is a critical boundary condition for numerical models of coupled heat and fluid flow, and previously an arbitrary value has been used for modelling (*Bense et al.*, 2009; *Rowland et al.*, 2011; *Grenier et al.*, 2013; *Bense et al.*, 2012). Therefore, the first aim is to develop a model to estimate lake bottom temperatures for different climatic scenarios and lake sizes.

A heat-conduction model is developed to study the temperature dynamics of a lake that seasonally freezes over by altering in a simplified manner the thermal regime from heat-conduction dominated in winter to heat-advection dominated in summer. Modelled lake bottom temperatures are then compared to measured lake bottom temperatures from the literature. This model serves as a tool to estimate the lake bottom temperatures for different lake sizes under different climatic settings, that can be used to model the thermal response of surface temperature increase on the sub-lake temperature regime, or the effect of lake size dynamics on the temperature regime.

Objective 2: Climate change and lake morphological changes are impacting the thermal regime and the hydrogeology of large areas in the northern hemisphere (e.g. *Yoshikawa and Hinzman*, 2003; *Smith et al.*, 2005; *Walter et al.*, 2006; *Marsh et al.*, 2009). The second aim is to estimate the response of the temperature regime underneath a lake with the influence of surface temperature warming, considering different hydraulic scenarios.

The modelled lake bottom temperatures from objective 1 are used to study talik development under a surface warming scenario and for lake formation and growing for four different lake models scenarios, namely heat conduction, a through-flowing lake, a discharging lake and a recharging lake. Advective heat flow can accelerate permafrost degradation, however the magnitude of advective heat flow is proportional to the hydraulic conductivity of the substratum. In frozen ground, the hydraulic conductivity is reduced by several orders of magnitude, resulting in permafrost that is to be literally impermeable. However, the hydraulic conductivity in partially frozen ground is not very well characterised. Therefore the impact of different permafrost-permeability-reduction-functions on the modelled groundwater flow in partially frozen ground are compared.

Objective 3: In the High Arctic where lakes and rivers are absent, a sub-permafrost groundwater connection cannot be explained with the concept of an insulating surface water body, as used in the objectives 1-2. Nevertheless spring systems can be observed that penetrate several hundred meters of permafrost (e.g. *Andersen et al.*, 2005; *Yoshikawa et al.*, 2007; *Haldorsen et al.*, 2010; *Grasby et al.*, 2012). Here, the aim is to better understand the dynamics of a spring system that is fed by a glacial meltwater source.

To evaluate the interaction between proglacial spring hydrogeology and formation of permafrost near the surface after the spring is exposed by a retreating wet-based ice sheet. The combination of a high permeable fault zone and high hydraulic head gradients result in a high advective heat flow component, responsible for the prevention of freezing of a talik.

Objective 4: The hydraulic boundary conditions in a small scale system of a talik lake or a spring are not very well known and are set as non-dynamic over time for objectives 2-3. This approach may be feasible in lowland areas, or models assuming a steady hydraulic head difference. In front of a dynamic ice sheet however, hydraulic heads are assumed to be altered with ice sheet dynamics. Therefore, the aim is to improve our understanding of talik evolution and groundwater movement in a proglacial environment infront of a

dynamic, wet-based ice sheet.

A larger scale model of a retreating ice sheet is used to control the hydraulic and thermal boundary conditions. These control the hydraulic head distribution and the sub-surface temperature distribution around a proglacial lake in front of a retreating ice sheet. In addition, the influence of open taliks on the regional scale hydrogeology is studied.

1.5.1 Thesis structure

The results chapters of this thesis are structured as self-contained chapters in the form of papers.

- Chapter 2 describes the modelling approach together with technical and theoretical background of this thesis. This numerical model is then applied to Chapters 3-6.

- Chapter 3, 'Evaluating lake bottom temperatures in permafrost terrain', develops a model to estimate the lake bottom temperature and addresses objective 1.

- Chapter 4, 'Control of advective heat flow on talik development in a dynamic permafrost landscape', studies the influence of lakes under a warming temperature scenario and under a scenario of lake growing. In addition, the influence of different hydraulic conductivity decrease functions on the talik evolution are evaluated. Chapter 4 addresses objective 2.

- Chapter 5, 'Transient nature of Arctic spring systems driven by subglacial meltwater', models a spring system along a high permeability fault zone after ice retreat and addresses objective 3.

- Chapter 6, 'Impacts of glacially recharged groundwater flow systems on talik evolution', uses a large scale model to study a glacially recharged groundwater source to proglacial lakes infront of a dynamic ice sheet and addresses objective 4.

- Chapter 7 summarises the results found in Chapters 3-6, discusses their limitations and raises questions for further research.

Chapter 2

Theoretical and technical background to numerical modelling

2.1 Introduction

In order to better understand the hydrogeological response to permafrost dynamics, as well as the response of permafrost to hydrogeological changes, modelling is used to test different temperature and hydrogeological scenarios in different environments. Generally, modelling serves as a tool to understand quantitatively how an environmental system behaves under different scenarios and input parameters, and explains causes and mechanisms behind observations.

In general, there are different approaches for mathematical modelling, and the choice depends on the objective of the study. The simplest model is a system approach, or black-box model, that describes a behaviour between variables on the basis of observations, or uses empirical relationships to describe input and output of a system (*Wainwright*, 2004). An empirical hydrological model is for example the unit hydrograph (*Abbott and Refsgaard*, 1996). In permafrost modelling, the measurement of temperatures at the base of winter snowpack (BTS) (*Gardaz*, 1997) or mapping of mountain permafrost with the criteria of aspect and elevation (*Keller*, 1992) are examples for empirical models. Generally, empirical models have a high predictive power as they are fitted to measured data, but have a low explanatory value, as the underlying processes are not explained (*Wainwright*, 2004).

In contrast, physics-based models solve the processes transforming input to output using the continuity equations for mass, momentum and energy

(*Wainwright*, 2004). Physical models can be used to study the key feature of the environment and its interaction between different environmental components (*Peng et al.*, 2002), as applied in this thesis where the interaction between permafrost dynamics and groundwater flow is studied. Physics based models can be complex, non-linear with different components interacting with each other, occur over a wide range of scales and be dynamic (*Peng et al.*, 2002). The physical description results in a high explanatory depth of the driving processes, but the model can have a lower predictive power than empirical models, as they often do not agree with observations, and usually need to be calibrated with field observations (*Wainwright*, 2004). This discrepancy can either be because not all processes are considered, or there are uncertainties in the parameter values. Physics based models are widely used in both hydrogeological science and permafrost science, however their coupling is less frequently studied.

For physics based models, different levels of approximation can be used. First, a reduced or simplified mathematical model identifies key mechanisms and captures the main behaviour of the relevant processes, however it misses out secondary physics and sacrifices in numerical accuracy. Second, full mathematical models capture a behaviour at high spatial and temperature resolution.

Examples of reduced or simplified mathematical model to study taliks are heat transport only models that ignore heat transport by heat advection (e.g. *Ling*, 2003; *Ling and Zhang*, 2004; *Taylor et al.*, 2008). Another example of a simplified mathematical model are models that describe the hydrogeology in a permafrost environment by prescribing the permafrost as an impermeable layer and do not couple heat and fluid flow (e.g. *Lemieux et al.*, 2008a).

Depending on the application of a model, the boundary between a simplified mathematical model and a full mathematical model is smooth; for example applications of groundwater flow use fully saturated fluid flow, other applications that study water movement in an unconfined aquifer or water movement in soil use unsaturated fluid flow, which is numerically more complex to solve than fully saturated fluid flow, but might be unnecessary for many applications. In addition, density- and salinity driven groundwater movement might be of relevance, or might unnecessarily complicate the model.

In this thesis, physics-based models are used describing transient coupled heat and fully saturated fluid flow including latent heat of fusion with the FlexPDE model (*Bense and Person*, 2008; *Bense et al.*, 2009). Other similar

models are SUTRA-ICE (*McKenzie et al.*, 2007; *Ge et al.*, 2011; *McKenzie and Voss*, 2013; *Wellman et al.*, 2013), Cast3M (*Grenier et al.*, 2013) or ARCHY (*Rowland et al.*, 2011) that are also applied to fully saturated conditions. SUTRA-ICE, in contrast to FlexPDE as used in this thesis, includes fluid density variabilities as a function of temperature, however if required this could be easily modified in the FlexPDE model. The model MarsFlo (*Painter*, 2011) uses a two component, three-phase model that is applied to unsaturated conditions.

The following section describes the theory of heat flow, Darcy's Law, coupling of heat and fluid flow, and solving of the equations with a finite element solution environment. This is followed by a theoretical discussion about model set-up and boundary conditions. The model used here is then validated against an analytical solution. Finally, model scaling, used in Chapter 6 is presented.

2.2 Fluid flow

Groundwater flow can be driven by different types of fluid motion. Forced convection is when the flow field is driven by external forces and in the absence of density gradients. An example for forced convection is topography driven flow, where groundwater is recharged in higher elevation areas, from where the flow is directed downwards and is discharged at lower elevation areas, at which point the flow is directed upwards with respect to the water table (*Tóth*, 1963). In addition, fluid flow can be driven by free convection due to density gradients caused by temperature or salinity variations and fluid flow is described by buoyancy forces, or by capillary forces, or tectonic strain (*Domenico and Schwarz*, 1998). However, in this thesis, only topographically driven flow is considered, which is described by Darcy's Law.

The groundwater flow equation is a combination of the Darcy's Law and the mass conservation law. Steady-state groundwater flow for an incompressible fluid in a fully saturated aquifer requires that fluid flow into an elementary control volume with specific discharge $q_{x,y,z}$ [m s^{-1}] and density $\rho_{x,y,z}$ [kg m^{-3}] is equal to the fluid flow out of the control volume:

$$\frac{\partial \rho_x q_x}{\partial x} + \frac{\partial \rho_y q_y}{\partial y} + \frac{\partial \rho_z q_z}{\partial z} = 0 \tag{2.1}$$

Considering water as an incompressible fluid, the fluid density $\rho_{x,y,z}$ is

constant and Equation 2.1 becomes:

$$\frac{\partial q_x}{\partial x} + \frac{\partial q_y}{\partial y} + \frac{\partial q_z}{\partial z} = 0 \tag{2.2}$$

Darcy's Law states that the specific discharge is proportional to the negative hydraulic gradient and the hydraulic conductivity K [m s^{-1}] of the porous medium:

$$q_x = -K_x \frac{\partial h}{\partial x}, q_y = -K_y \frac{\partial h}{\partial y}, q_z = -K_z \frac{\partial h}{\partial z} \tag{2.3}$$

where h [m] is the hydraulic head and x, y, z are the flow lengths. Darcy flux is directed from high to low hydraulic head.

Substituting Equation 2.3 into Equation 2.2:

$$\frac{\partial}{\partial x}\left(K_x \frac{\partial h}{\partial x}\right) + \frac{\partial}{\partial y}\left(K_y \frac{\partial h}{\partial y}\right) + \frac{\partial}{\partial z}\left(K_z \frac{\partial h}{\partial z}\right) = 0 \tag{2.4}$$

results in the groundwater flow equation. For an isotropic and homogeneous porous material with constant K-values Equation 2.4 can be simplified to the Laplace Equation:

$$\nabla^2 h = 0 \tag{2.5}$$

where the nabla symbol ∇ represents a vector differential operator.

Under transient conditions, the mass inflow rate minus the mass outflow rate is equal to the change in mass storage with time. Equation 2.4 becomes:

$$\nabla \cdot [K \nabla h] = S_s \frac{\partial h}{\partial t} \tag{2.6}$$

where t [s] is time, and S_s [m^{-1}] is the specific aquifer storage.

The specific storage is defined as a proportionality constant relating the volumetric changes in fluid volume per unit volume to the time rate of change in hydraulic head. However, in confined flow, a drop in hydraulic head is not accompanied by drainage from storage, as the aquifer remains fully saturated at all times. However, water and the porous structure are elastically compressible, and changes in head are accompanied by changes in both water and pore volume (*Domenico and Schwarz*, 1998).

2.3 Heat transport

Heat transport in the subsurface occurs in a porous media through conduction, and advection. Heat conduction is directly proportional to the temperature gradient, the higher the the geothermal gradient, the higher the conductive heat flow at the surface. Heat advection is the heat transport through groundwater flow, or in unsaturated ground through air flow.

Conductive heat transport is described by Fourier's Law and the conservation of energy. Fourier's Law describes heat conduction from regions of high temperatures to regions of lower temperatures with the heat flux $\vec{q}_{heat}$ [W m^{-2}] being proportional to the temperature gradient:

$$\vec{q}_{heat} = -\kappa_a \nabla T \tag{2.7}$$

where T[°C] is the temperature distribution and κ_a [W m^{-1} K^{-1}] is the effective thermal conductivity of the material. The negative sign states that heat flows is in the direction of decreasing temperature. In the subsurface, $\vec{q}_{heat}$ [W m^{-2}] can be understood as the geothermal heat flux, and ∇T [°C m^{-1}] the geothermal gradient.

For steady state problems, the temperature profile in the ground is proportional to κ_a:

$$\nabla \cdot [\kappa_a \nabla T] = 0 \tag{2.8}$$

For a constant κ_a, the temperature profile in the ground is linear with depth and follows the Laplace Equation.

$$\nabla^2 T = 0 \tag{2.9}$$

However, the temperature distribution in the subsurface rarely follows a steady state and transient heat flow components influence the temperature distribution (*Williams and Smith*, 1989). Generally, the rate of heat flow into the system equates to the rate of heat flow out of the system plus the rate of change in heat storage and is expressed as follows:

$$\nabla \cdot [\kappa_a \nabla T] = C_a \frac{\partial T}{\partial t} \tag{2.10}$$

where C_a [J m^{-3} K^{-1}] is the effective heat capacity, and t [s] time.

In frozen soil, the temperature profile is further influenced by the effects of latent heat of fusion L_i [J m^{-3}] and the change of the thermal properties in the frozen or unfrozen state (*Williams and Smith*, 1989). The change of

heat storage is determined by the change in temperature and the change in the unfrozen water content Θ_w [-]:

$$\nabla \cdot [\kappa_a \nabla T] = C_a \frac{\partial T}{\partial t} + L_i \frac{\partial \Theta_w}{\partial t} \tag{2.11}$$

In systems with a moving fluid, advective heat transport influences the temperature distribution. Adding an advective heat flow term to Equation 2.11 results in the complete heat conduction-advection equation including phase change of pore water:

$$\nabla \cdot [\kappa_a \nabla T] - C_w \vec{q} \, \nabla T = C_a \frac{\partial T}{\partial t} + L_i \frac{\partial \Theta_w}{\partial t} \tag{2.12}$$

where C_w [J m^{-3} K^{-1}] is the effective heat capacity of water, and $\vec{q}$ [m s^{-1}] (Equation 2.3) is the Darcy flux.

2.4 Hydraulic and thermal properties over the freezing interval

The presence of ice and water near their freezing / thawing temperature has a dominant effect on the thermal and hydraulic properties of soil. When water freezes, its thermal conductivity increases four-fold, its mass heat capacity decreases by half, it releases heat equivalent to that required to raise the temperature of an equal volume of rock by about 150°C and its hydraulic conductivity decreases several orders of magnitudes (*Williams and Smith*, 1989; *Woo*, 2012). In the model used in this thesis, the water saturated pore-space, calculated with the soil freezing function, is used to calculate the effective thermal conductivity, the effective volumetric heat capacity and a permafrost-permeability-reduction function that is then multiplied with the hydraulic conductivity to obtain an effective hydraulic conductivity over the freezing interval. This section describes the soil freezing function and thermal and hydraulic properties over the freezing interval as they are implemented in the model used in this thesis.

2.4.1 Soil freezing function

Water in the subsurface freezes over a range of temperatures. Pure water freezes at 0°C, but the occurrence of salts lowers the free energy and there is a depression of the freezing point. An additional effect is that of capillarity and adsorption; the migration of water to the freezing front and the forces

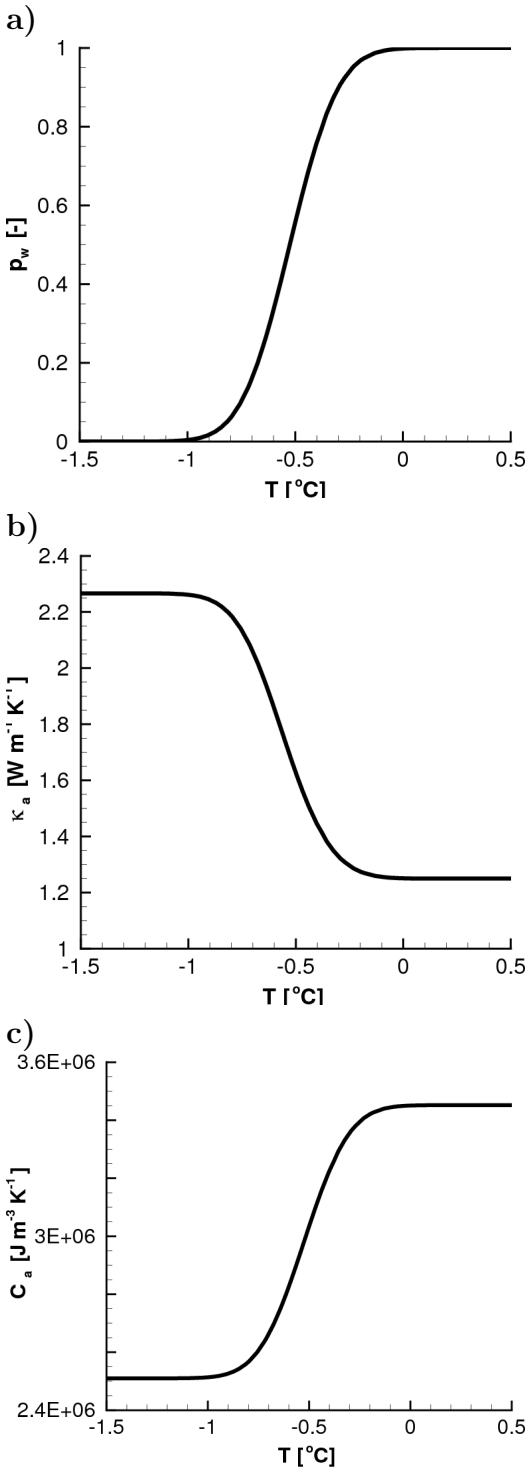

Figure 2.1: Change of the thermal properties over the freezing interval for a substrate with 40% pore space, as implemented in FlexPDE. a) p_w is for the water occupied pore space, b) κ_a the thermal conductivity, and c) C_a the heat capacity.

emanating from the mineral particle surfaces reduces the free energy in the absorbed layer on the particles. The remaining unfrozen supercooled water in frozen soil is the residual saturation p_{res} (*Williams and Smith*, 1989). A review of different mathematical representations of functions describing the freezing and thawing process can be found in *McKenzie et al.* (2007) and *Kurylyk and Watanabe* (2013).

Even though, in this thesis, the influences of salts and capillarity effects are not mathematically described, a temperature interval over which the freezing process is used in order to maintain numerical stability.

There are different ways of describing the freezing function, which should be smooth and easily differentiated (*McKenzie et al.*, 2007). The simplest way of describing the freezing process is with a linear function, however this function is not smooth at the point of residual saturation and at the point of full saturation. Another possibility is using a smooth stepping function, and here the error function is used:

$$\theta_w = n(erf(2.1 + T/0.25) + 1) \tag{2.13}$$

where θ_w is the water occupied porosity, n the total porosity, and erf the error function. Figure 2.1a presents the water occupied pore space interval, $p_w = \theta_w/n$, between 0°C and -1°C.

For Chapters 3, 4, and 6 a freezing interval between 0°C and -1°C and for Chapter 5, a freezing interval between 0°C and -0.25°C is applied. A wider freezing interval stabilises the numerical code and decreases computation time.

2.4.2 Thermal conductivity

The thermal conductivity of ice is more than four times higher than that water, and thus frozen soils have a higher thermal conductivity than unfrozen soils. Around the freezing point, the volume fractions of ice and water are temperature dependent and thus the thermal conductivity is a function of temperature. In addition, the thermal conductivity is strongly influenced by the soil mineralogy; quartz for example has a very high conductivity (*Williams and Smith*, 1989).

The model used in this thesis assumes fully water saturated conditions with all the free pore space being water/ice saturated:

$$\theta_s + \theta_w + \theta_i = 1 \tag{2.14}$$

where the subscripts s, w, and i stand for solid, water and ice (*Cutler et al.*, 2000). For a given aquifer porosity (n[-]) the ice content θ_i follows the porosity and water content as:

$$\theta_i = n - \theta_w \tag{2.15}$$

and the solid grain fraction (θ_s [-]) is equal to 1-n.

The effective thermal conductivity is calculated as a weighted geometric mean from the thermal conductivities of rock, water and ice as specified in Equation 2.15:

$$\kappa_a = \kappa_s^{\theta_s} \kappa_w^{\theta_w} \kappa_i^{\theta_i} \tag{2.16}$$

The change of the thermal conductivity is implemented in the model code as presented in Figure 2.1b.

2.4.3 Heat capacity

The volumetric heat capacity C_a [J m^{-3} K $^{-1}$] is the amount of heat required to change the temperature of 1 m^3 by 1°C. For a composite material, a weighted average for heat capacities is used (Equation 2.17) (*Williams and Smith*, 1989).

$$C_a = C_s\theta_s + C_w\theta_w + C_i\theta_i \tag{2.17}$$

The change in heat capacity over the freezing interval is described here as presented in Figure 2.1 c.

2.4.4 Permafrost-permeability-reduction function

In permafrost, where all pore fluids are frozen, water is immobile and the hydraulic conductivity approaches effectively zero. However, over the freezing process, porewater freezes progressively from larger pores through to smaller pores and there will be a steep decrease in hydraulic conductivity (*Ireson et al.*, 2013).

Very few field studies and modelling studies investigating the decrease in hydraulic conductivity exist (e.g. *Burt and Williams*, 1976; *Mualem*, 1976; *Kleinberg et al.*, 2003; *Kleinberg and Griffin*, 2005; *Watanabe and Flury*, 2008; *Azmatch et al.*, 2012), however they all describe the hydraulic conductivity decrease of soil and not solid rock. Next to empirical formulas or semi-theoretical approaches, hydraulic conductivity can be obtained from a combination of classical retention curves by van Genuchten, Mualems model

for relative permeability and the Clausius-Clapeyron equation, relating temperature and pressure of freezing soils (*Mualem*, 1976; *van Genuchten*, 1980; *Painter*, 2011). An in depth discussion of various forms of the Clapeyron equation, the relationship between the soil moisture curve and the soil freezing curve, and models relating the soil freezing curves and hydraulic conductivity models for partially frozen soils is reviewed in *Kurylyk and Watanabe* (2013). A comparison of some of these different models and their effect on hydrogeological modelling is presented in Chapter 4.

The hydraulic conductivity decrease used in the model presented in this thesis, is based on the study by *Kleinberg et al.* (2003); *Kleinberg and Griffin* (2005) and is modified by *Bense and Person* (2008); *Bense et al.* (2009). *Kleinberg and Griffin* (2005) compare theoretical models of hydraulic conductivity decrease to measured data. The models used are ice coating the walls of capillary tubes, ice occupying the centre of capillary tubes, ice coating the surfaces of a grain pack, and ice occupying the centres of a grain pack pore space. The model where ice occupies the grain pack pore space best represents the measured data (Figure 2.2); the model assumes that the pore surface area increases as ice is forming in the centre of the pore. The permeability reduction (k_{rw}) can be described as a function of water-saturation state:

$$k_{rw} = \frac{p_w^{m+2}}{(1 + (1 - p_w)^{0.5})^2} \tag{2.18}$$

where the water-saturation state ($p_w = \theta_w / n$) is defined from the water content θ_w [-] and porosity n [-], and m is the saturation exponent, which increases from $m = 0.4$ at $p_w = 0.9$ to unity at $p_w = 0$ (*Kleinberg et al.*, 2003; *Kleinberg and Griffin*, 2005).

This equation has been simplified by *Bense and Person* (2008); *Bense et al.* (2009) to:

$$k_{rw} = \frac{p_w^4}{(1 + (1 - p_w)^{0.5})^2} \tag{2.19}$$

which is applied for the model used in this thesis. However, a lower limit is set for p_w=$\sim$2%, resulting in a permeability reduction of eight orders of magnitude to stabilise the numerical code (*Bense et al.*, 2009).

The effective hydraulic conductivity is then obtained by multiplying the permeability reduction function (k_{rw}) with the hydraulic conductivity K. Including the permafrost -permeability-reduction function, Equation 2.6 can be updated as follows.

$$\nabla \cdot [k_{rw} K \nabla h] = S_s \frac{\partial h}{\partial t} \tag{2.20}$$

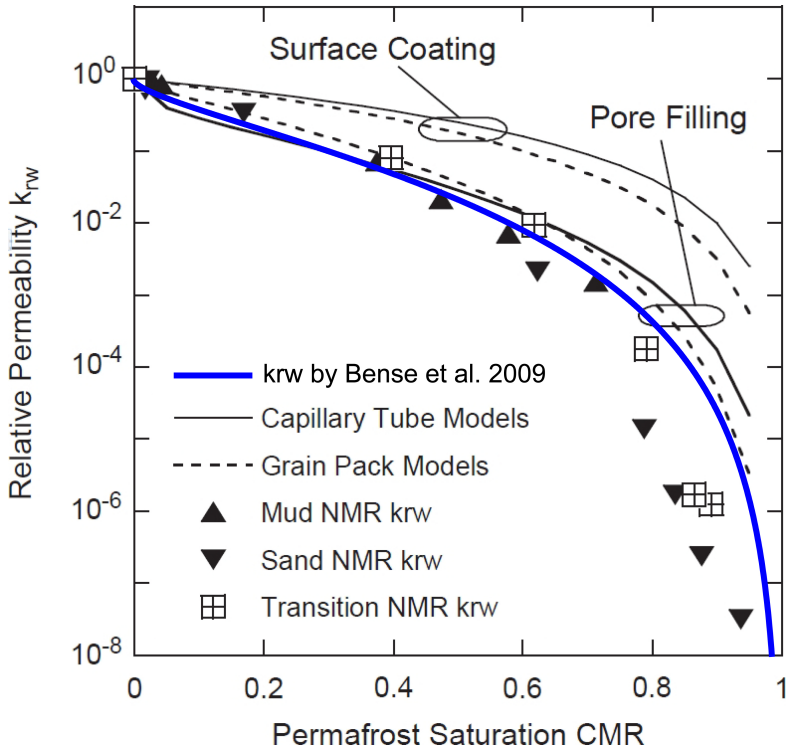

Figure 2.2: Relative permeability (k_{rw}) with permafrost saturation for NMR measured sand and mud at the base of permafrost compared to modelled relative permeability in which ice coats grains or fills the centre of pores. Figure taken from (*Kleinberg and Griffin*, 2005), with the k_{rw} function from Equation 2.19 added.

2.5 Finite element modelling

There are several methods available for solving differential equations; and the most widely used ones are finite differences, integrated finite differences, also known as finite volumes, and finite elements. All schemes discretise the partial differential equations (PDEs) in the spatial dimension to convert the PDE to an ordinary differential equation (OED) in time.

The finite difference method (FDM) is the oldest method and is based upon the application of a local Taylor expansion to approximate the differential equations. The problem domain is discretised with a rectangular grid, based on lines. FDM is flux conserving, but not mass conserving. A problem with the FDM approach is that the grid used can only change in grid size over an entire row or column. This issue motivated the use of an integral form of the PDEs and the development of the finite element (FEM) and finite volume (FVM) methods (*Wainwright*, 2004; *Peiró and Sherwin*, 2005).

Finite element methods (FEM) on the other hand use regular shapes, such as triangles, cubes, cuboids, hexahedrons, to divide the model domain. Triangular elements as used in this thesis, are defined by three nodes that locate the unknown variable (e.g. hydraulic head or temperature). The unknown

variable within each element is defined in terms of the nodal value by basis of an interpolation function. Numerical modelling predicts the value of the unknown variable at each nodal point. In contrast to the finite difference approach, the unknown value in the finite element approach is interpolated over one element (*Wang and Anderson*, 1982). This approach is advantageous as it provides a more natural treatment of the Neumann boundary conditions as well as that of discontinuous source terms due to their reduced requirement on the regularity or smoothness of the solution (*Peiró and Sherwin*, 2005). The advantage of finite elements over finite difference is that the size of the elements can vary over space and time, so that locations where changes occur more rapidly are represented by a smaller grid. This results in a minimisation of the errors in the approximation (*De Cogan and De Cogan*, 1997; *Wainwright*, 2004). In addition, irregular boundaries or problems in which the medium is heterogeneous or anisotropic can be implemented. Moreover, the flexibility of finite elements is useful for coupled problems or solving moving boundary problems (*Wang and Anderson*, 1982). Another advantage of the finite element method over the finite difference method is that the boundary conditions are directly included in the formulation in the finite element approach, and it is not necessary to approximate gradients at the boundary. On the other hand, finite element calculation requires more computer memory and power than the finite difference approach (*Wainwright*, 2004).

Finite volume method (FVM) combines the advantages of an integral formulation with the simplicity of finite difference gradients. Like for FEM, FVM enables complex geometries and multi-dimensional problems, as the integral formulation does not rely in any special mesh structure. In addition, FVM approach is flux-conserving, similar to the FDM (*Narasimhan and Witherspoon*, 1976; *Peiró and Sherwin*, 2005).

The software used in this thesis, FlexPDE, is a scripted finite element model builder and numerical solver. FlexPDE has a built in mesh generator for building finite element meshes, a finite element solver to find solutions, and a graphic system to plot results (*PDE Solutions*, 2006).

2.6 Model design

2.6.1 Conceptualisation of the real world

Numerical modelling provides a useful tool to quantitatively understand how an a system behaves under different constraints. A model can be used to explain observations, reconstruct past or predict futures scenarios to input

parameters and boundary constraints. By comparing model results to observations, missing processes can be identified. Where field observations are absent, the sensitivity of different input parameters can be found that drive a system.

However, it is important to notice that a model in environmental science is an abstraction and simplification of the real world. Some processes may be neglected, the geometry simplified, the material properties homogenised, and the forcing factors simplified.

2.6.2 Initial conditions and boundary conditions

Initial and boundary conditions of a model define the extent of the model domain. The boundary conditions represent processes or values at the border of the spatial domain of the model. The initial conditions represent values of the model domain at $t=t_0$ (*Allen et al.*, 1988; *Wainwright*, 2004). Model results are usually very sensitive to the choice of the initial and boundary conditions and are discussed in this section.

2.6.2.1 Initial condition

The initial conditions specify a solution to the problem domain at $t=t_0$. Commonly, a steady state problem is assumed for the initial condition (e.g. *McKenzie et al.*, 2007; *Bense et al.*, 2009). For systems with a long response time, the initial conditions should be calculated early enough in order for any relevant past changes to be included in the model. For example, the hydrogeology of a previously glaciated area may still be influenced by past conditions, and therefore setting the initial conditions to present day in order to model future responses may neglect past glacial influences. In addition, *Bense et al.* (2012) use an initial condition of an intra-permafrost talik, for which a transient model has been used.

2.6.2.2 Boundary conditions

The choice of boundary conditions of any model is crucial and determines what happens at the edge of the model domain and how they change over time (*Wainwright*, 2004). At the boundary, either a value to the solution can be specified, also known as Dirichlet boundary condition, or the normal derivative of the equation, the Neumann boundary condition can be given.

The Dirichlet boundary condition specifies a value at the boundary; for heat flow this can be the ground surface temperature at the top boundary,

or for Darcy flow the hydraulic head distribution over the model domain. The value specified at the boundary can be a function of length along the boundary and time.

The Neumann boundary specifies a flux into or out from the model domain. Considering a Laplace equation:

$$\nabla \cdot \nabla u = 0 \tag{2.21}$$

here for two dimensions, the Divergence Theorem states that the flux outward of a vector field is equal to the volume integral of the equation (*Kreyszig et al.*, 2011) as follows:

$$\iint_A \nabla \cdot \nabla(u) \mathrm{d}A = \oint_S \mathbf{n} \cdot \nabla u \mathrm{d}S \tag{2.22}$$

where u is a variable, A the area of the domain, S the surface, and $\mathbf{n}$ the normal vector. $\mathbf{n} \cdot \nabla u$ is the gradient at the boundary and describes the Neumann boundary condition (*PDE Solutions*, 2006).

A flux boundary can either be equal to zero, when no fluxes enters or leaves the system, be a set value over the entire side, as for example a heat flux defined at the base of the model, or be defined with an equation, as for example regions with high groundwater discharge whose temperature is defined by the component of advective heat flow normal to the surface.

How the initial and boundaries are implemented for each model scenario, will be discussed in each chapter separately.

2.6.3 Model geometry

The implementation of the model can be done in different coordinate systems: 1D, 2D Cartesian, 2D radial, and 3D. Each of the geometries have their advantages and disadvantages for modelling different systems.

In this section, the model geometries for a lake, surrounded by bedrock is evaluated. In order to model the real world lake geometry, the lake geometry is measured and its coordinates imported into a 3D geometry. When conceptualised and simplified, the lake geometry could be simplified to a circular or elliptical lake geometry and modelled in 3D. However, in FlexPDE, using coupled heat and fluid flow including phase change in 3D is computationally very expensive. Therefore, the model has to be implemented into 2D geometry. Here the choice is either with cylindrical coordinates or 2D Cartesian coordinates. Cylindrical coordinates would be ideal to model a circular

Type	a:b [m/m]
3D circular	50:50
3D elliptical	50:100
3D elliptical	50:150
3D elliptical	50:200
3D rectangular	50:250
2D cartesian	50
2D radial	50

Table 2.1: Definition of lake geometries compared in Figure 2.3. A lake modelled in 3D is defined by its major axis **a**, and the minor axis **b**. In a 2D model, the lake size is defined by its major axis, the radius.

lake. However, in cylindrical coordinates heat conduction only models can be done, as fluid flow could only flow radially either into or from the lake. Thus, to incorporate a flow from one side to the other side of the model domain, 2D Cartesian coordinates have to be used. However, assigning the thermal boundaries for a lake in 2D is difficult, as 2D models a cross section through the lake and is essentially a river. In 2D Cartesian, the thermal disturbance of a lake is only influenced from the sides of the model and the depth, whereas in 2D cylindrical or 3D, the thermal disturbance is influenced by the x-y plain and the depth. Therefore, the thermal disturbance is larger if modelled in 2D Cartesian than for 2D radial or 3D.

In order to find the relative importance of the lake geometry, different lake geometries modelled in a steady state are compared. Compared geometries are a circular lake, elongated lakes, and square lakes modelled in 3D and 2D radial and 2D Cartesian lake (Table 2.1).

Figure 2.3a compares the talik distributions, where the permafrost boundary is defined as 95% ice saturation ($p_i = \Theta_i/n$), under elliptical lakes with different proportions of major radius a [m] versus minor radius b [m]. For a circular lake modelled in 3D, there is no through talik modelled, whereas for an oval lake with $a/b = 2$ a through talik exists for the set boundary conditions. For a longer major radius, the permafrost boundary becomes shallower, and approaches the one of a river or an infinite long lake.

Figure 2.3b compares a talik under a 2D Cartesian lake and a 3D infinite rectangle, or river and demonstrates a good match. The mesh of the 3D simulation is coarser, resulting in a less smooth permafrost boundary than for the 2D simulation. In addition, Figure 2.3b compares a circular lake modelled in 3D and 2D radial coordinates and shows that the 2D talik is deeper than the 3D talik. This is possibly due to numerical instability and the coarser mesh of the 3D model.

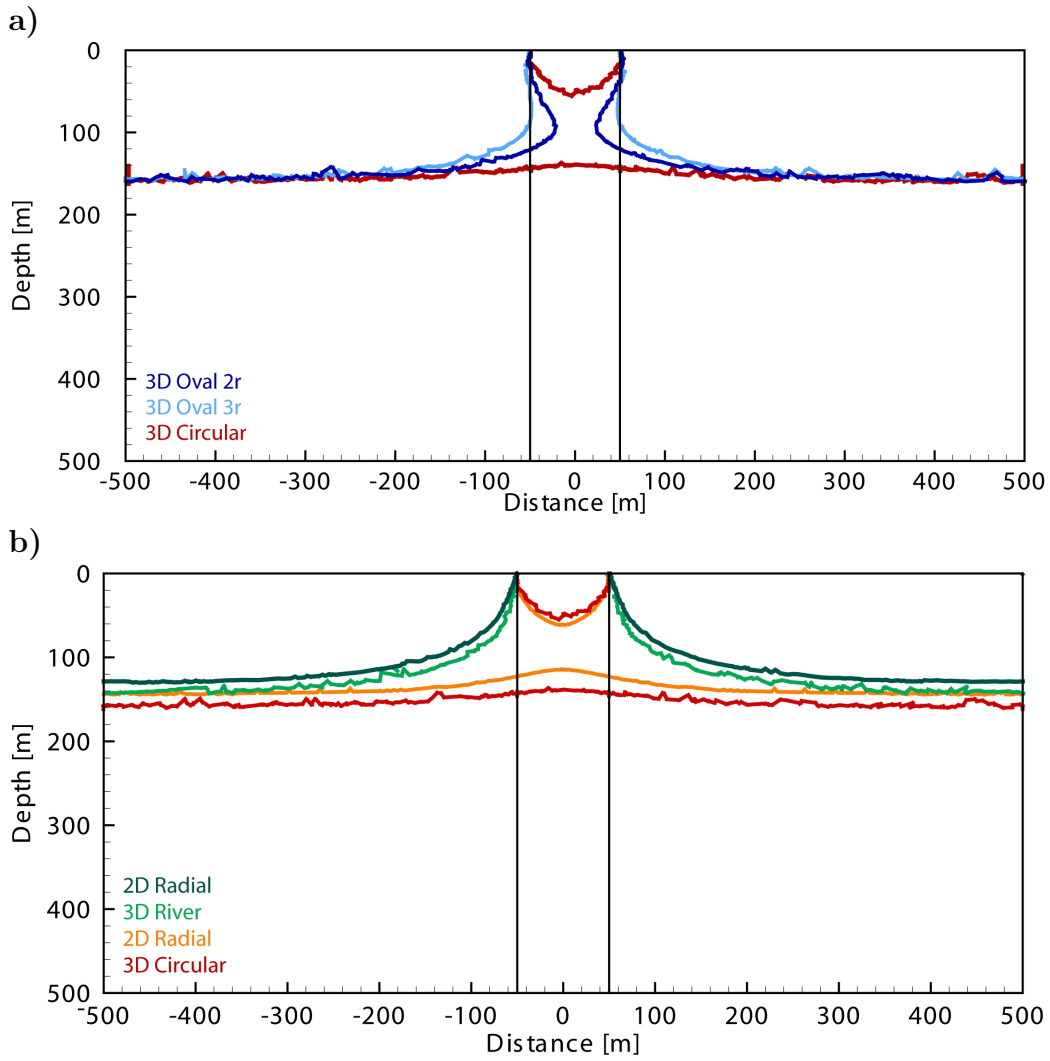

Figure 2.3: a) Comparison of permafrost geometry under lakes with different elongation. b) Comparison of permafrost geometry under lakes for a 2D and 3D model domain. The permafrost boundary represented is defined as 95% ice saturation.

2.7 Code validation

Model validation of coupled heat and fluid flow including phase change with an analytic function is impossible, as there is no analytic function describing temperatures including phase change and advective heat flow.

One option is intercomparison of different models modelling the same model, or benchmarking. However, comparison of model results is an assessment of model consistency rather than an evaluation of model accuracy (*Konikow et al.*, 1997). The HYDROCOIN benchmark has found that the accuracy of a solution depends much more strongly on the proper conceptualisation of the problem and the scale of discretisation than it does on which appropriate code is used.

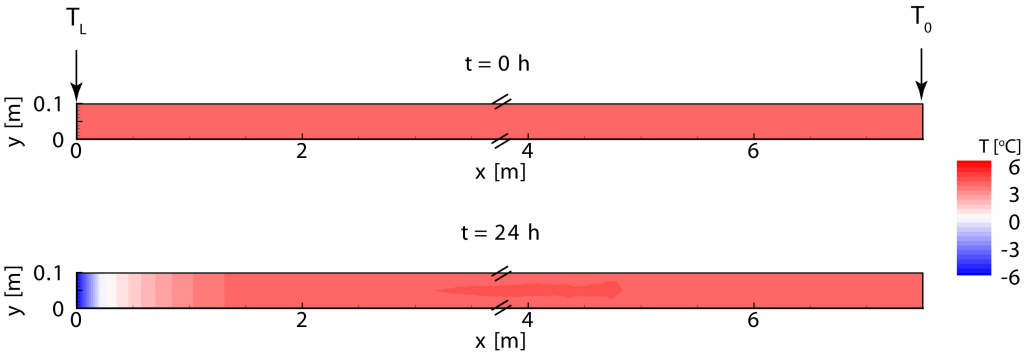

Figure 2.4: Model set-up with initial conditions and modelled temperatures after 24 h for a one-dimensional heat flow example that is used for model comparison to the Lunardini Solution.

An intercomparison of models with mass and energy transport with ice formation has been suggested by (*McKenzie et al.*, 2007), however no such comparison has been done yet. This intermodel comparison is difficult to do, as for example the boundaries specified for the comparison are unclear (e.g. Neumann or Dirichlet boundary, definition of hydrostatic pressure of the lake water column when no lake depth is specified, or implementation of a surface boundary layer).

Nevertheless, there is a analytic function for 1D temperature profile including phase change, which is compared to the FlexPDE solution in Section 2.7.1, and has been compared to SUTRA-ICE before by *McKenzie et al.* (2007). In order to compare a 2D temperature profile, the FlexPDE solution is compared to a temperature under a circular lake, that is surrounded by permafrost (Section 2.7.2), however this analytic solution does not take into account a variation in thermal properties for the frozen, partially frozen or unfrozen state.

2.7.1 Comparison of FlexPDE with an exact 1D analytical solution after Lunardini

In this section, the FlexPDE model is compared with the tree-zone analytic solution by *Lunardini* (1985). This comparison has been previously done for the SUTRA-ICE code by *McKenzie et al.* (2007); and here the same approach and parameters are used for this comparison. The domain is divided into a fully frozen zone ($T1$), a mushy zone ($T2$) with both ice and water, and a fully thawed zone ($T3$). The solution simulates the movement of a freezing zone for an initially unfrozen medium over time t. The Lunardini solution

Parameter	Symbol	Value	Units
initial temperature	T_0	4	°C
temperature at surface	T_s	-6	°C
temperature of liquidus	T_f	0	°C
temperature of solidus	T_m	-1	°C
thermal conductivity frozen zone	κ_1	3.46	W m^{-1} K^{-1}
thermal conductivity mushy zone	κ_2	2.94	W m^{-1} K^{-1}
thermal conductivity thawed zone	κ_3	2.41	W m^{-1} K^{-1}
volumetric heat capacity frozen zone	C_1	690360	J m^{-3} K
volumetric heat capacity mushy zone	C_1	690360	J m^{-3} K
volumetric heat capacity thawed zone	C_1	690360	J m^{-3} K
kg water / kg solid frozen conditions	ξ_f	0.0782	-
kg water / kg solid thawed conditions	ξ_0	0.2	-
volumetric latent heat of fusion	L_f	334720	J kg^{-1}
dry unit density of solid	γ_d	1680	kg m^{-3}
parameter	γ	1.395	-
parameter	ψ	0.1375	-

Table 2.2: Parameters used for the Lunardini analytical solution, after *McKenzie et al.* (2007)

for temperatures $T1 - T3$ over x is:

$$T1 = (T_m - T_s)\frac{erf(x/2\sqrt{\alpha_1 t})}{erf(\psi)} + T_s \tag{2.23}$$

$$T2 = (T_m - T_f)\frac{erf(x/2\sqrt{\alpha_4 t - erf(\gamma)}}{erf(\gamma) - erf(\psi\sqrt{\alpha_1/\alpha_4})} + T_f \tag{2.24}$$

$$T3 = (T_0 - T_f)\frac{-erfc(x/2\sqrt{\alpha_3 t})}{erfc(\gamma\sqrt{\alpha_4/\alpha_3})} + T_0 \tag{2.25}$$

where T_0 is the temperature of the initial conditions, T_m the temperature of the solidus, T_f the temperature of the liquidus and T_s the temperature of the boundary; α_1 and α_3 are the thermal diffusivity for the zones 1 and 3 and are defined as κ_1/C_1 and κ_3/C_3, where C_1 and C_3 are the volumetric bulk-heat capacities of the frozen and thawed zones and κ_1 and κ_3 are the bulk thermal conductivities for the frozen and unfrozen zones.

The thermal diffusivity α_4 is regarded as constant over the mushy zone and is defined as:

$$\alpha_4 = \frac{k_2}{C_2 + \frac{\gamma_d L_f \Delta\xi}{F_f - T_m}} \tag{2.26}$$

where $\gamma_d = (1 - \epsilon)\rho_s$ is the dry unit density of soil solids, and $\Delta\xi = \xi_0 - \xi_f$ where ξ_0 and ξ_f are the ratio of unfrozen water to soil solid mass for the fully thawed and frozen conditions.

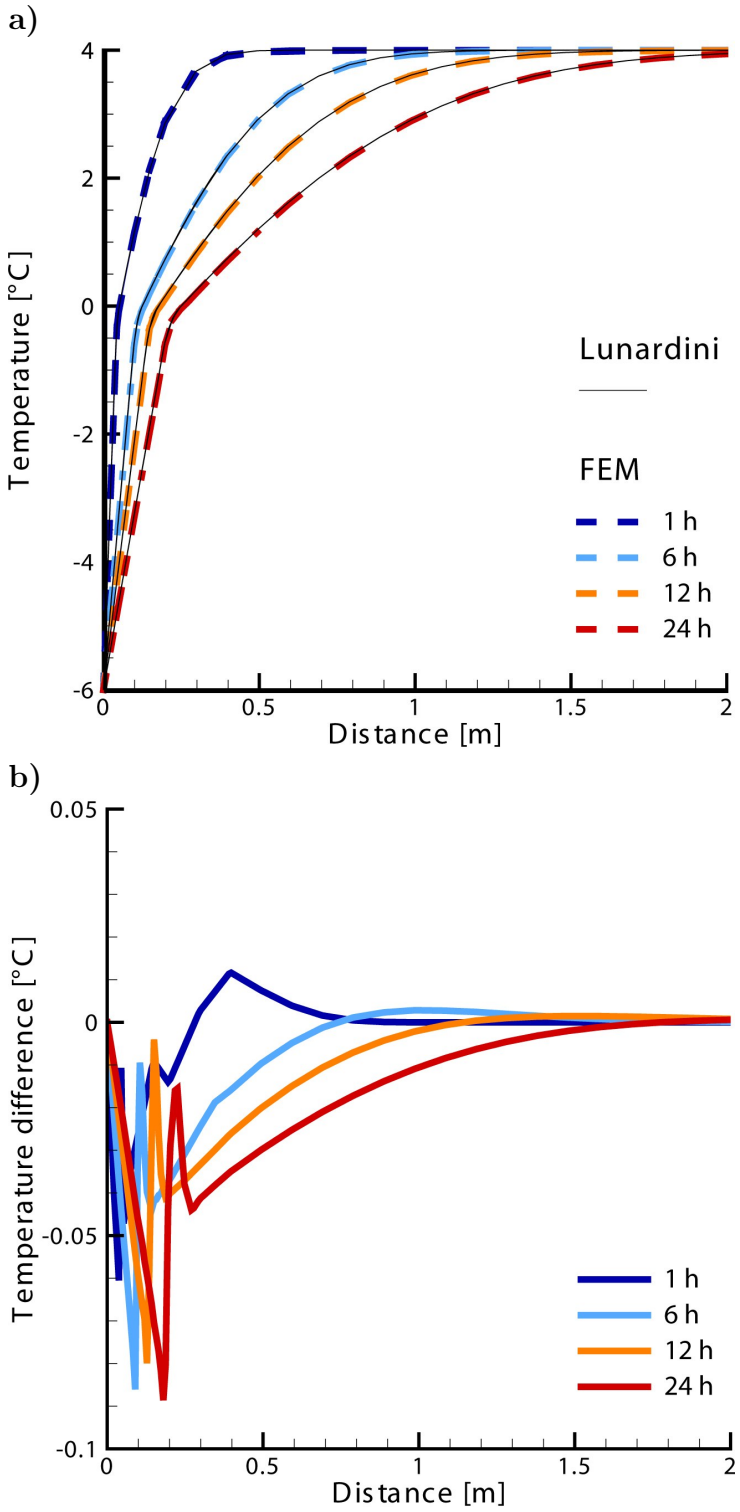

Figure 2.5: a) Comparison of modelled temperatures of the analytic Lunardini Solution with the numeric solution from FlexPDE for four time steps. b) Temperature difference between the analytic and numeric solution for the same time steps as in a).

T_1 is valid for a time t in the region from $0 \leq x \leq X_1(t)$ where $X_1(t) = 2\psi\sqrt{\alpha_1 t}$; T_2 is valid from $X_1(t) \leq x \leq X(t)$, where $X(t) = 2\gamma\sqrt{\alpha_4 t}$, and for $x \geq X(t)$, T_3 is valid.

The parameters γ and ψ are found iteratively. For description in more detail and derivation of specific parameters, see *McKenzie et al.* (2007).

Initially, the temperature of the model domain (Figure 2.4) is $T_0 = 4°C$ and the temperature of the left boundary (T_L) at x=0 is then cooled from T_0 to T_s = -6°C over 50 s. The temperature response of the model domain is calculated with both the analytical and the numerical solution. There is a very good match between the numeric solution and the analytic solution by Lunardini (Figure 2.5). The temperature difference is largest at the left boundary, but the maximum error is less than 0.1°C. Overall, for a 1D heat conduction model including phase change, FlexPDE provides an excellent solution.

2.7.2 Comparison of FlexPDE with analytical solution of a temperature profile under a circular lake

In order to validate the model for a 2D heat conduction including phase change model, the following section compares ground temperatures under a circular lake derived from an analytical solution after *Mackay* (1962) and *Burn* (2002) with FlexPDE. The analytical model for ground temperatures with depth (T_z) is:

$$T_z = T_g + \frac{z}{I} + (T_p - T_g)\left(1 - \frac{z}{\sqrt{z^2 + R^2}}\right) \tag{2.27}$$

where T_g and T_p are the mean annual ground surface temperature (MAGST) and mean annual lake bottom temperature (MALBT), z the depth, I the geothermal gradient and R the lake radius.

The model set-up is described with the temperature at the lake location at 4°C and elsewhere set to -6°C, a geothermal heat flux at the base of the model domain of 75 [mWm^{-2}], and no flow boundaries at the sides (Figure 2.6). Figure 2.7 compares the temperature under a circular lake for the analytical function and the numeric function with FlexPDE.

Figure 2.7 a presents a comparison between the solution from FlexPDE, including the effect of latent heat and change of thermal conductivity depending on the ice / water / ice-water mixture. The difference with the analytical solution is especially large around the freezing point, where there is a maximum difference of 1.3°C. This large difference is caused because the

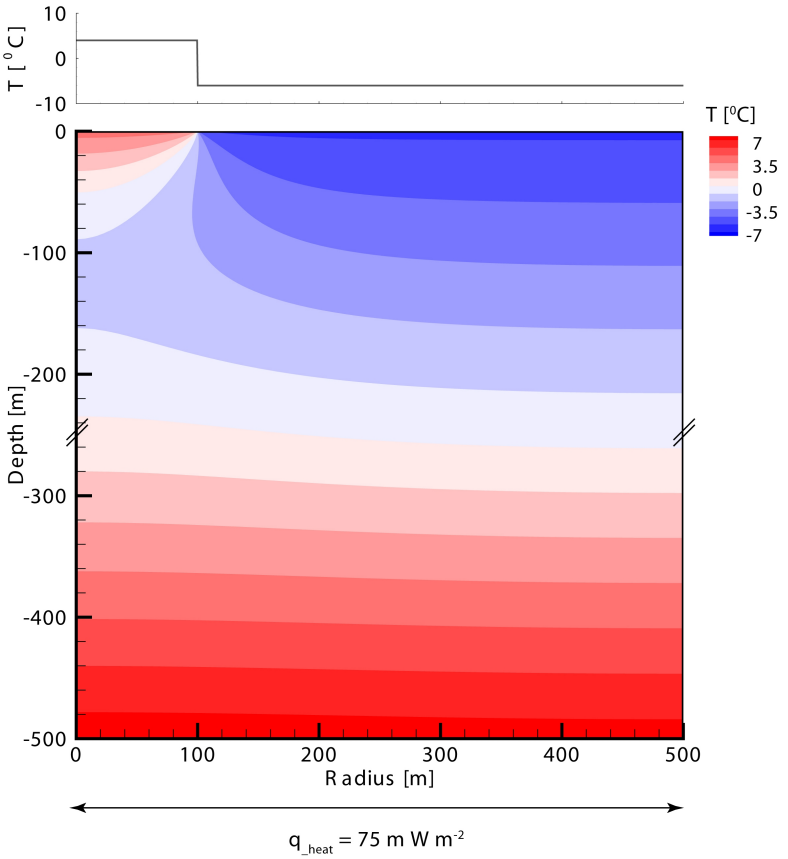

Figure 2.6: Model set-up and temperature distribution for a circular lake with lake bottom temperature of 4°C and ground surface temperature of -6°C.

analytical solution does not take into account any effects of latent heat or change in thermal conductivity with ice saturation.

When the variability in thermal conductivity is removed of frozen, unfrozen or partially frozen substrate from the FlexPDE code, a good match can be obtained (0.05°C) (Figure 2.7 b). However, the local geothermal gradient I varies depending on the distance from the lake. When geothermal gradient is taken 500 m from the lake centre for a 100 m lake, then the analytic model fits the FlexPDE model best. As the analytic solution from *Mackay* (1962) does not take account of variation in geothermal gradient depending on permafrost thickness or a changing thermal conductivity for ice / water / ice-water mixture, a direct comparison to the model used in this thesis is not possible. However, for a simplified case with no variation in thermal conductivity the numeric solution can be fitted to the analytic model.

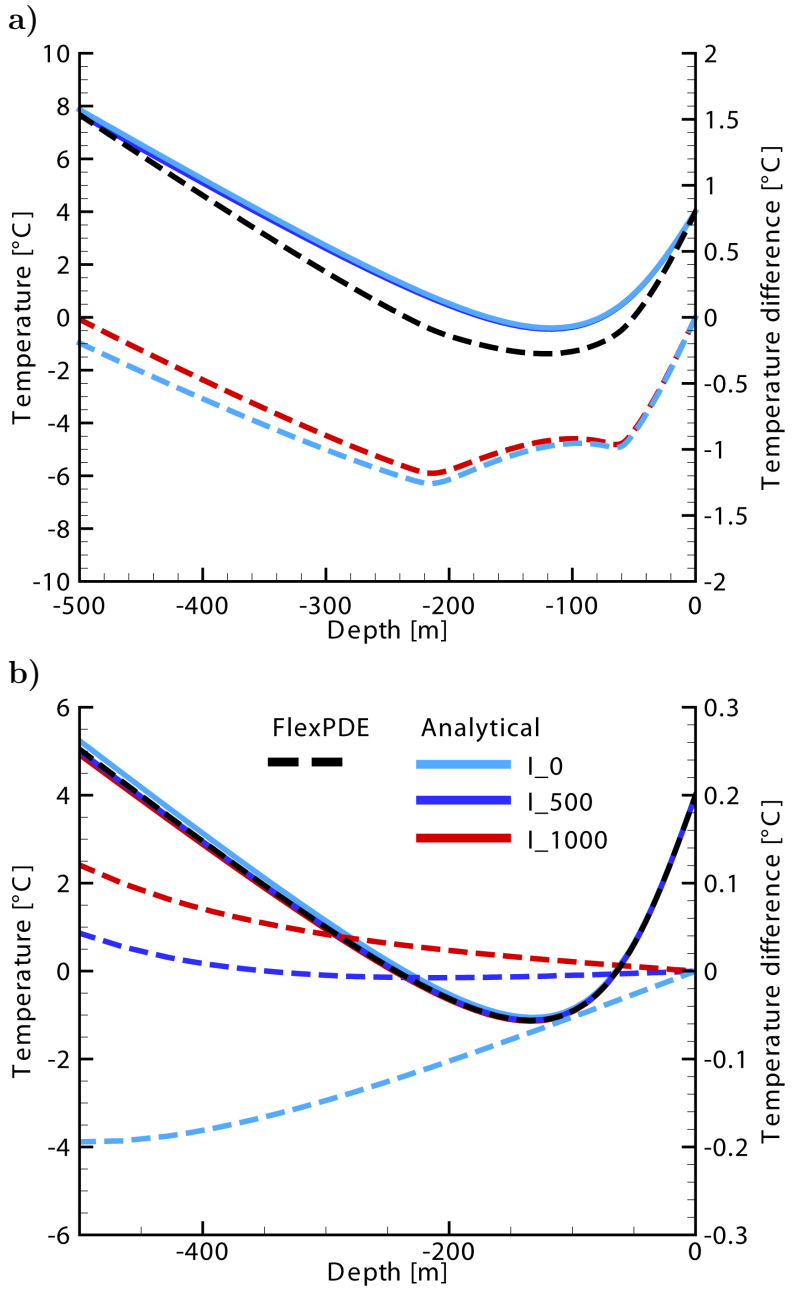

Figure 2.7: Comparison of the results for the ground temperatures under a circular lake derived from an analytical solution after *Mackay* (1962) with that of FlexPDE. The solid coloured lines represent the analytical model, whereas the coloured dashed lines represent the temperature difference between the analytical model and the numerical model. a) FlexPDE includes latent heat of fusion and varies the thermal conductivity depending on the proportion of frozen and unfrozen state. b) FlexPDE does not take into account the variability in thermal conductivity for frozen and unfrozen state.

2.8 Scaling issues

For models whose length and thickness differ by several orders of magnitudes, coordinate scaling makes the code more stable and increases the number of nodes in the shorter dimension. This is applied in Chapter 6, where a model domain of 400 km x 1 km is used.

A scaling factor s is multiplied with the physical coordinate w, resulting in the FlexPDE coordinate z.

$$z = s \cdot w \tag{2.28}$$

An equation gets scaled as follows:

$$\mathrm{dw}(f) = s \cdot \mathrm{dz}(f) \tag{2.29}$$

$$\frac{\partial f}{\partial w} = s \cdot \frac{\partial f}{\partial z} \tag{2.30}$$

and for steady state heat flow as implemented in FlexPDE this is as follows:

$$s\frac{\partial}{\partial z} s\kappa_a \frac{\partial T}{\partial z} + \frac{\partial}{\partial y}\kappa_a \frac{\partial T}{\partial y} = 0 \tag{2.31}$$

FlexPDE assumes continuity of the surface integrals generated by integration by parts of the second-order terms. The z-directed flux terms in the transformed equation therefore assume that $s^2 \cdot \kappa_a \partial T/\partial z$ is continuous across cell interfaces. This is equivalent to flux conservation in the physical system as long as s is constant throughout the domain.

As continuity over surface integrals generated through scaling, the fluxes must be unscaled. Fluxes in the scaled direction must be multiplied by the scale factor, but when they are integrated over a surface, they do not need to be modified. Fluxes in the unscaled direction however are correctly computed in true coordinates, but they must be divided by the scale factor for surface integrals. For the natural boundary conditions, components in the unscaled direction have to be divided by the scaling factor. In the scaled direction however, the components are unmodified. The scaling example is a domain of 2000 m by 200 m which is scaled in x dimension by a scaling factor of 0.1. Initially, the model domain has a ground surface temperature of 1°C with a lake in the middle of the model domain with a lake surface temperature of 4°C. Over one year, the ground surface temperatures decrease to -5°C. Hydraulic head is left constant over time and groundwater flow is forced to discharge into the lake. The initial conditions are characterised in Figure 2.8.

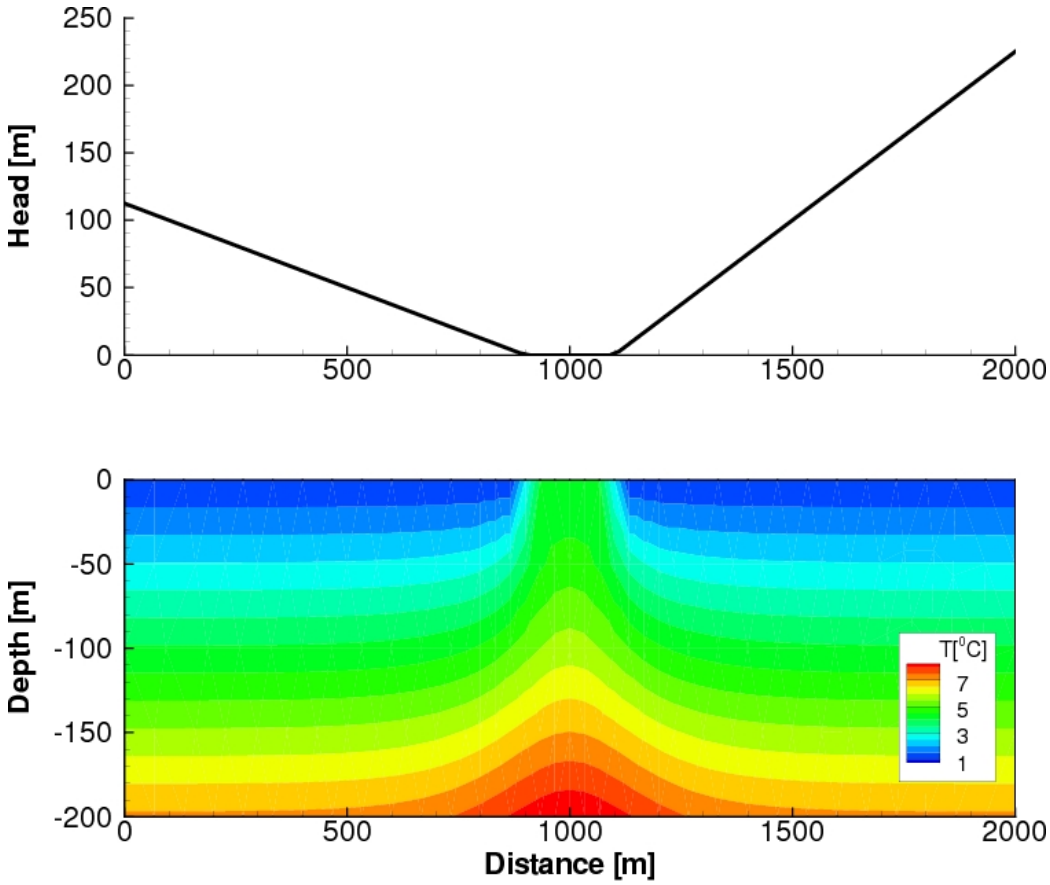

Figure 2.8: Initial conditions for hydraulic head at the top boundary and the temperature distribution for a model scaling example.

Model output for a scaled and unscaled model are compared after 1000 years of simulation time (Figure 2.9). Hydraulic head compares well between the scaled and unscaled model (Figure 2.9a), with a maximum difference of around 1 m compared to a range of 225 m. The temperature distribution next to the lake (250,-150) is well represented with a temperature difference of 0°C between the scaled and the unscaled model, however under the lake centre at (1000, -150), there is a temperature difference of 0.48°C. This difference may result from the error at the top boundary and propagate to the bottom of the model. The maximum difference of the flow velocity is around the permafrost permafrost border in the order of 10^{-10} m s^{-1}. The permafrost extent in is well represented in Figure (2.9d).

It is impossible to evaluate the error of the scaled model, as the 'true' solution is unknown. However, generally, the scaled and the unscaled model compare well and no difference in permafrost extent is apparent.

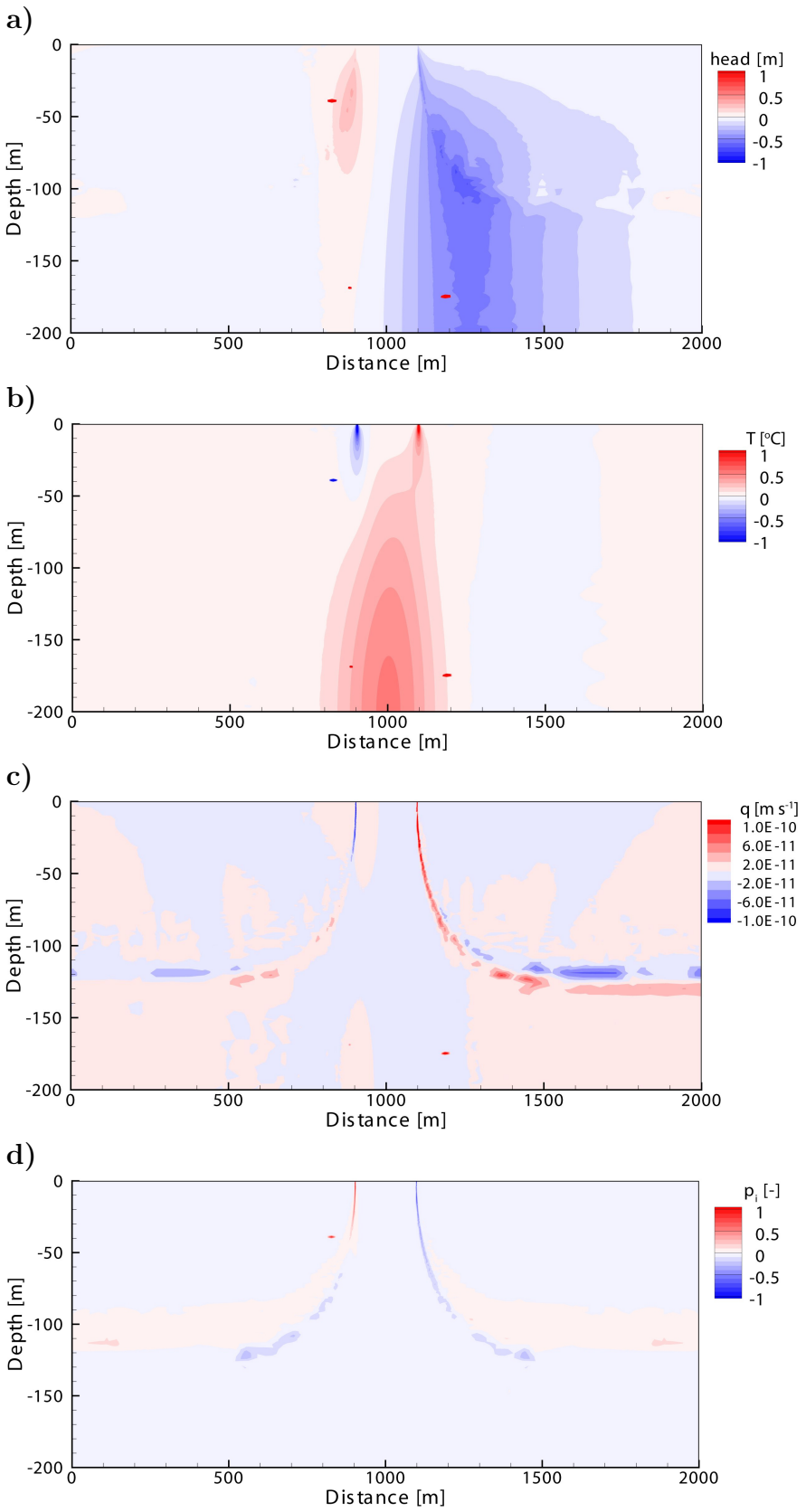

Figure 2.9: Difference of scaled and unscaled model for 1000 years of simulation time for a) hydraulic head, b) temperature, c) flow magnitude, and d) ice saturation.

2.9 Summary of Chapter 2

In this chapter the theoretical framework for heat and fluid flow are given, and it is shown how latent heat flow can be added and the equations can be coupled in order to model groundwater flow in permafrost covered areas. Finite element modelling with FlexPDE is presented. Theoretical thoughts about model set-up, the choice of initial conditions and boundary conditions are given. Then model validation with analytical solutions and their constraints are given.

This model is applied in Chapters 4-6, with specific modifications described in each Chapter.

Chapter 3

Evaluating lake bottom temperatures in permafrost terrain [1]

Abstract

The thermal regime below lakes in permafrost terrain exerts an important control on the hydrogeology. Through-taliks underneath lakes can form a rare pathway for hydrological exchange between surface water and sub-permafrost groundwater. In numerical hydrogeological models of lake-talik systems, a critical boundary condition is the temperature at the lake bed for which earlier studies have often used arbitrary values. In this chapter, a process-based numerical model evaluation is presented, considering different lake sizes and ground surface temperature regimes to estimate lake-bottom temperature regimes for lakes that seasonally freeze-over and are fully mixed in the open season. The thermal regime in the lake is considered to be dominated by heat-conduction (winter) and mixing (summer). We conclude that lakes with a radius $\geq$20 m and for a mean annual ground surface temperature $\geq$-10°C should have average temperatures above freezing at their bed. Hence, only such lakes have the potential to form taliks underneath their bed.

[1] This chapter under review in Geophysical Research Letters. The chapter is a modified version of the paper in which the model description as been deleted here to avoid repetition from Chapter 2, and the results and discussion sections are rewritten in part. JMS was responsible for the majority of the work under supervision of Victor Bense, who provided scientific input and helped revise the manuscript for publication.

3.1 Introduction

In permafrost terrain, mean annual ground surface temperatures are below freezing. However, locally unfrozen zones (taliks) within the permafrost can occur underneath surface water bodies, where the lake bottom temperature differs profoundly from the surrounding ground surface temperatures. Ground underneath lakes is subject to the greatest difference from climatic driven ground temperature regime (*Lachenbruch et al.*, 1982), and is warmer than the surrounding permafrost, because lake bottom temperatures do not fall below 0°C in winter, unless the water body freezes through (*Burn*, 2002). This thermal disturbance results in the formation of a talik underneath the lake. The depth of this talik, and whether it penetrates to the permafrost base and forms a through talik, depends on the climatic conditions, the size of the lake, the lake bottom temperature, and the thermal properties of the underlying material. Taliks that penetrate the entire thickness of low-permeability permafrost can form hydraulic pathways between sub-permafrost aquifers and surface water systems. Hence, the possible occurrence of through-taliks is of primary importance when the potential for groundwater flow in permafrost terrain is evaluated (e.g. *Rowland et al.*, 2011; *Bense et al.*, 2012; *Grenier et al.*, 2013; *Wellman et al.*, 2013).

Groundwater-surface water interaction in permafrost areas is likely to have intensified over the past decades under the influence of permafrost degradation (*Bense et al.*, 2009). Indirect evidence for this comes from river discharge records that suggest an increase of groundwater discharge to provide river baseflow during winter months (e.g. *Walvoord and Striegl*, 2007; *Brabets and Walvoord*, 2009; *Brutsaert and Hiyama*, 2012). Observed dynamics of lake size have been more difficult to assess for the role of increased groundwater inputs (*Yoshikawa and Hinzman*, 2003; *Smith et al.*, 2005; *Wang et al.*, 2012). Changes in lake size and number can be caused by changes in the surface-water balance, or by hydrological changes potentially related to permafrost dynamics. An example of the latter system is the thaw-lake cycle which starts with the ponding of water below which a talik forms leading to ground subsidence (thermokarst). Subsequently, water from the lake might drain over the surface or via a subsurface supra-permafrost pathway (*Yoshikawa and Hinzman*, 2003; *Wang et al.*, 2012; *Wellman et al.*, 2013).

The potential of groundwater-surface water interaction via through-taliks is further illustrated by geophysical imaging of permafrost thickness, for example, as reported by *Minsley et al.* (2012) for the Yukon Basin. The latter

study clearly shows the occurrence of through taliks underneath river and lakes. However, the relative importance of lake size, lake depth, groundwater flow and geothermal heat flow on the potential for occurrence of through-taliks underneath lakes remains uncertain. The study of the hydrogeological relevance of thaw lakes has a pan-Arctic relevance as thaw lakes occur across vast areas such as the Alaskan Coastal Plain, along the Arctic coast of Canada, in Siberia, and on the Qinghai-Tibet Plateau (e.g. *Frohn et al.*, 2005; *Plug and West*, 2009; *Marsh et al.*, 2009; *Ling et al.*, 2012; *Wellman et al.*, 2013).

Where direct field evidence of talik occurrence and geometry is absent, numerical modelling of the relevant heat-flow processes can be used to evaluate the potential for the occurrence of through taliks in a given area. Previous studies have considered heat-flow by conduction only (*Ling*, 2003; *Ling and Zhang*, 2004; *Ling et al.*, 2012), or also include the impacts of heat-advection by groundwater flow (e.g. *Bense et al.*, 2009; *Rowland et al.*, 2011; *Bense et al.*, 2012; *McKenzie and Voss*, 2013; *Wellman et al.*, 2013; *Grenier et al.*, 2013). When heat-conduction is considered, surface temperature, geothermal heat flux and thermal properties of the subsurface are the main parameter controlling subsurface temperature distribution. Surface temperature displays strong spatiotemporal variability both as result of annual seasonality and longer-term climatic changes, but also due to slope, aspect, vegetation patterning, snow cover and the occurrence of surface water such as rivers and lakes (*Jorgenson et al.*, 2010). The mean annual lake bottom temperature will be a primary control on the existence of a talik underneath a lake. However, in numerical models of talik lakes, the temperature at the lake bottom is often arbitrarily assigned as a temperature several degrees above freezing to allow for a talik to form underneath the lake (*Rowland et al.*, 2011; *Bense et al.*, 2012; *Grenier et al.*, 2013; *Wellman et al.*, 2013). The aim of this chapter is to provide a more accurate and robust way to assess lake bottom temperatures for inclusion in heat-flow models simulating talik lakes.

The relatively high mean annual lake bottom temperature has been attributed to a convective heat exchange and absorption of heat by radiation through the water column (*Harris*, 2002). Field data (e.g. *Burn*, 2002, 2005) show that when the lake is unfrozen, the temperature in the lake is homogenized by turbulence driven by wind shear at the lake surface, but that after the formation of an ice layer across the lake surface, the temperature distribution within the now still water column is dominated by heat conduction. This change from strongly forced wind driven mixing in summer to

conduction through snow and ice and weak convection in winter has been stated to be the most important factor for estimating the thermal influence of lakes on permafrost distribution (*Riseborough*, 2006). In addition, storage of accumulated summer heat beneath the lake snow cover and asymmetry of lake-ice freezing thawing geometry influences the thermal distribution at the lake bottom (*Riseborough*, 2006).

A generic talik-lake heat-conduction model is used to evaluate the seasonal dynamics of lake bottom temperatures. Our model includes the latent heat effects of phase-change of freezing and thawing water/ice in the subsurface and also mimics the heat flow dynamics in the lake water itself. The focus here is on representing relatively shallow lakes of less than 20 m depth in which the thermal regime is dominated by wind driven mixing during the open season, and by heat conduction during the ice covered season. This shift in thermal regime in the lake alternating between heat conduction and heat convection dominated as function of the occurrence of an ice-cover over the lake surface results in a stratified water column during the ice covered season and a completely mixed water column for when there is open water.

First, the model is applied generically to evaluate the sensitivity of lake bottom temperature to surface air temperatures and lake depth, and using surface air temperature directly as being equivalent to ground surface temperature. These generic models show that once a lake exceeds a critical depth between 2-3 m, the temperatures at the lake base are insensitive to the lake shape and maximum lake depth. Model performance are evaluated by simulating field data of lake bottom temperature dynamics reported in *Burn* (2002, 2005). In the latter model runs the surface air temperature is modified to account for snow cover dynamics.

3.2 Methodology

3.2.1 Lake thermal regime

The lake thermal regime is modelled using the heat-conduction equation including the latent-heat effects of freezing and thawing (Equation 2.11), with the thermal properties altered over the freezing interval as described in Section 2.4.

It is assumed that the lake thermal regime varies as function of surface temperature as follows. When the lake is ice free, thermally homogenized conditions are established by setting the thermal conductivity of the lake water to an artificially high value of κ_{wMix}=1000 W m^{-1} K^{-1}. When surface

Parameter	Symbol	Value	Units
Effective porosity lake	n	1	-
Average matrix porosity sediment	n	0.4	-
Average matrix porosity bedrock	n	0.01	-
Volumetric heat capacity of water	C_w	$4190 \cdot 10^3$	J m^{-3} K^{-1}
Volumetric heat capacity of ice	C_i	$1835 \cdot 10^3$	J m^{-3} K^{-1}
Volumetric heat capacity of sediment	C_r	$2960 \cdot 10^3$	J m^{-3}K^{-1}
Volumetric heat capacity of bedrock	C_r	$2160 \cdot 10^3$	J m^{-3}K^{-1}
Volumetric heat capacity of snow	C_s	$80 \cdot 10^6$	J m^{-3}K^{-1}
Volumetric latent heat of fusion	L_i	$3.03 \cdot 10^8$	J m^{-3}
Thermal conductivity of water	κ_w	0.58	W m^{-1} K^{-1}
Thermal conductivity of ice	κ_i	2.37	W m^{-1} K^{-1}
Thermal conductivity of sediment	κ_r	2.2	W m^{-1} K^{-1}
Thermal conductivity of bedrock	κ_r	2.5	W m^{-1} K^{-1}
Thermal conductivity of snow	κ_s	0.22	W m^{-1} K^{-1}
Heat flow density	q_{heat}	$100 \cdot 10^{-3}$	W m^{-2}
Gravitational acceleration	g	9.81	m s^{-2}

Table 3.1: Thermal properties of modelled bedrock. Sediment occurs in the top 25 m of the model domain.

temperatures are below 0°C, ice is assumed to be forming on the lake surface, halting convection and thermal homogenization. In this case, the thermal conductivity of the unfrozen lake water is equivalent to that of water.

3.2.2 Model scenarios

Two model scenarios (A & B) are considered, applying different model geometries and thermal boundary conditions (Figure 3.1). Models are two-dimensional and radially symmetric. The top 25 m of the model has the thermal and hydraulic properties of fine-grained material such as silt, overlaying bedrock (i.e. granite). This geometry would represent a common situation where till, or lake sediments are overlying bedrock material, such as for example reported in *Minsley et al.* (2012). The temperatures in the model domain are driven by a heat flow density (q_{heat} [W m^{-2}]) at the base of the model and the temperature at the surface, for which we use the same value for land and the lake surface. The sides of the model are no-flow. Thermal properties of all model units are provided in Table 3.1.

For both scenarios seasonal variability is considered. Model simulations are spun up using several seasonal cycles. Running the model for several cycles demonstrates that the lake bottom temperatures show the same temporal pattern after the first year of simulation time.

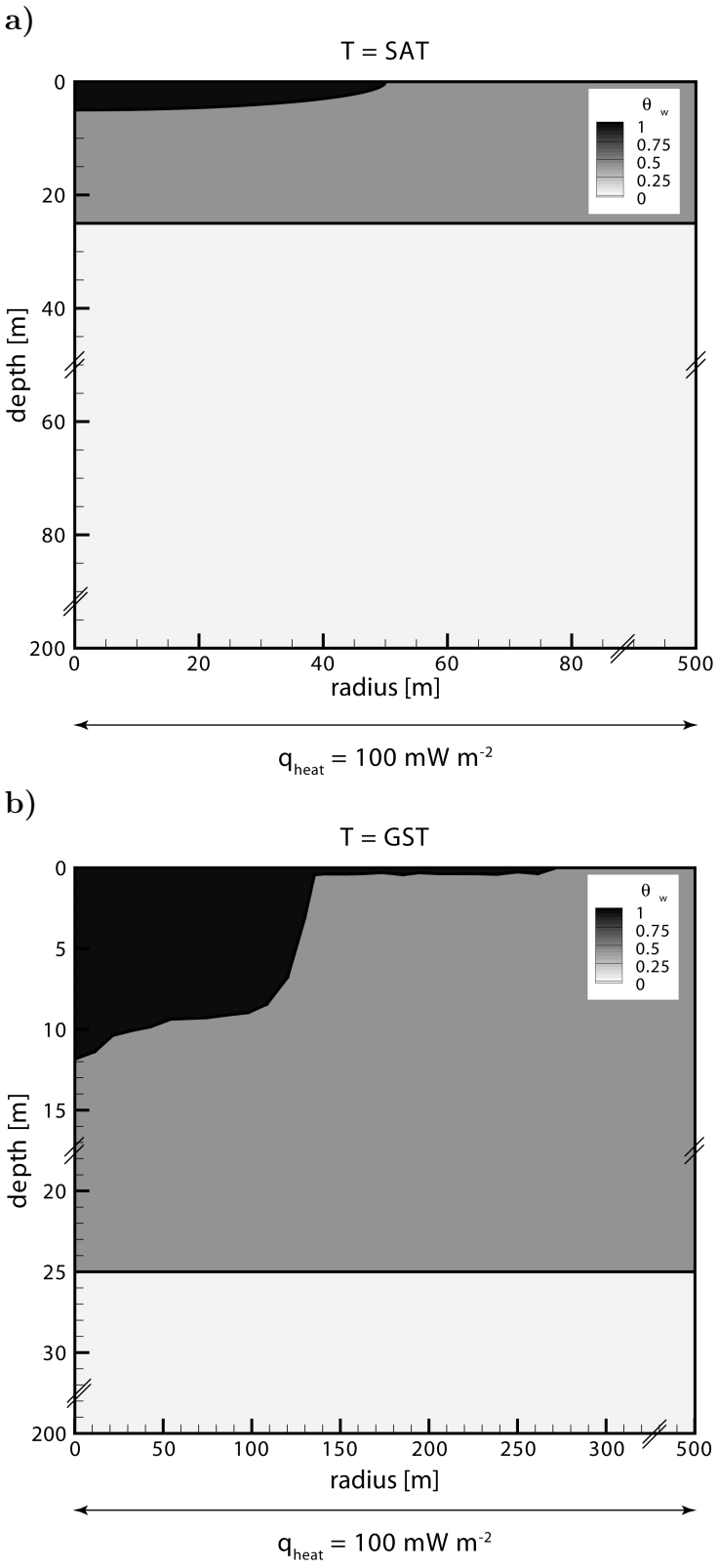

Figure 3.1: Model set-up of lake bottom temperature calculations with water content for different units for a) the generic model scenario A for r = 50 m and b) model scenario B, representing Todd lake. Please note the different scales and the broken axis.

Scenario A: In scenario A, a relatively simple generic model is used for a sensitivity study of lake bottom temperature to lake size and surface air temperature. In this scenario surface air temperature is assumed to be equal to ground surface temperature. The lake shape is circular and a synthetic depth profile ($z(x)$ [m]) is calculated as a function of distance from the shore, x [m], as follows:

$$z(x) = \sqrt{1 - \frac{x}{r_l}} \cdot z_{max} \tag{3.1}$$

where r_l [m] is the lake radius and z_{max} [m] is the maximum lake depth.

In models run for scenario A, a range of lake radii are considered between 15 m and 100 m, with z_{max}=0.1·r_l. Mean annual ground surface temperature is varied between -2°C and -10°C. In this scenario, the seasonal air temperature variation is assumed to follow a sine function with an amplitude of 20°C.

Scenario B: Scenario B is used to test the performance of our approach to simulate lake bottom temperature dynamics as observed in the field using a well-documented case-study (*Burn*, 2002). In scenario B, lake bathymetry is taken from that study, but assuming a circular lake.

Ground surface temperature is calculated from the observed surface air temperature at Todd Lake (*Burn*, 2002) by using the 1D Snow-Permafrost Interaction Soil Model (*Heikenfeld et al.*, 2012; *Westermann et al.*, 2011). Surface air temperature and snow depth at a daily interval are used to calculate an effective ground surface temperature, using heat conduction. SnowPI model parameters (snow duration and thickness, and soil composition) are optimized by imposing SnowPI calculated ground surface temperatures values as a surface boundary condition in the talik model, at a location away from the lake, and visually inspecting the resulting temperature trends at a depth of 1 meter with temperature data measured in the field (from *Burn*, 2002). Snow thermal properties used are shown in Table 3.1.

3.3 Results

Calculated temperatures along the lake bed are extracted from the model grid.

Scenario A: For selected values of mean annual ground surface temperature and lake radius, Figure 3.2a shows the calculated mean annual lake

bottom temperature along the lake bed and mean annual ground surface temperature at the land surface outside of the lake. Our results show that at a lake radius of 15 m, the mean annual lake bottom temperature is still being affected by the proximity of the lake shore, whilst for larger radii this effect progressively disappears. For larger, and therefore deeper lakes, the mean annual lake bottom temperature becomes less sensitive to mean annual ground surface temperature as the range of mean annual lake bottom temperature as function of mean annual ground surface temperature decreases for larger lakes. In general mean annual lake bottom temperature is warmer for increasing lake size, which is less pronounced for relatively high mean annual ground surface temperature (e.g. -2°C) than it is for lower mean annual ground surface temperature (e.g. -10°C).

Model results for scenario A are plotted in relation to lake depth in Figure 3.2b. This clearly illustrates that where any depth in any lake is larger than ∼2.5 m, temperatures at the bed are primarily controlled by mean annual ground surface temperature with only a very small sensitivity to further increases in depth. This is due to the insulating property of pure water in the lake with a relatively low thermal conductivity as compared to the substratum. Mean annual lake bottom temperature will have to become as low as ∼-15°C for even deep lakes (i.e. ≥10 m) to be on average below freezing at the lake bed.

Figure 3.2c presents the maximum mean annual lake bottom temperature at the lake centre for different ground surface temperature and different lake size scenarios, as obtained by interpolation of individual model results. Modelled mean annual lake bottom temperature tend near-linearly from a radius of ∼20 m and depth of 2 m in an environment with mean annual ground surface temperature -10°C to a radius of ∼5 m and depth of 0.5 m in climates with a mean annual ground surface temperature -2°C. Therefore, only very shallow lakes that are found in cold environments have a mean annual lake bottom temperature below freezing.

Scenario B: The site-specific model effort represented by scenario B is making use of published data (*Burn*, 2002), which reports on a field study carried out near Todd Lake, Richards Island, western Arctic coast, Canada. At Todd Lake, mean annual air temperature is -11.8°C with an annual range of 56°C. The mean annual ground surface temperature at 1 m depth is -6.4°C with a range of 15°C. Permafrost thickness is over 400 m with a geothermal gradient of 0.02-0.025°C m^{-1}. At Todd Lake, when the monthly mean air

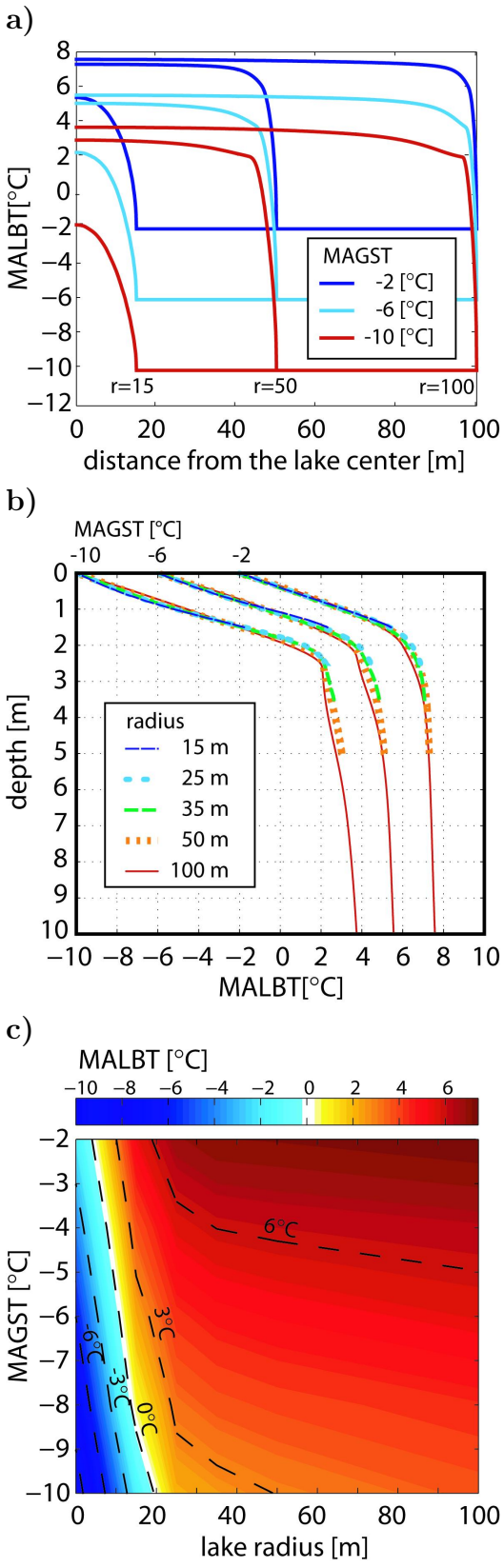

Figure 3.2: Simulated mean annual lake bottom temperature (MALBT) for different lake sizes and mean annual ground surface temperature (MAGST). a) MALBT with distance from the lake centre for lake radii of 15 m, 50 m and 100 m for a MAGST of -2°C to -10°C. b) MALBTs over lake depth for different lake radii and imposed MAGST of -2°C to -10°C. c) Maximum MALBT for different lake radii and imposed MAGST.

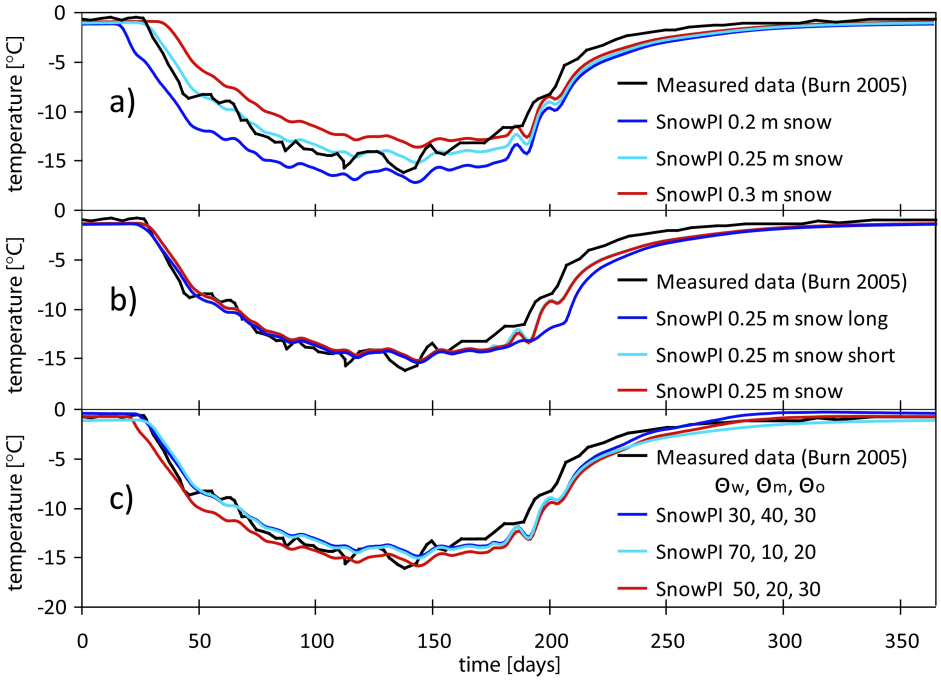

Figure 3.3: Comparison of ground temperatures derived from SnowPI at 1 m depth for a) different snow depths, b) different snow durations, c) different soil properties with measured ground temperatures (*Burn*, 2002). a) Snow thicknesses are 20 cm, 25 cm and 30 cm. b) The snow free season is for reference model from day 122-273, the short snow covered season from day 146-273 and the long snow season from 112-273. c) The soil properties specified in the legend correspond to water content (Θ_w), mineral content (Θ_m) and organic content (Θ_o) [%].

temperatures are below 0°C, the snow depth is estimated as 20 - 30 cm and from October to May. Todd Lake is about 1.6 km long and up to 800 m wide with a single basin and well developed littoral terraces with a water depth of less than 1 m and a width of up to 150 from the shore. The maximum water depth is 16 m (*Burn*, 2002).

Figure 3.3 shows how choices of different parameter values for snow duration, average thickness, and soil parameters affect the agreement between simulated and observed soil temperatures at 1 m depth. The best fit is found with a snow thickness of 0.25 m, a snow free period from day of year 112-273, and a soil composed of 30% water, 40% mineral and 30% organic matter. For this parameter set, the average difference between the observed and the modelled mean annual temperature at 1 m depth is less than 0.1°C. However, clearly snow thickness is the most important parameter by which a fit with the field data can be accomplished within SnowPI (Figure 3.3 a).

The observed temperature data at Todd Lake (solid lines, Figure 3.4a) show how at shallow depth (0.4 m) seasonal temperature fluctuations are strong throughout the season, whilst at 10.6 m depth, winter temperatures

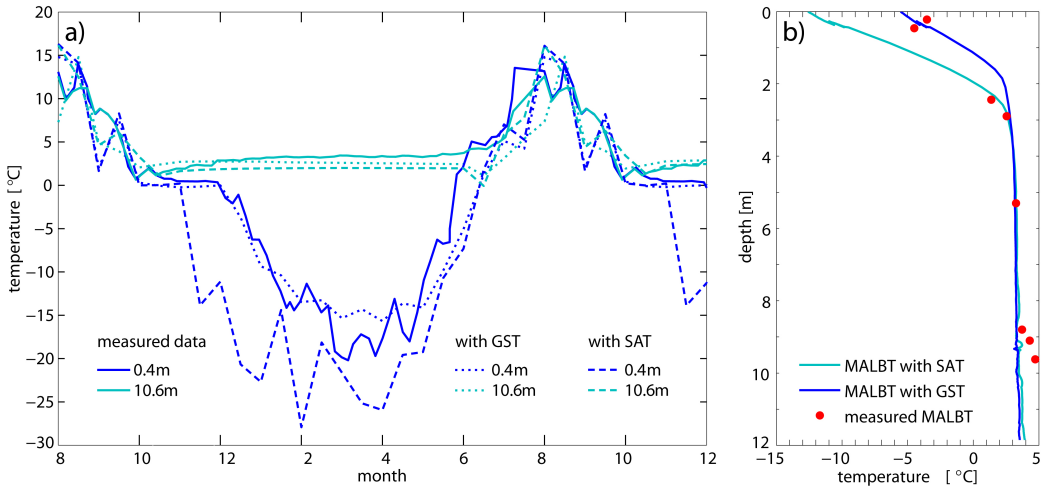

Figure 3.4: Comparison of measured and modelled lake bottom temperatures for Todd Lake (*Burn*, 2002). a) Comparison of the lake bottom temperature at different depths of a seasonal cycle for measured lake bottom temperatures and modelled lake bottom temperature with ground surface temperature (GST) and surface air temperature (SAT) as model input. Two temperature measurements at the same depth at different locations are taken. b) Comparison of modelled and measured mean annual lake bottom temperature (MALBT) with water depth. Ground surface temperature (GST) is the surface air temperature (SAT) corrected for the influence of snow cover.

stabilize to +2-3 °C. The modelled temperature trends for those depths shows analogous patterns. When surface air temperature is used directly without correction for snow cover (as in Scenario A) as the surface temperature boundary condition, the simulated temperatures are too cold when compared to observations. However, when the thermal insulating effects of the presence of snow are included, the match between observed and simulated lake bottom temperature for 0.4 m depth improves significantly. For a depth of 10.6 m, for which data from Todd lake are available, consideration of snow cover does not make an important difference, and the agreement between observed and simulated lake bottom temperature for this depth remains as satisfactory as it was.

Figure 3.4b compares the simulated trends and observed data in terms of mean annual lake bottom temperature for different depth for Todd lake. As observed from the analysis of the seasonal trends, the agreement between modelled and observed lake bottom temperature seems to improve significantly for relatively shallow depths (e.g. $\leq\sim$2 m), while for larger depth the consideration of snow cover effects does not impact the mean annual lake bottom temperature.

3.4 Discussion and Conclusion

In this chapter we aim to provide a process-based estimate of lake bottom temperature dynamics in permafrost terrain if the lake is perfectly mixed under open conditions. A numerical heat flow modelling approach is used that alters between heat-conduction (winter) and heat-convection (summer), and provides a good first order estimate of the lake bottom temperatures as a function of surface temperatures and water depth.

Previously, estimating lake bottom temperatures for a changing climate has been undertaken by *Burn* (2002), by altering the measured lake bottom temperatures with longer open water duration and maximum water temperature. This may be a very good approach for a lake where existing water temperatures are available, however, if they are absent, a more general approach, as presented in this study may be more suitable. Another attempt to model lake bottom temperature with changing climate has been undertaken by *Matell et al.* (2013) by modelling 1D heat conduction through a lake - permafrost system, including subsidence. In contrast to our temperature approach, *Matell et al.* (2013) define the temperature at the lake surface with an energy balance.

Our model simulations of lake bottom thermal regimes in a generic context (scenario A) suggest that the variation of mean annual lake bottom temperature for different ground surface temperature forcing is largest for smaller and shallower lakes, and smaller for larger and deeper lakes (Figure 3.2a). This implies that the temperature regime of smaller lakes is more sensitive to rising ground surface temperature or lake expansion associated with climate change, than that of larger lakes. In addition, results suggest that there is a simple relationship between ground surface temperature and lake bottom temperature as a function of water depth (Figure 3.2b). When the water depth is larger than ∼2.5 m, the temperatures are dominated by ground surface temperature and only increase slightly in temperature with increasing water depth. The depth from which mean annual lake bottom temperature remains above 0°C varies predominantly depending on the ground surface temperature, whereas lake size has a minor influence, and is for the sensitivity study presented here between ∼0.5 m and ∼2 m, depending on ground surface temperature (Figure 3.2b). For this generic description of lakes bathymetry, lakes that have been modelled with a mean annual lake bottom temperature below freezing at their deepest location, tend near-linearly from a radius of ∼20 m in an environment with mean annual ground surface temperature -10°C to a radius of ∼5 m in climates with a

with mean annual ground surface temperature -2°C. Lakes that have a mean annual lake bottom temperature above 0°C might still freeze to the base for some time in winter; however essential for talik evolution is the mean annual lake bottom temperature.

When our modelling approach is focused on a specific field situation (Scenario B), a consideration of the thermal effects of seasonal snow cover on the upper model boundary temperature (Figure 3.3) is improving agreement between observed and simulated temperature dynamics for shallow depth, but does not substantially impact the lake bottom temperature for depths over ∼2.5 m (Figure 3.4b).

In order to estimate the temperature along a lake bed for a specific lake, the model has to be run for each lake geometry. However, neglecting lateral heat flow for locations near the lake shore, the model domain could be simplified to a 1D vertical profile, similar to the approach by *Matell et al.* (2013). Figure 3.2b demonstrates that regardless of the size of the lake, the mean annual lake bottom temperatures for a given depth and surface temperature scenario is very similar. Therefore, the lake shape is of minor importance and the main driving factors found from this modelling determining the mean annual lake bottom temperature is found to be the ground surface temperature and the water depth.

The model presented here is valid for a fully mixed lake and can be used to estimate the mean annual lake bottom temperature for shallow lakes or littoral terrace that freeze to the ground in winter, and intermediate deep lakes where wind driven mixing dominates in the ice free season and which do not freeze to the ground in winter. This model however, does not represent deep lakes where the temperature-density relationship of water controls the thermal regimes. For future work, the model could be expanded to include this relationship.

Ongoing climate change has several implications on the thermal regime of lakes as described in this letter. A rising mean annual ground surface temperature and associated shorter ice covered period will increase the mean annual lake bottom temperature and a larger area of the lake will remain >0°C. However, changes in the duration, thickness and properties of the snow cover will also influence the thermal regime of the lake base. Moreover, the thermal effect of lake dynamics is primarily driven by the local water depth, and thus only a change in water depth, as through thermokarst processes or lake drainage has a considerable influence of the temperature at the lake centre. In contrast, a lake's thermal regime of an expanding or shrinking

lake that is not associated with the lake becoming deeper or shallower will only be influenced near the shore. It is likely however, that a combination of these factors will influence the future thermal regime of a lake.

In principle, this modelling approach can be used to assign surface temperature boundary conditions for hydrogeological models for permafrost terrain that include thaw lakes as potential locations for surface-water groundwater interaction. We doubt that our modelling approach for the lake water thermal regime will be applicable for rivers, since river flow continues underneath the ice after ice forms over the river surface. Hence, temperature dynamics in the unfrozen water column in rivers cannot be properly approximated by assuming heat conduction-only conditions once the ice has formed.

Our modelling efforts provide no answer to the question as to a lake has a through-talik underneath it or not. This will depend on many more parameters than have been considered here. Whether this talik penetrates the entire depth of the permafrost, and how this talik responds to altering surface temperatures and lake bottom temperatures, is subject of the following chapter. Nevertheless, the existence of temperatures at the lake bed of on average (seasonally) above freezing is a first prerequisite for a talik of any dimension or shape to exist which is to a large degree independent of the thermal regime in the substratum. Therefore, the analysis presented in this chapter is an important step to improve the representation of lakes in numerical permafrost hydrogeological models. With the dearth of hydrogeological field data from permafrost areas, numerical models will continue to be a primary mean of improving our understanding of the rapid hydrological changes observed in these part of the Earth system.

Chapter 4

Control of advective heat flow on talik development in a dynamic permafrost landscape [1]

Abstract

The thermal regime under lakes in permafrost terrain is an important control on the hydrogeology, because taliks can form a sub-permafrost surface water connection. Climate warming can potentially open new groundwater-surface water connection through taliks underneath lakes, influencing the hydrology of large areas pan-arctically. In the absence of field data, numerical modelling of coupled heat and fluid flow provide a first order estimate to elucidate potential hydrogeological changes associated with climate change. Here, we aim to estimate the response of the temperature regime underneath a lake with the influence of surface temperature warming, considering different hydraulic scenarios. Simulation results suggest that the thermal regime under lakes takes hundreds to thousand years to respond to surface temperature changes. Advective heat flow can accelerate permafrost degradation. However a comparison of different permafrost-permeability-reduction-functions from the literature demonstrates that the transition from a heat-conduction dominated environment to a heat-advection dominated system can be highly variable, depending on the permafrost-permeability-reduction-function used.

[1] This chapter is in preparation to be submitted to Geophysical Research Letters. The following changes to the paper have been made; the methods section in this Chapter has been deleted in order to avoid repletion with Chapter 2, the result section is expanded and some figures added. JMS was responsible for the majority of the work under supervision of Victor Bense, who provided scientific input and helped revise the manuscript for publication.

4.1 Introduction

Thaw lakes are found pan-arctically and have recently undergone changes, such as lake expansion or shrinkage, or have increased in numbers (*Yoshikawa and Hinzman*, 2003; *Frohn et al.*, 2005; *Smith et al.*, 2005; *Walter et al.*, 2006; *Plug and West*, 2009; *Marsh et al.*, 2009; *Ling et al.*, 2012). Although, it is not always clear whether the observed hydrological changes are part of a natural thermokarst cycle of surface water ponding, subsequent lake formation and eventual lake drainage, or whether such changes are driven by surface temperature increase and/or changes in the pattern of precipitation (*Yoshikawa and Hinzman*, 2003; *Wang et al.*, 2012; *Wellman et al.*, 2013).

Ground underneath lakes in permafrost terrain is usually warmer than the surrounding permafrost, because lake bottom temperatures do not fall below 0°C, unless the water body freezes to the lake bed (*Burn*, 2002). This thermal regime explains the presence of a talik, layer of unfrozen ground in permafrost terrain, underneath a lake. The depth of a talik, whether it penetrates to the permafrost base and forms a through talik, depends on a combination of surface temperature, the size and depth of the lake, the thermal properties of the subsurface, and the magnitude of geothermal heat flow. Moreover, the impact of transient thermal conditions needs to be considered when the potential existence and geometry of taliks is evaluated (*Rowland et al.*, 2011; *Bense et al.*, 2012; *Grenier et al.*, 2013; *Wellman et al.*, 2013). In the absence of field data, numerical models of coupled heat and fluid flow provide a first order estimate of whether a lake can be underlain by a through talik, incorporating the parameters outlined above. In addition, these models can be used to evaluate how permafrost hydrogeological systems may change under the influence of projected climatic changes.

When permafrost, and permafrost evolution are considered in hydrogeological models, permeability is a function of ice-content (θ_i). The temperature range over which the transition occurs between a fully frozen (θ_i=1) and fully thawed (θ_i=0) open pore space, is called the freezing interval. How groundwater flow decreases over the freezing interval will have a profound control on how permafrost and changes in permafrost distribution will impact groundwater flow, and also how advective heat flow influences the permafrost distribution.

Several experimental or theoretical relations describing the change of permeability as function of ice-content or temperature varying over the freezing interval are described in the following literature. Hydraulic conductivity decrease as a function of temperature has been measured by *Burt and Williams*

Parameter	Symbol	Value	Units
Average matrix porosity sediment	n	0.25	-
Average matrix porosity bedrock	n	0.01	-
Hydraulic conductivity sediment	K	10^{-4}	m s^{-1}
Hydraulic conductivity bedrock	K	10^{-6}	m s^{-1}
Volumetric heat capacity of water	C_w	$4220 \cdot 10^3$	J m^{-3} K^{-1}
Volumetric heat capacity of ice	C_i	$1835 \cdot 10^3$	J m^{-3} K^{-1}
Volumetric heat capacity of sediment	C_s	$2960 \cdot 10^3$	J $m^{-3}K^{-1}$
Volumetric heat capacity of bedrock	C_s	$2160 \cdot 10^3$	J $m^{-3}K^{-1}$
Volumetric latent heat of fusion	L_i	$3.03 \cdot 10^8$	J m^{-3}
Heat flow density	q_{heat}	$100 \cdot 10^{-3}$	W m^{-2}
Gravitational acceleration	g	9.81	m s^{-2}

Table 4.1: Hydraulic and thermal properties of modelled bedrock and sediment. Sediment occurs in the top 25 m of the model domain.

(1976) for sand, silt and clay, by *Watanabe and Flury* (2008) for silt and sand, by *Kleinberg and Griffin* (2005) for mud and sand, and by *Azmatch et al.* (2012) for silt under different consolidation pressures. Model descriptions of how the permeability decreases over the freezing interval, commonly assume that an analogue to unsaturated fluid flow can be made, in which the increase in ice content resembles a drying up of pore space (*McKenzie et al.*, 2007; *Kurylyk and Watanabe*, 2013). Alternatively, different theoretical models relating permafrost saturation and permeability (*Kleinberg et al.*, 2003; *Kleinberg and Griffin*, 2005), or temperature and permeability (*Watanabe and Flury*, 2008) for capillary tube models and grain pack models have been compared to experimental data.

In this chapter, the aim is to address the relative control of advective heat flow on talik development for a surface warming scenario with numerical modelling of coupled heat and fluid flow under consideration of different hydraulic scenarios and by applying different published models of permeability decrease over the freezing interval. For all simulations, a temperature scenario without seasonal variation is considered, as the objective here is to study the influence of advective heat flow from a deep groundwater source. In addition, we believe that a talik at 200 m depth is influenced to a minor extent by advective heat flow in the active layer. However, the influence of advective heat flow in the active layer for more shallow lake taliks would be an interesting topic for future work.

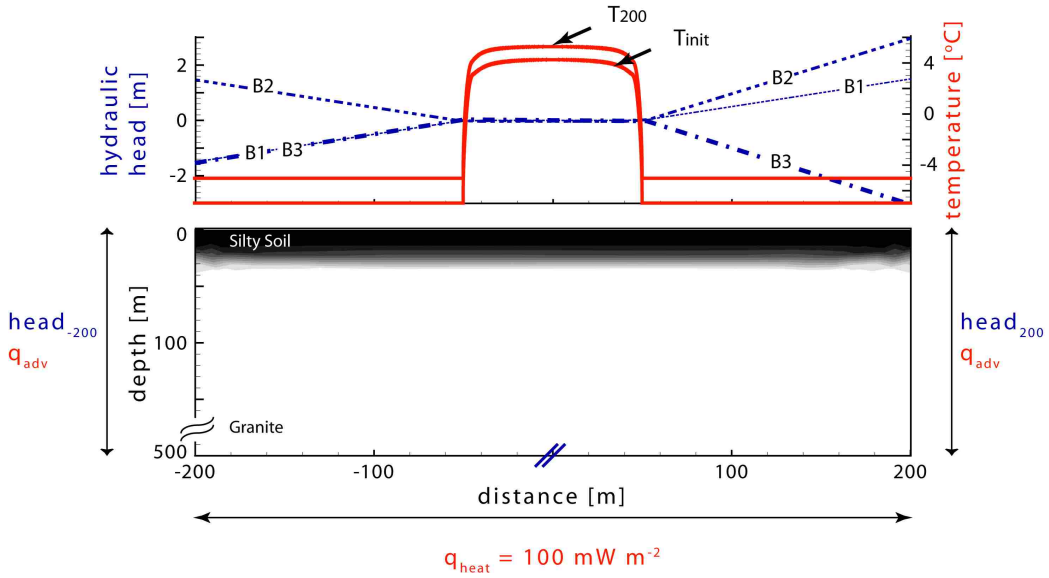

Figure 4.1: Model set-up and initial conditions for talik model. The thermal boundaries are given in red and the hydraulic boundaries in blue. The surface temperature is forced from T_{init} to T_{200} over 100 years. Three hydraulic head scenarios are used, representing groundwater entering and exiting the lake (B1), groundwater discharging into the lake (B2), and lake-water recharging the aquifer (B3). The hydraulic and thermal parameters represent silty soil in the upper 25 m, transitioning to the parameters of granite below.

4.2 Modelling approach

The model set-up is presented in Figure 4.1. The thermal boundaries are given in red and the hydraulic boundaries in blue. The surface temperature is forced from T_{init} to T_{200} over 100 years. The sides of the model are open for advective heat flow, and at the base of the model, a heat flux of 100 mW m^{-2} is applied. Three hydraulic head scenarios are used, representing groundwater entering and exiting the lake (B1), groundwater discharging into the lake (B2), and lake-water recharging the aquifer (B3). The sides of the model are open for flow whereas the value of hydraulic head as used at the top boundary is assigned at the sides. The base of the model is closed for fluid flow. The top 25 m of the model domain is characterized as silt overlaying bedrock and the thermal and hydraulic properties change with a smooth stepping function. The model geometry is cross-sectional and 2D, 400 m across and 500 m deep, however, only the upper 200 m of the results are presented. Hydraulic and thermal properties assigned to the model are listed in Table 4.1.

The temperature is driven from the surface and two different scenarios are considered: firstly a lake warming scenario, and secondly a lake growing scenario.

First, for the lake warming scenario an increase of ground surface temperature of 2°C from -7°C to -5°C between 100 a and 200 a simulation time is imposed for a lake of 100 m width. The warming of the lake bottom temperature is estimated using a process-based numerical model for different lake sizes and ground surface temperature regimes to estimate lake bottom temperature regimes, as presented in Chapter 3. In this example, the temperatures in the centre of the lake increase by $\sim$ 1°C (from T_{init} to T_{200} in Figure 4.1) when ground surface temperatures rise from -7°C to -5°C. The warmer conditions are then run for an additional 5000 a.

We first consider in scenario A, a heat-conduction only case. In Scenario B, we considered heat advection by groundwater flow for three different modes of groundwater flow in addition to heat conduction. Scenario B1 mimics a scenario of the lake being embedded in a regional scale groundwater flow system in which groundwater enters and exits the lake. In scenario B2 groundwater discharges into the lake, whereas in scenario B3 the lake recharges the aquifer (Figure 4.1).

In addition, in scenario C, a lake growth scenario is considered, in which a lake gets formed and grows over a thousand years to a radius of 100 m. A lake starts to grow at 100 a of simulation time, and the radius grows with a growth rate of 10 m per century. Again, the temperatures of the lake bed are calculated as presented in Chapter 3. Similar to the lake warming scenario, three different hydraulic scenarios are considered; scenario C1 mimics a lake being embedded in a regional scale groundwater flow system in which groundwater enters and exits the lake, in scenario C2 groundwater discharges into the lake and in scenario C3 groundwater recharges the aquifer.

We use the permafrost-permeability-reduction-functions (PPRFs) as used in earlier studies (e.g. *Bense et al.*, 2009; *Scheidegger et al.*, 2012) for calculating talik evolution for Scenario B1-3 (Equation 2.19). Using a suite of other PPRFs from the literature listed in Table 4.2, we calculate steady-state talik geometries (using the hydraulic boundary conditions of B2). Then we use a selection of three PPRFs to evaluate the varying impact of these on talik evolution in Scenario B2. Please note that only the PPRF is altered and that the freezing function, the calculation of thermal conductivity and heat capacity are calculated as described in Chapter 2.

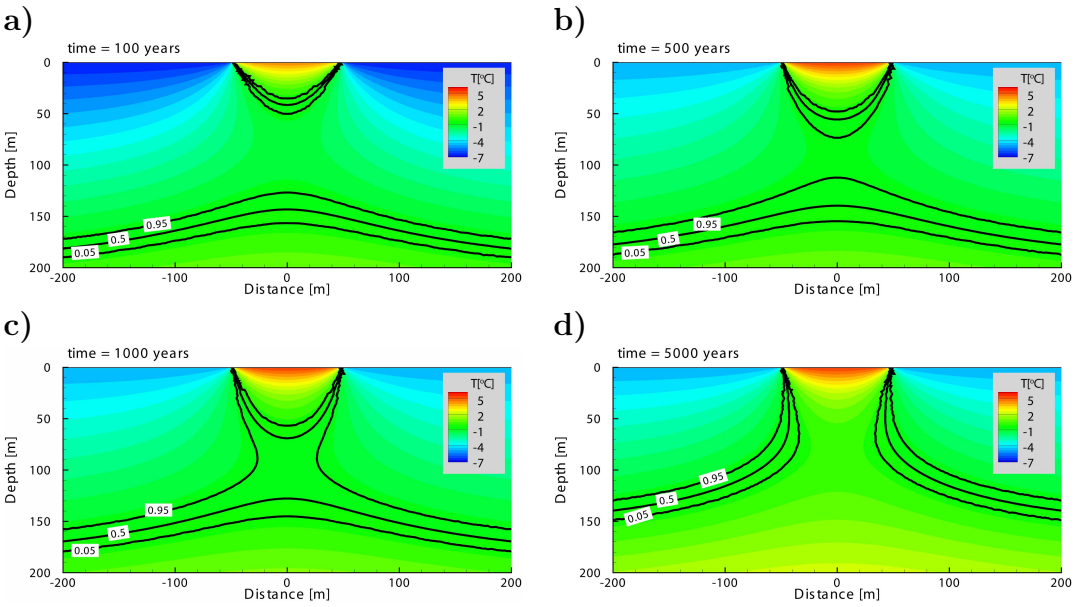

Figure 4.2: Temperature distribution and lines of equal ice saturation for a lake warming case, scenario A, for 100 a, 500 a, 1000 a, and 5000 a.

4.3 Results

4.3.1 Influence of surface warming on talik development

In the heat-conduction only case (scenario A), temperatures near the surface respond fast to changing boundary conditions, whereas the ice saturation underneath the talik takes millennia to respond to the warmer surface temperatures, and only 3000 a after temperature increase, a through talik develops under the lake (Figure 4.2). The impact of advection on talik evolution relative to the base case of this heat conduction only simulation is now discussed.

For a scenario of the lake being embedded in a regional groundwater flow system (scenario B1), after 1000 a simulation time, the ice saturation is still high enough to hinder a significant groundwater surface water connection with the sub-permafrost aquifer and no significant difference from the conduction only model can be found (not shown). However, after 3000 a, the ice saturation is lower, disappears by 3100 a (not shown) and is open for a groundwater-surface water connection thereafter (Figure 4.3c-d). The flow is concentrated in the lower half of the model domain at 5000 a simulation time (Figure 4.3b) and the flow magnitude increases with depth. This is also where the temperature difference between the conduction and the advection model is largest, (Figure 4.3e-f) and where advective cooling can be

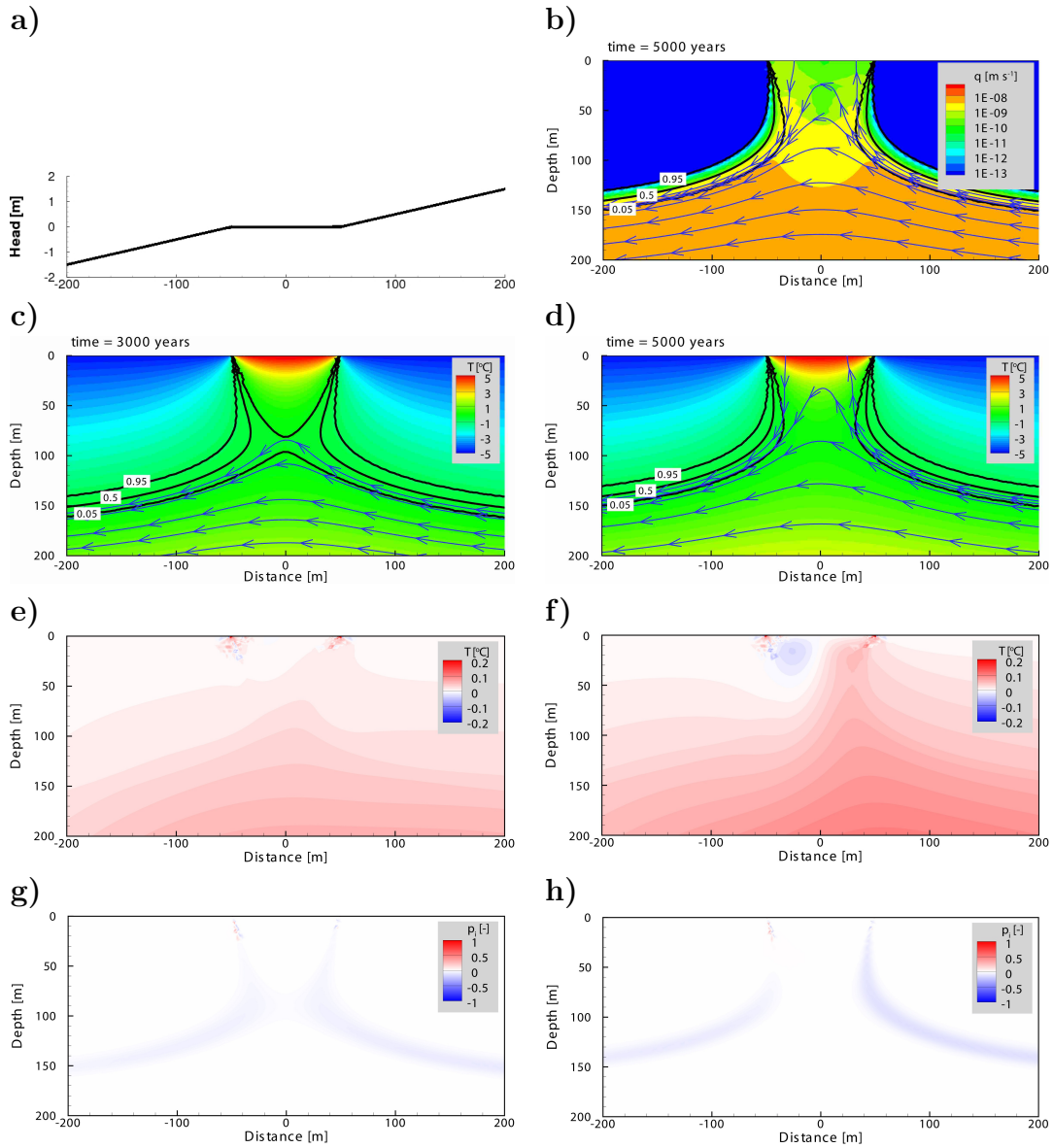

Figure 4.3: Model results for a scenario in which groundwater enters and leaves the lake (B1). Panel a) shows the hydraulic head boundary, b) the flow magnitude after 5000 a simulation time, c) the temperature field with lines of equal ice saturation after 3000 a, and d) after 5000 a simulation time, e) the temperature difference between the conduction model with the advection model after 3000 a, and f) after 5000 a simulation time, g) the difference in ice saturation between the conduction model and the advection model after 3000 a, and h) after 5000 a simulation time.

observed. This advective cooling propagates to the surface in Figure 4.3f where groundwater upwells, and where there is groundwater downwelling, there is a slight advective warming, which has also increases or decreases the ice content (Figure 4.3g-h). The ice content at the permafrost base is higher than for the conduction only model. The effect of the advective cooling is also observed by the timing of the opening of the lines of equal ice content; the opening time of the 5% line is delayed by 100 a relative to the conduction model, whereas the timing of the opening of the 95% and the 50% lines are not influenced (Figure 4.3a-b) by advective heat flow. In general however, the effect of advective heat flow for scenario B1 is small.

For a scenario B2 where groundwater discharges into the lake, the flow magnitude is largest in the talik at the top of the model domain (Figure 4.4a-b). This is where the advection model is cooler compared to the conduction only model after 3000 a, and ice gets aggregated (Figure 4.4c, e and g). Below the permafrost however, there is warming relative to the conduction model and the permafrost base is eroded. This warming effects becomes the dominant effect after 5000 a (Figure 4.4d, f and h) and approximately 50 m of permafrost get eroded near the lake. The opening of the 50% ice content line is delayed by a 100 a relative to the conduction model, as the cooling effect is dominant in the upper half of the model domain at around 2000 a simulation time, but for the 5% ice content line, the warming effect becomes dominant at 2950 a simulation time, and opens up 50 a earlier than for the conduction only model (Figure 4.4c-d).

For scenario B3, in which the lake recharges the aquifer, the opposite effect as for scenario B2 can be observed. Permafrost gets eroded in the upper half of the model domain and aggregated in the lower half. The flow magnitude is largest in the talik and the right side of the model domain under the permafrost (Figure 4.5b-d) and transports warmer surface water into larger depths. This results in a warmer temperature field and smaller permafrost extent under the lake (Figure 4.5e-h). At the permafrost base however, the temperature field is cooler than for the conduction only model and permafrost gets aggregated. The warming effect of the downwelling surface water is dominant for the timing of the permafrost degradation, as the 50% line of equal ice content opens 50 a earlier and the 5% line of equal ice content opens 800 a earlier than the conduction only model (Figure 4.5e-f).

Generally, it needs a high hydraulic head gradient, for advective heat flow to have an effect, and here a hydraulic gradient of 0.01 to 0.02 is used. If the hydraulic head gradient is two orders of magnitudes lower (not shown) then

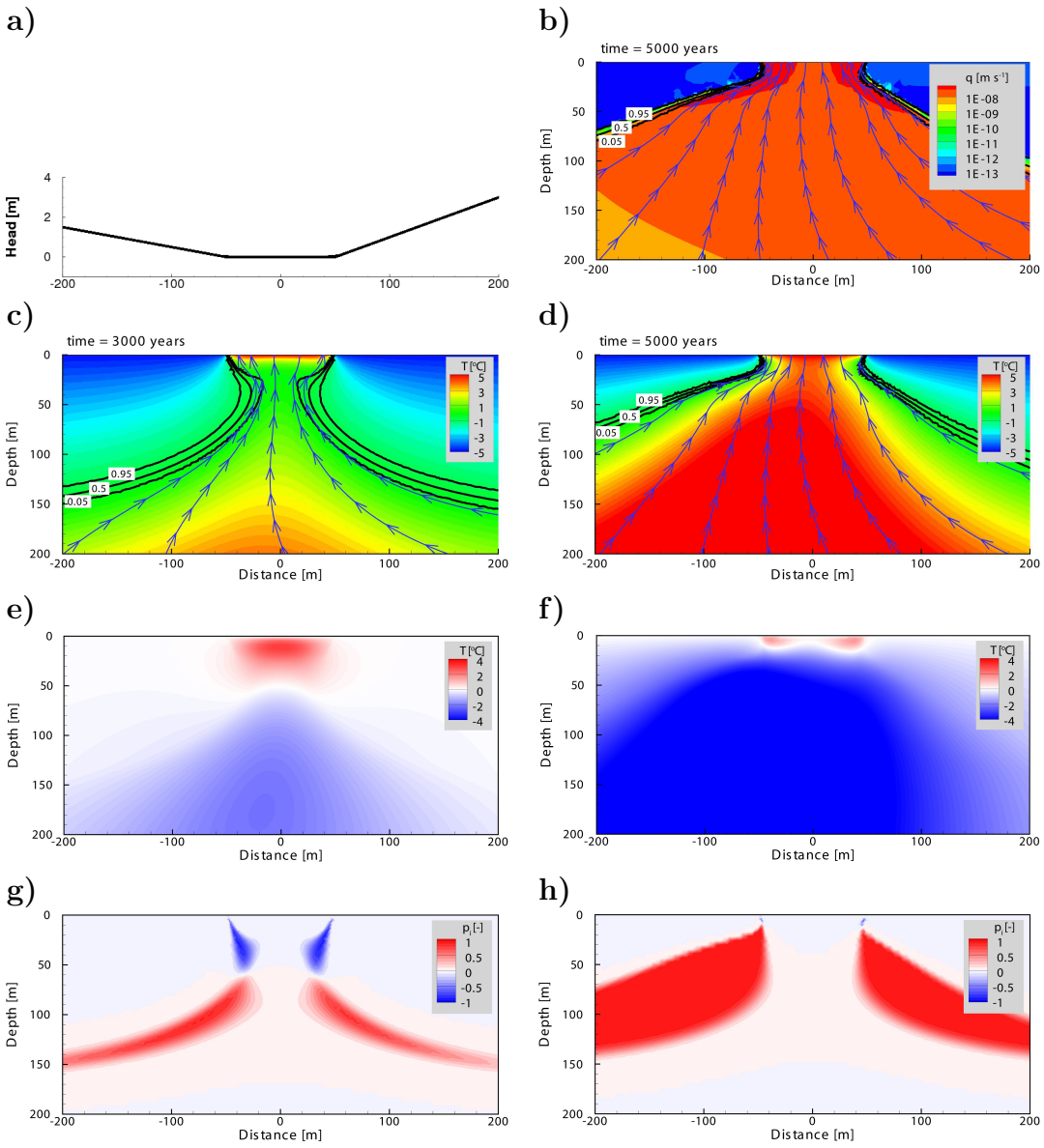

Figure 4.4: Model results for a scenario in which groundwater discharges into the lake (B2). Panel a) shows the hydraulic head boundary, b) the flow magnitude after 5000 a simulation time, c) the temperature field with lines of equal ice saturation after 3000 a, and d) after 5000 a simulation time, e) the temperature difference between the conduction model with the advection model after 3000 a, and f) after 5000 a simulation time, g) the difference in ice saturation between the conduction model and the advection model after 3000 a, and h) after 5000 a simulation time.

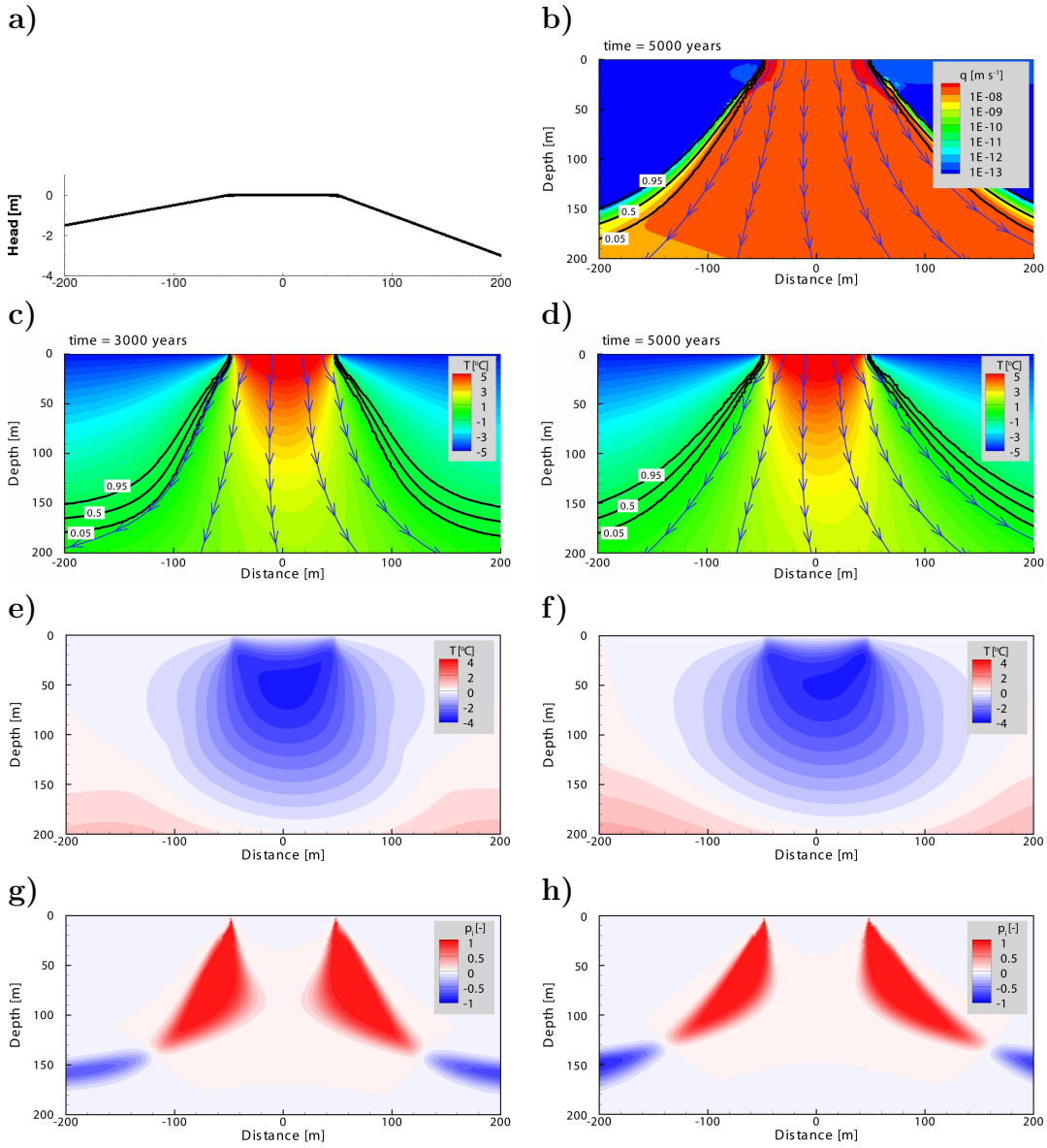

Figure 4.5: Model results for a scenario in which lake water recharges the aquifer (B3). Panel a) shows the hydraulic head boundary, b) the flow magnitude after 5000 a simulation time, c) the temperature field with lines of equal ice saturation after 3000 a, and d) after 5000 a simulation time, e) the temperature difference between the conduction model with the advection model after 3000 a, and f) after 5000 a simulation time, g) the difference in ice saturation between the conduction model and the advection model after 3000 a, and h) after 5000 a simulation time.

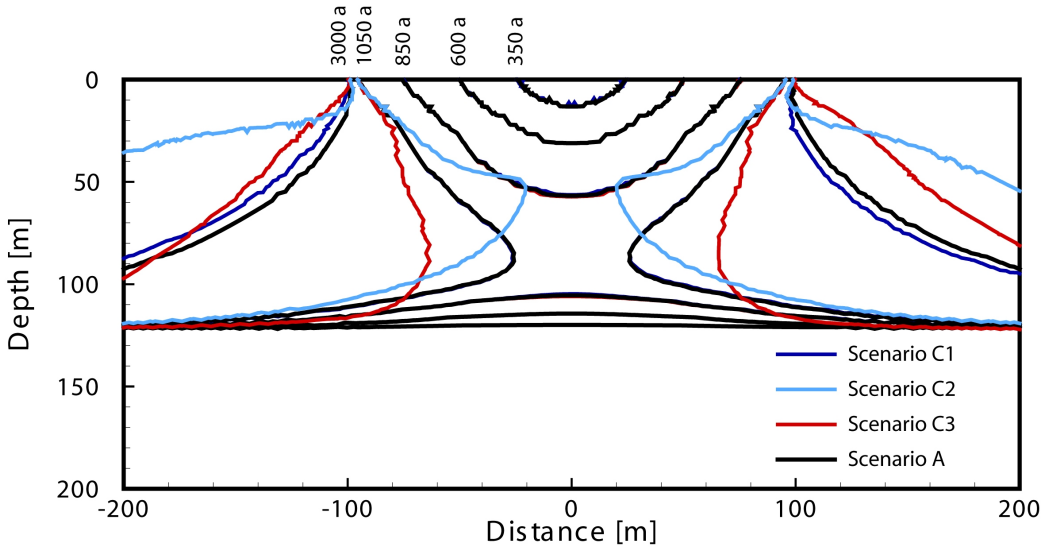

Figure 4.6: Lines of 5% ice saturation for a lake growing case for the conduction only scenario A (black), and the advection scenarios at 350 a, 600 a, 850 a, 1050 a and 3000 a simulation time. The advection scenario represent: C1 (blue) groundwater entering and leaving the lake, C2 (light blue) groundwater discharging into the lake, and C3 (red) lake water recharging the aquifer.

there is no difference between the conduction only scenario and the advection scenario.

4.3.2 Influence of lake growth on talik development

The 5% ice saturation under a growing lake for a conduction only and advection scenario C1, C2 and C3 are presented in Figure 4.6. As long as there is no through talik, the permafrost distribution for all models is similar, because heat conduction is the dominant process. It takes ∼1000 a for the permafrost to disappear underneath the lake. Once a groundwater-surface water interaction is established (at 1050 a of simulation time), the conduction and advection models diverge. The time until a through talik develops is similar for all model runs, except for model scenario C3 for which the through talik disappears 50 a earlier than for all other runs.

The direction of the permafrost migration depends on the direction of advective heat flow. For scenario C1, no difference at 1050 a of simulation time can be seen. At 3000 a, the right side of the talik, where there is groundwater upwelling, undergoes cooling, and the left side of the talik, where there is groundwater downwelling, there is warming relative to the conduction only model. This can also be observed in the distribution of the permafrost, as the permafrost gets aggregated where there is groundwater upwelling and eroded where there is groundwater downwelling. This pattern

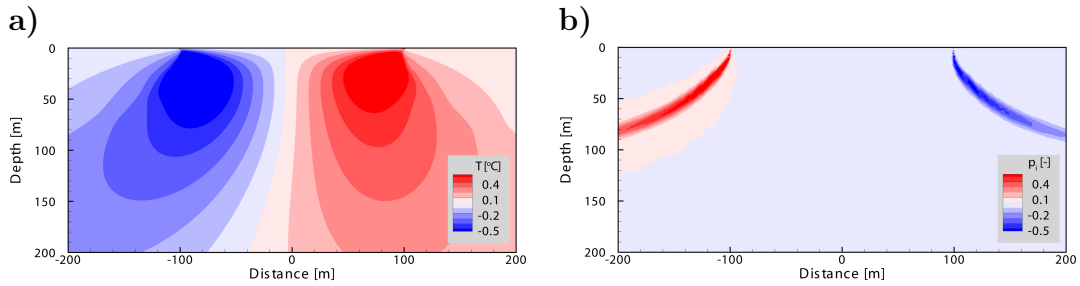

Figure 4.7: Difference between the conduction only model and an advection model for a) temperature and b) ice content for a lake growing scenario C1 in which groundwater enters and leaves the lake.

is different to the one observed for a lake warming scenario B1 (Figure 4.3a-b), as presented in (Figure 4.7a-b) .

The permafrost distribution of the head scenario C2 follows a similar pattern to the one described in Figure 4.4c-d, with erosion of the permafrost base and ice aggregation in the talik at 1050 a of the simulation time. This pattern changes over time, when the erosion by heat advection becomes dominant, and erodes the permafrost by around 50 m near the talik at 3000 a of simulation time. Then, the temperatures have risen up to 6°C due to advective heat flow.

The permafrost gets eroded in the talik for the head scenario C3, and aggregates at the permafrost base, similar as observed in Figure 4.5e-f. For this downwelling scenario, the opening of the talik occurs 50 a earlier than for all other scenarios.

When and over which temperature/ice content range a decrease in hydraulic conductivity will occur, is strongly dependent on the choice of the permafrost-permeability-reduction function, whose impact on talik evolution is discussed in the following section.

4.3.3 Impact of different permafrost-permeability-reduction function on modelled permafrost degradation

The hydraulic conductivity decrease with temperature using different permafrost permeability reduction functions (PPRFs) is presented in Figure 4.8a. The shape of the PPRFs as well as the magnitude of the total decrease varies between the different functions. For example, the PPRFs by *Burt and Williams* (1976) (K11-K13), *Watanabe and Flury* (2008) (K9-K11) and *McKenzie et al.* (2007) and *Ge et al.* (2011) (K7) show a sharper decrease

Model	Characteristics	Reference
K1	ice coating walls of capillary tubes	Eq. 13 in *Kleinberg et al.* (2003)
K2	ice coating surface of a grain pack	Eq. 15 in *Kleinberg et al.* (2003)
K3	ice in centre of capillary tubes	Eq. 14 in *Kleinberg et al.* (2003)
K4	ice in centres of a grain pack pore space	Eq. 16 in *Kleinberg et al.* (2003) with n=2 (*Bense et al.*, 2009)
K5	ice in centres of a grain pack pore space	Eq. 16 in *Kleinberg et al.* (2003) with n=0.4 for p_w=0.9 and n=1 for p_w=0
K6	modelled	Eq. 11 in *McKenzie et al.* (2007)
K7	modelled	Eq. 12 *McKenzie et al.* (2007); *Ge et al.* (2011) after *Hansson et al.* (2004)
K8	modelled decrease for Devon Silt	Fig. 6 in *Azmatch et al.* (2012)
K9	modelled decrease for sand	Fig. 9 in *Watanabe and Flury* (2008)
K10	modelled decrease for silt loam	Fig. 9 in *Watanabe and Flury* (2008)
K11	measured decrease for densely lensed silt	*Burt and Williams* (1976)
K12	measured decrease for fine sand	*Burt and Williams* (1976)
K13	measured decrease for clay	*Burt and Williams* (1976)
K14	modelled	log-linear decrease of 6 orders of to p_i=0.8 and 30 orders of magnitudes at p_i=0.99, *Wellman et al.* (2013)
K15	modelled	2/3 for T <0°C and T>-1.5°C, and 6 orders of magnitudes < T=-1.5°C, *Grenier et al.* (2013)
K16	Mualem's model	Eq. 12 in *Painter* (2011) with λ=0.9
K17	Mualem's model	Eq. 12 in *Painter* (2011) with λ=0.7
K18	Mualem's model	Eq. 12 in *Painter* (2011) with λ=0.5
K19	Mualem's model	Eq. 12 in *Painter* (2011) with λ=0.3

Table 4.2: Modelled and measured permafrost-permeability-reduction functions.

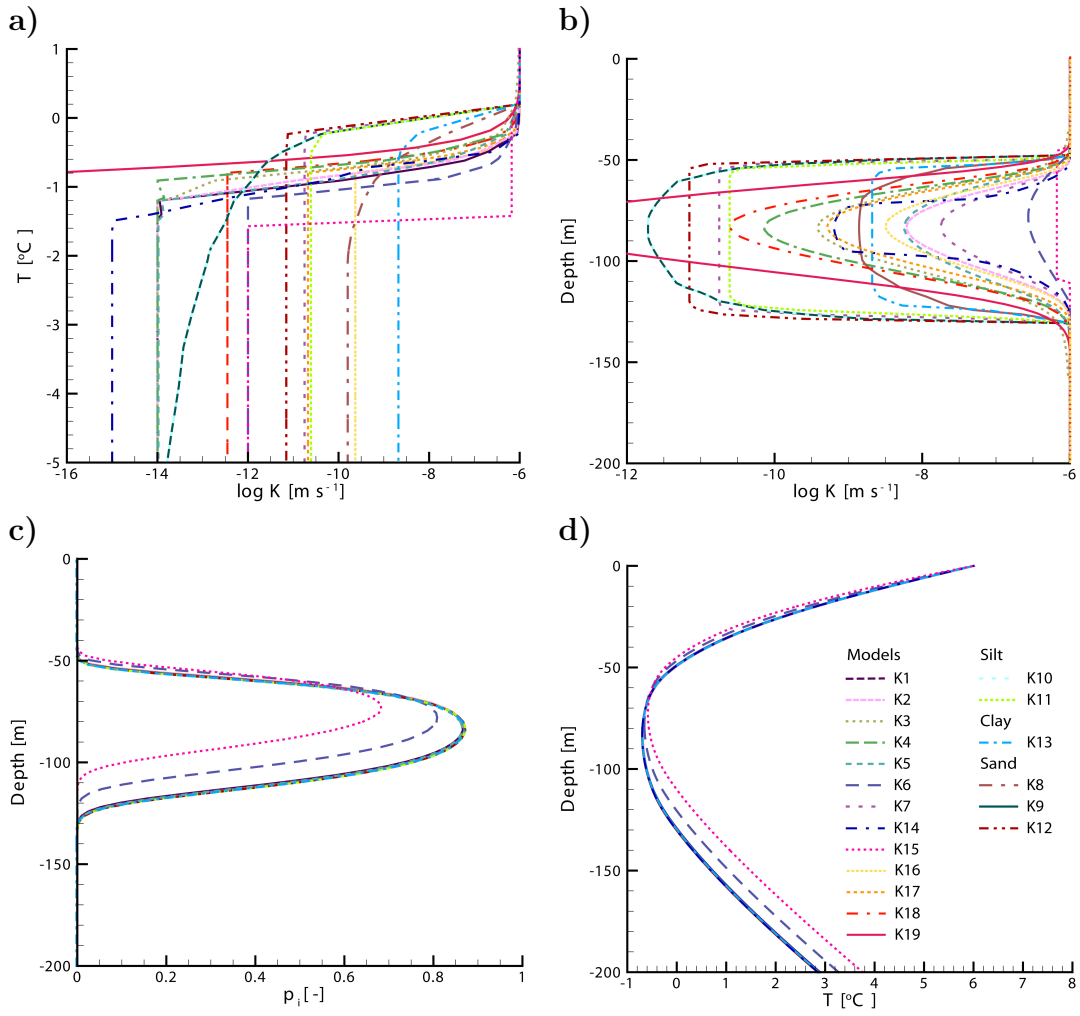

Figure 4.8: a) Hydraulic conductivity - temperature relationships as outlined in Table 4.2. These hydraulic conductivities are applied to a steady state model with a hydraulic head scenario B2. Depth profiles for b) log hydraulic conductivity, c) ice saturation, and d) temperature.

closer to 0°C than the PPRFs by *Kleinberg et al.* (2003) (K1-K5), *McKenzie et al.* (2007) (K6) and *Mualem* (1976) and *Painter* (2011) (K16-K19). This results in a profound difference in hydraulic conductivities at temperatures close to 0°C. In addition, the total decrease varies between 2.5 and 8 orders of magnitudes, and in general, measured PPRFs decrease less than modelled PPRFs.

The effect of applying these different PPRFs on a steady state model with coupled heat and fluid flow for model scenario B2 is shown in Figure 4.8b-d. The variability between the different estimates for hydraulic conductivity in partially frozen ground is several orders of magnitudes, and ranges from less than one order of magnitude (K6 and K15, *McKenzie et al.*, 2007; *Grenier et al.*, 2013) to over five orders of magnitudes (K9-K10, *Watanabe and Flury*

2008 and K19, *Painter* 2011). In addition, the rate of decrease varies from smooth to abrupt. In general, the decrease of hydraulic conductivity after the freezing onset is steeper for measured freezing functions and smoother for modelled ones. The influence of the different PPRFs on an ice saturation-depth profile and temperature-depth profile is presented in Figure 4.8c-d, and shows that all except models K6 and K15 show a very similar profile. Both models K6 and K15 remain higher K for temperatures below 0°C compared with other models, and thus advective heat flow is higher, resulting in lower ice saturation and higher temperatures. Model K15 merely uses two different values for the PPRF, a decrease in 2/3 for temperatures between 0°C and -1.5°C and for temperatures below -1.5°C a decrease of 6 orders of magnitudes (*Grenier et al.*, 2013). Model K6 uses a linear decrease of 6 orders of magnitudes between 0°C and -0.9°C. The fact that only these two models differ notably from all other models implies that the initial decrease in hydraulic conductivity with decreasing temperature has the most profound impact for this model, and that the total decrease in hydraulic conductivity is of lesser importance for a steady state model.

Figure 4.9 compares a transient model with lake formation using the FlexPDE (K4) model, the model by *Ge et al.* (2011) (K6) and the model by *McKenzie et al.* (2007) (K7) for model scenario B2. The timing for the opening of the talik varies considerably for the different models. Model K6 opens 500 a prior to the K4 model and about 1000 a prior to the K7 model. Therefore, the choice of freezing function for transient talik modelling can considerably alter the role of advective heat flow and thus result in earlier or later talik development.

4.4 Discussion and Conclusions

In this chapter, talik evolution under a developing lake is studied and scenarios of heat conduction only (scenario A) with heat advection (scenario B&C) are compared for a lake in a regional scale groundwater system, a lake into which groundwater discharges, and a lake recharging an aquifer for a lake warming case and a lake growing case. We find that the thermal state of an evolving lake landscape is in transient condition and it takes hundreds to several thousands of years to respond to changing surface boundary conditions. Therefore, taliks under newly formed lakes have possibly not reached a steady state. This implies that for deeper permafrost the effect of anthropogenic climate change on talik evolution might not be observed for several

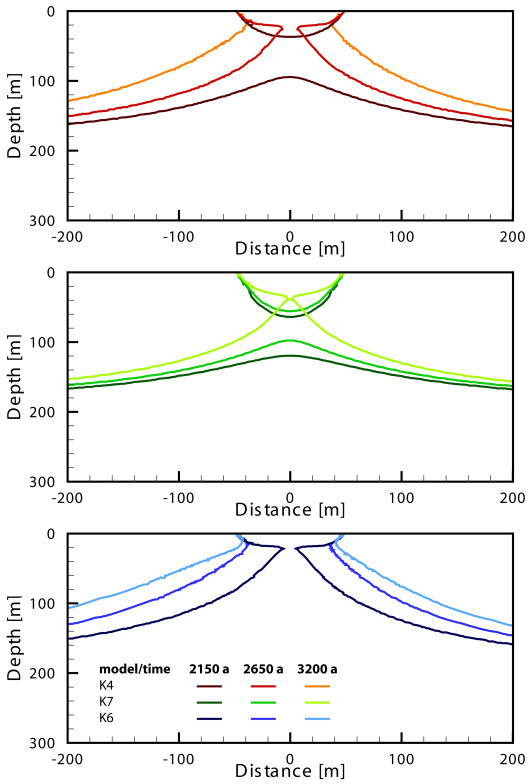

Figure 4.9: Transient model of a through talik formation for scenario B2, using different permafrost-permeability-decrease functions for model K4 (FlexPDE, this study), K6 (*McKenzie et al.* (2007)) and K7 (*Ge et al.* (2011)).

hundreds to thousands of years, and present changes in talik configurations may be a response to past climate change.

Model results imply that when a lake gets formed, it behaves in a purely conductive manner, as long as permafrost impedes a groundwater surface water connection. Although, as soon as a through talik is established, the systems changes to advective-conductive, and heat advection through groundwater flow can considerably change the permafrost distribution and the temperature field under a talik. This is in contrast with *Rowland et al.* (2011) and *Wellman et al.* (2013) who find that advective heat flow can accelerate the development of a talik and permafrost thaw and accelerates the breakthrough of sub-lake taliks. We confirm the relative importance of heat conduction for when there is no through talik, but as soon as a through talik exists and there is a high hydraulic head gradient, heat-advection can be equally as important as heat conduction. The influence of advective heat flow can erode and migrate permafrost, either into (scenario B2) or from (scenario B3) the talik. The pattern of cooling close to the surface due to groundwater upwelling and warming due to groundwater downwelling has previously been found by *Grenier et al.* (2013). This is in contrast with the results found

by *Wellman et al.* (2013), who states that both gaining and loosing lakes contribute to faster talik formation. *Grenier et al.* (2013) however observe a stronger cooling from groundwater upwelling, whereas we only observe a near surface cooling initially, which then changes into a warming dominated pattern.

For predicting the permafrost dynamics with projected climate change impacts, the influence of advective heat flow has been stated to accelerate permafrost degradation in newly forming taliks underneath lakes (*Rowland et al.*, 2011; *Wellman et al.*, 2013). Difference between the relative importance of advective heat flow on talik evolution between this study and *Wellman et al.* (2013) is likely due to a different choice of the PPRF function and the soil freezing function. The PPRF function K14 decreases at lower temperatures compared with K4 used in this study, which allows a higher magnitude of advective heat flow at temperatures close to 0°C. The PPRF in the study by *Rowland et al.* (2011) is dependent on fluid pressure, but their function is not described and is thus impossible to compare to this study. In addition, different model structure, boundary conditions, as well as including either suprapermafrost flow (*Wellman et al.*, 2013) or density driven flow (*Rowland et al.*, 2011) can influence the relative importance of advective heat flow in permafrost degradation. These examples and results from this chapter demonstrate that use of a different PPRF has a major role in determining the impact of advective heat flow on opening new taliks.

The question whether advective heat flow from groundwater movement in permafrost significantly contributes to permafrost thaw is difficult to be answered with this type of modelling, as the permafrost-permeability-reduction function (PPRF) determines the magnitude of groundwater flow and with it the advective heat transport in partially frozen and frozen ground. In partially frozen ground, the hydraulic conductivity can differ by several orders of magnitudes, depending on the choice of PPRF (Figure 4.8). Another uncertainty in estimating the advective heat flow component is that the freezing functions found in the literature were only measured in soil samples and thus might be different for sedimentary, igneous or fractured rock aquifers.

The choice of the PPRF can largely impact the dynamics of permafrost under surface water bodies, as shown in Figure 4.9. In addition, the onset of the impact of advective heat flow under a newly formed or warming lake is different depending on the PPRF, which results in the timing of a through talik development to be different by ∼1000 a. In this study, using an average PPRF (K4), we do not find a large influence of advective heat

flow on partially frozen ground, the onset is when the subsurface is fully thawed. In contrast, using a hydraulic conductivity decrease function that starts at cooler temperatures (K6) emphasizes the effect of advective heat flow in partially frozen ground.

An alternative approach of using an empirical or semi-theoretical approach relating temperature and hydraulic conductivity, the hydraulic conductivity can be obtained from a combination of classical retention curves by van Genuchten, Mualem's model for relative permeability and thermodynamical constraints for ice with a form of the Capeyron equation (*Mualem*, 1976; *Loch*, 1978; *van Genuchten*, 1980). This approach has been applied in e.g. *Painter* (2011); *Frampton et al.* (2011, 2013) and *Karra et al.* (2014) and can be applied to fully saturated, fully unsaturated or partially saturated porous media. An advantage of this approach is that the soil freezing curve or the soil water curves and the saturated hydraulic conductivities are easier to determine in a laboratory than the conductivity-temperature relationship (*Kurylyk and Watanabe*, 2013). A review of various forms of the Clapeyron equation, the relationship between the soil moisture and the soil freezing curve, and processes for developing soil freezing curves and hydraulic conductivity models for partially frozen soils is given in *Kurylyk and Watanabe* (2013).

In summary, in this chapter we find that the choice of PPRF has a profound impact on advective heat flow in partially frozen ground. Therefore, more research is needed to compare theoretical models with laboratory studies of PPRFs for different lithologies.

Chapter 5

Transient nature of Arctic spring systems driven by subglacial meltwater [1]

Abstract

In the High Arctic, supra- and proglacial springs occur at Borup Fiord Pass, Ellesmere Island. Spring waters are sulphur bearing and isotope analysis suggests springs are fed by deeply circulating glacial meltwater. However, the mechanism maintaining spring flow is unclear in these areas of thick permafrost which would hamper the discharge of deep groundwater to the surface. It has been hypothesized that fracture zones along faults focus groundwater which discharges initially underneath wet-based parts of the ice. With thinning ice, the spring head is exposed to surface temperatures, tens of degrees lower than temperatures of pressure melting, and permafrost starts to develop. Numerical modelling of coupled heat and fluid flow suggest that focused groundwater discharge should eventually be cut off by permafrost encroaching into the feeding channel of the spring. Nevertheless, our model simulations show that these springs can remain flowing for millennia depending on the initial flow rate and ambient surface temperature. These systems might provide a terrestrial analogue for the possible occurrence of Martian

[1] This chapter consists of a paper published in Geophysical Research Letters in June 2012 with the same title as this chapter (*Scheidegger et al.*, 2012). The chapter is unchanged from the paper apart from the the model description which has been deleted here to avoid repetition from Chapter 2, and the layout of the figures. JMS was responsible for the majority of the work under supervision of Victor Bense and collaboration with Stephen Grasby, who both provided scientific input and helped revise the manuscript for publication. In addition, comments by Pablo Wainstein and three anonymous reviewers helped to improve the quality of the manuscript.

springs recharged by polar ice caps.

5.1 Introduction

Groundwater flow in permafrost regions is generally thought to be restricted to unfrozen zones, taliks, which may occur above, below or within permafrost. Groundwater discharge to the surface can occur through taliks penetrating the entire depth of the permafrost, found under sufficiently large lakes and rivers insulating the ground from subzero air temperatures (*Williams*, 1970; *Sloan and Van Everdingen*, 1988). In High Arctic regions, characterized by thick permafrost, where insulating surface water bodies and hence through taliks are absent, groundwater discharge can nevertheless be observed in spring systems. Examples of spring systems which penetrate permafrost can be observed in Svalbard (*Haldorsen et al.*, 2010), and the Canadian High Arctic (*Andersen et al.*, 2002; *Moorman*, 2003; *Grasby et al.*, 2003). In the Arctic desert, precipitation is unlikely to sufficiently recharge springs, because groundwater recharge is inhibited by a confining permafrost layer. Thus, glacier meltwater (*Haldorsen and Heim*, 1999; *Grasby et al.*, 2003; *Haldorsen et al.*, 2010) or meltwater fed surface water bodies (*Andersen et al.*, 2002; *Moorman*, 2003) are believed to provide recharge for spring flow in areas of thick permafrost.

Subglacial water can either originate from in situ melt, or drain from the surface to the ice base (*Zwally et al.*, 2002). The meltwater at the glacier bed can then either migrate along the bed, or recharge a subglacial aquifer (*Boulton et al.*, 1993; *Piotrowski*, 2006). For strongly consolidated sedimentary or crystalline basement rocks, fracture systems, often associated with fault zones, provide the permeability required for substantial subglacial recharge. Therefore, discharge along fractures is often focused, and results in the formation of spring systems (*Fairley*, 2009).

At Borup Fiord Pass, Ellesmere Island, Nunavut, Canada, springs discharge from bedrock underneath glacial ice, and emerge at the surface as supra-glacial springs (Figure 5.1a). Evidence for a subglacial melt water source is provided by stable isotope analyses, and high concentrations of dissolved solids suggest a circulation depth of at least 1.5 km through fracture systems in the bedrock (*Grasby et al.*, 2003). The presence of abandoned spring mounds in the proglacial area illustrate the evolution from initial formation to their eventual demise. *Grasby et al.* (2012) propose that the abandoned spring mounds in the proglacial area reflect the retreat of the ice

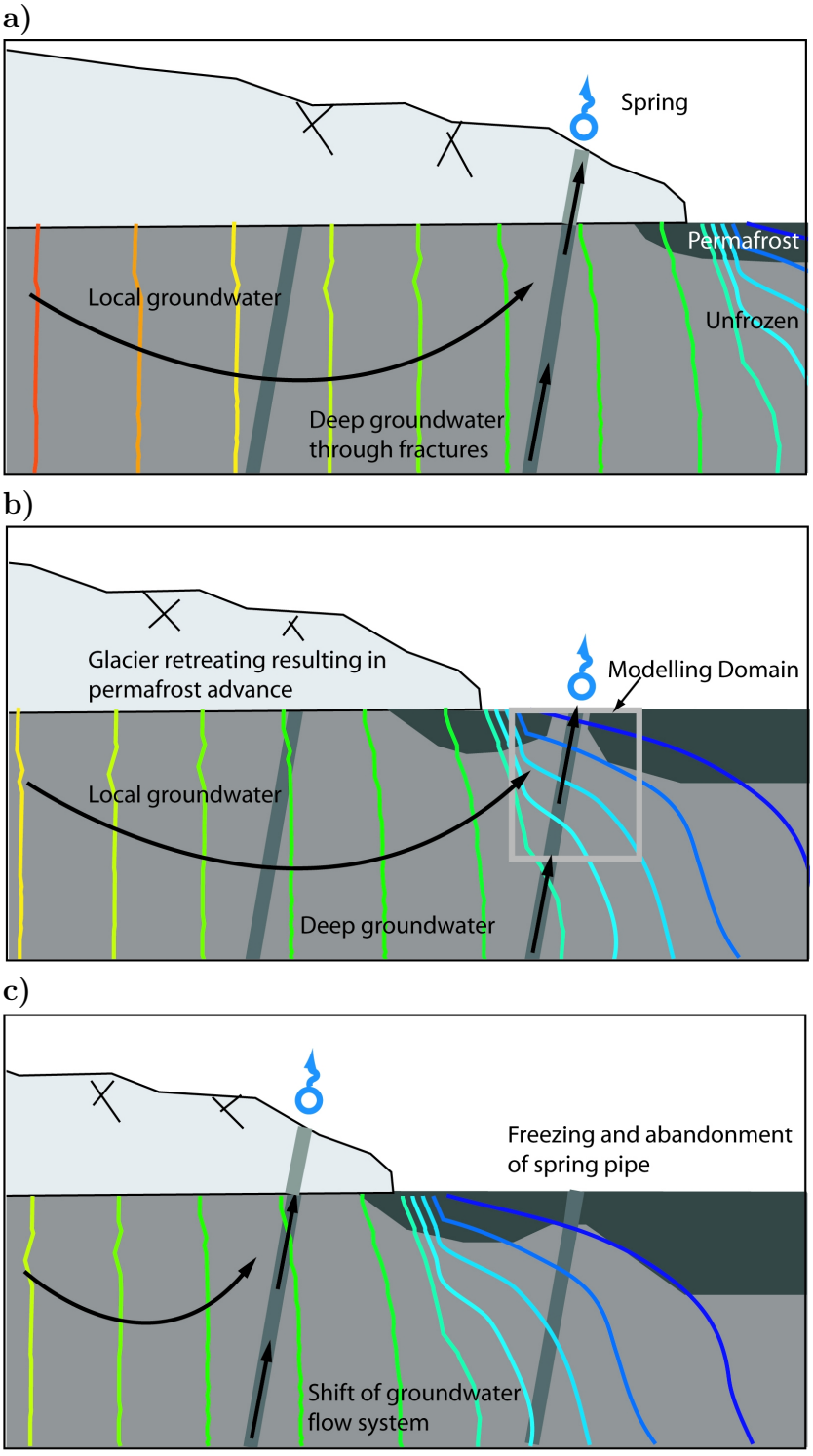

Figure 5.1: Conceptual model of supraglacial- and proglacial spring evolution modified after (*Grasby et al.*, 2012). Hydraulic head contours indicate low values (blue) at the ice margin and high values (red) underneath thick ice.

since the last glacial maximum. When springs get exposed to air temperatures 20°C lower than temperatures found underneath wet-based parts of the glacier (Figure 5.1b), permafrost growth surrounding the spring eventually cuts off the flow to the spring mound (Figure 5.1c). This site shows subglacial groundwater may play an important, but perhaps poorly recognized role in hydrogeologic systems in polar regions. How such perennial spring systems can operate in regions of thick permafrost (> 500 m) and low average air temperatures (<-20°C), and how transient these features are, remain uncertain.

Numerical models describing the transient nature of high-latitude spring systems have so far not been published. These are needed, since available analytical models address steady-state conditions, and can only be used to model temperatures of upwelling water from a isothermal reservoir through a cylindrical pipe surrounded by permafrost with no explicit description of permafrost formation and thaw (*Andersen et al.*, 2002; *Wainstein et al.*, 2008).

In this chapter, we aim to improve understanding of the occurrence of groundwater discharge in the High Arctic by means of numerical modelling, in which the relevant transient processes can be incorporated. Based upon the conceptual model depicted in Figure 5.1, we have developed a set of numerical model simulations which consider transient groundwater flow and heat transport, and include the latent heat effects of permafrost formation. Climatic and geological parameters are partially constrained by those encountered on Borup Fiord Pass. The scope of our model study here is to evaluate the interaction between the spring hydrogeology and the formation of permafrost near the surface when the spring is exposed in the proglacial area. Our model is thus inspired by, but not meant to be an exact representation of, the site at Borup Fiord pass. The model aims to be a generic, i.e. a heuristic description of a spring system surrounded by permafrost. Thus, the description of fault zone hydrogeology is simplified, and is represented as a relatively high permeability zone embedded in low permeability host rock.

5.1.1 Modelling approach

We numerically simulate that part of the conceptual model (Figure 5.1) directly surrounding the spring. The modelling domain is depicted in Figure 5.2. The 2D models are cross-sectional perpendicular to the strike of the fault zone and contain two hydrogeological units, the low-permeability bedrock, K_r, and a permeable fault zone, K_f. Parameter values and units

Parameter	Symbol	Value
Hydraulic conductivity in bedrock	K_r	10^{-13} m s^{-1}
Hydraulic conductivity in fault	K_f	10^{-6} m s^{-1}
Specific storage of the aquifer	S_s	10^{-4} m^{-1}
Volumetric heat capacity of water	C_w	$4220 \cdot 10^3$ J m^{-3} K^{-1}
Volumetric heat capacity of ice	C_i	$1835 \cdot 10^3$J m^{-3} K^{-1}
Volumetric heat capacity of solids	C_s	$1875 \cdot 10^3$J m^{-3}K^{-1}
Volumetric latent heat of fusion	L_i	$3.03 \cdot 10^8$ J m^{-3}
Gravitational acceleration	g	9.81 m s^{-2}

Table 5.1: Parameters used for a scenario in which hydraulic conductivity in the fault is homogeneous.

used are listed in Table 5.1. We set $K_{f,y} = 10 \cdot K_{f,x}$, which mimics the permeability anisotropy in the fault zone as a result of the presence of fracture networks predominantly located parallel to the orientation of the fault zone (*Caine et al.*, 1996). In a first set of models, hydraulic conductivity is homogeneous in the fault zone, and heterogeneous in a second set. Where the fault permeability is heterogeneous, a log-normal distribution of hydraulic conductivities, K, gradually increasing from 10^{-11} m s^{-1} at the edge of the fault zone, and 10^{-6} m s^{-1} in the middle of the spring, was used as being representative of fractured limestone or weathered crystalline rocks (*Freeze and Cherry*, 1979) across a 5 m by 5 m grid (Figure 5.3 a). Functions for predicting hydraulic conductivity follow a power law distribution (*Dardis and McCloskey*, 1998), and here, porosity, n, is calculated as a function of the initial, unfrozen hydraulic conductivity, K; $n = 10 \cdot K^{0.25}$ (Figure 5.3 b).

Fluid flow is driven by a hydraulic head differential, Δh, between the base and the top of the modelling domain. The upward pointing hydraulic head gradient imposed onto the model domain represents the high pressures underneath the wet-based ice that propagate underneath the proglacial area, and result in elevated heads at depth (Figure 5.1). At the top, a uniform temperature, T_g, represents ground surface temperature; except at the fault location, where temperatures are dominated by the outflow of groundwater. Here, the component of advective heat flow normal to the surface is assigned at the boundary. At the base, a heat flux (q_T) of 60 mW m^{-2} is imposed (*Grasby et al.*, 2003). The sides of the model are closed for both heat- and fluid flow.

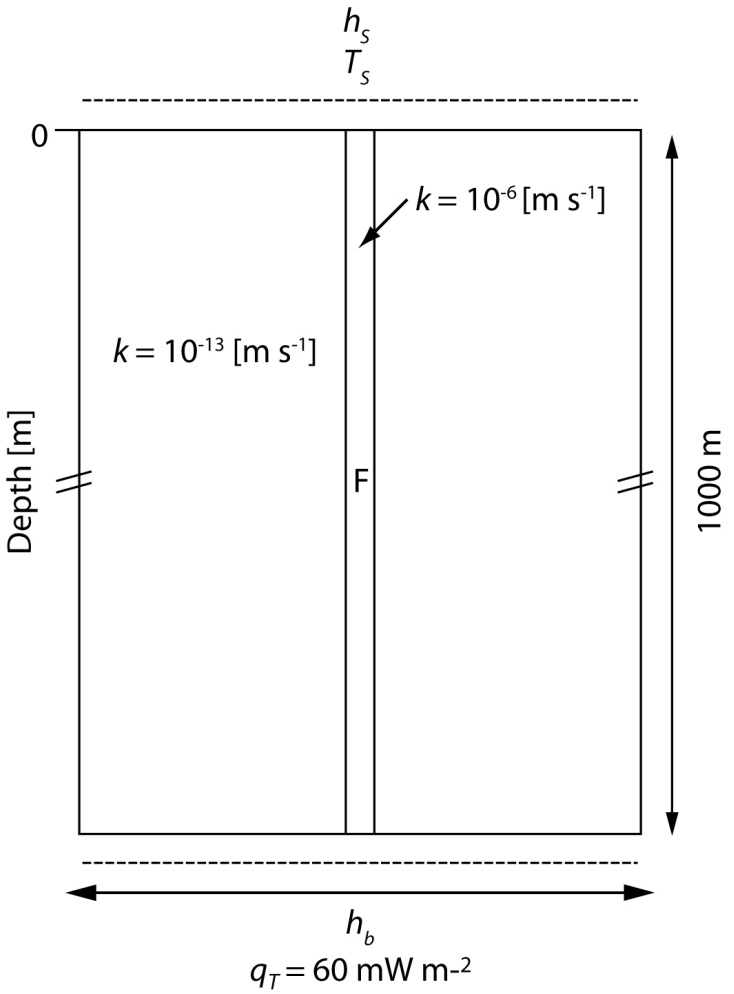

Figure 5.2: Modelling domain with boundary conditions for heat transport and fluid flow. At the base and at the fault location on top, a heat flux q_T is applied, ground surface temperature T_g is forced from 1°C to -19°C over a period of 200 a. T_s is equal to T_g, except at the fault location, where the surface temperature is dominated by advective heat flow. A head difference h_b - h_s from 1 m to 2.8 m from the base to the top is defined. The sides are no-flow for heat and fluid flow.

5.1.2 Modelling scenarios

The initial values are calculated at steady state, with ground-surface temperatures of +1°C, representing unfrozen conditions underneath a wet-based part of the glacier (Figure 5.1a). Temperatures slightly above freezing (+1°C) are imposed to ensure that all modelled pore space is unfrozen, and to enhance numerical stability. The exposure of the spring system to air temperatures following glacier retreat is represented with a ground surface temperature (T_g) decrease from 1°C to -19°C over a period of 200 years. Sensitivity scenarios are conducted for hydraulic head differential (Δh) between the base and the top of the spring from 1 m to 2.8 m, and the width of the fault zone (W_f) from 25 m to 100 m.

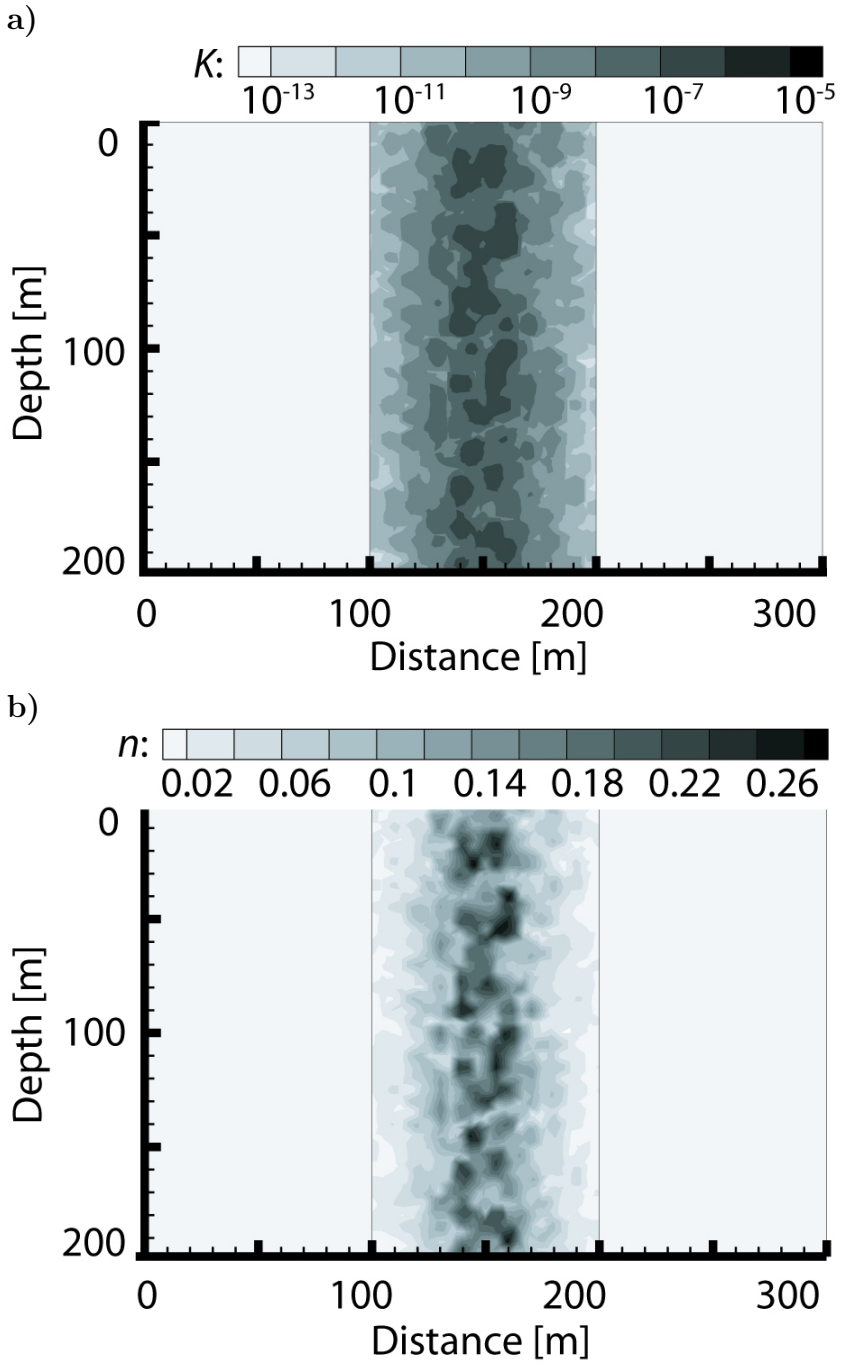

Figure 5.3: a) Hydraulic conductivity b) and porosity distribution for the heterogeneous model are shown, hydraulic conductivity is a log normal distribution, increasing towards the middle of the spring, and porosity is a function of hydraulic conductivity.

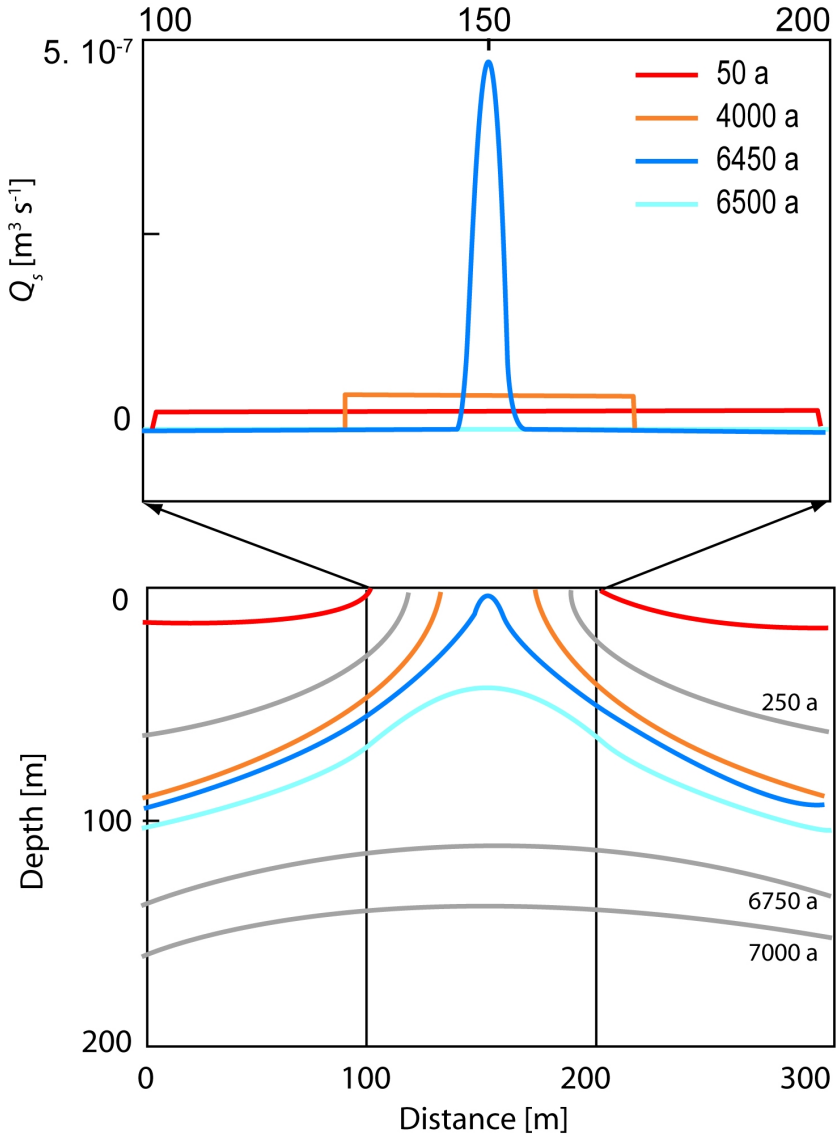

Figure 5.4: Freezing front migration and discharge Q_s evolution around the spring after initiation of cooling for a model with a homogeneous permeability structure. The contours represent discharge (top) along the fault zone and the location of the freezing front (bottom) over time. Discharge is specified for a model thickness of 1 m and Δh is set to 2.6 m.

5.2 Results

Modelling results for the example of a hydraulic head differential of 2.6 m, show that the position of the freezing front (95 % ice saturation) and evolution of the discharge at the spring location over time are fundamentally different for a homogeneous (Figure 5.4) or a heterogeneous fault permeability structure (Figure 5.5). After exposure of the spring location to surface air temperatures, permafrost develops in the surrounding bedrock and then starts to grow sideways. Then, permafrost develops at the near-surface parts of the fault zone, freezing the flow channel from the sides and focusing the flow

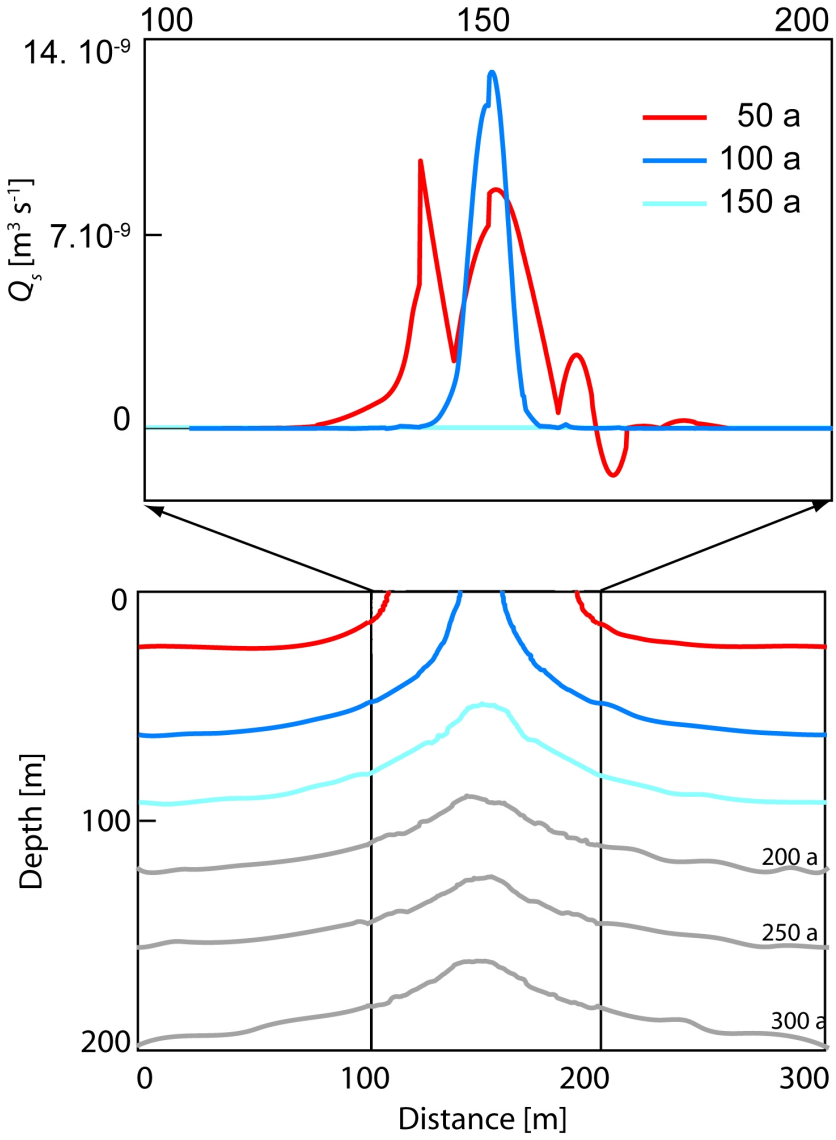

Figure 5.5: Freezing front migration and discharge Q_s evolution around the spring after initiation of cooling for a model with a heterogeneous permeability structure. The contours represent discharge (top) along the fault zone and the location of the freezing front (bottom) over time. Discharge is specified for a model thickness of 1 m and Δh is set to 2.6 m.

in the centre until the spring has completely frozen down and the flow to the surface is finally cut-off (Figures 5.4 and 5.5). For the case in which hydraulic conductivity is heterogeneous, the freezing front migration, and groundwater discharge (Figure 5.5), is modelled with the hydraulic conductivity and porosity distribution shown in Figure 5.3. Zones with lower porosity and hydraulic conductivities freeze faster, resulting in a nonuniform freezing front migration. The spring in this model freezes down considerably faster than in the model incorporating a homogeneous fault permeability structure, as the zone of the higher porosity and hydraulic conductivity is narrower, and

consequently, discharge and associated advective heat flow are lower.

Modelled temperatures and discharges are evaluated in the middle of the spring and illustrate the dynamics of the system in response to changing ground-surface temperature conditions. When the surface temperature (T_g) drops below freezing, spring temperatures decrease steadily to 0°C. Then, temperatures remain steady until all the latent heat is removed. Subsequently, the temperature decreases at a faster rate, decelerates with decreasing temperature, and the spring temperature approximates the ambient temperature (Figure 5.6a). Similarly, the discharge integrated over the width of the fault zone (Q_S) decreases steadily (Figure 5.6b) until the spring freezes down, when the discharge falls abruptly to zero.

A sensitivity study was carried out, using different scenarios for the hydraulic head differential (Δh) across the top and bottom of the model domain, and by varying fault widths (W_f). This results in a variation of the timing of the spring cut-off (Figures 5.7a and 5.7b). The variation of head difference and fault width both show a non-linear relationship with the timing of the cut-off.

5.3 Discussion and Conclusion

Numerical modelling suggests that springs in continuous permafrost cannot be explained as a steady state phenomenon. Our first-order modelling evaluation suggests that glacier meltwater fed spring systems in Arctic areas can persist for millennia after having been exposed from underneath thermal or polythermal glaciers. Hence, our modelling results support the conceptual models by *Haldorsen et al.* (2010) and *Grasby et al.* (2012), suggesting that flow channels in permafrost can persist as a transient feature for a finite time period. This considerably expands the analytical model by *Andersen et al.* (2002).

The most important parameter controlling the cut-off time, after having been exposed to surface air temperature, is spring discharge. With a higher discharge, more energy is provided to prevent permafrost encroaching into the feeding channel. Depending on discharge, a spring may freeze down within a few years, or several thousand years, implying that a sufficient hydraulic head differential is crucial for maintaining spring flow. Both variation of hydraulic head differential and width of the fault zone relate nonlinearly with the cut-off timing of the spring. By assuming that hydraulic head distribution at the glacier bed is equal to the ice flotation level, a small decrease in the

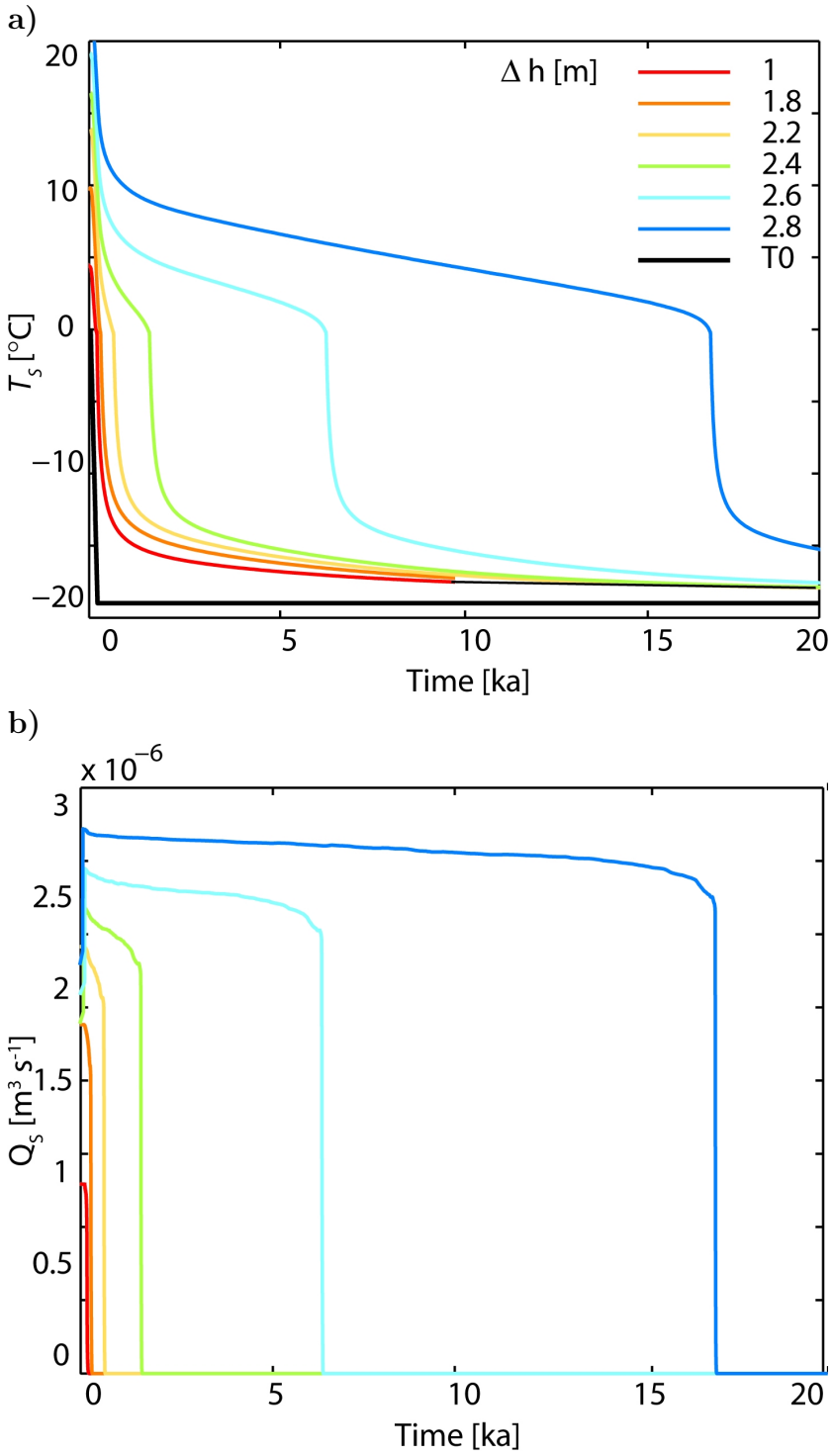

Figure 5.6: Sensitivity study for the model in which permeability structure is homogeneous and with a fault width of 100 m. a) Spring temperature T_s and b) Spring discharge Q_s, over time for different head scenarios Δh. The legend in (a) is valid for (b).

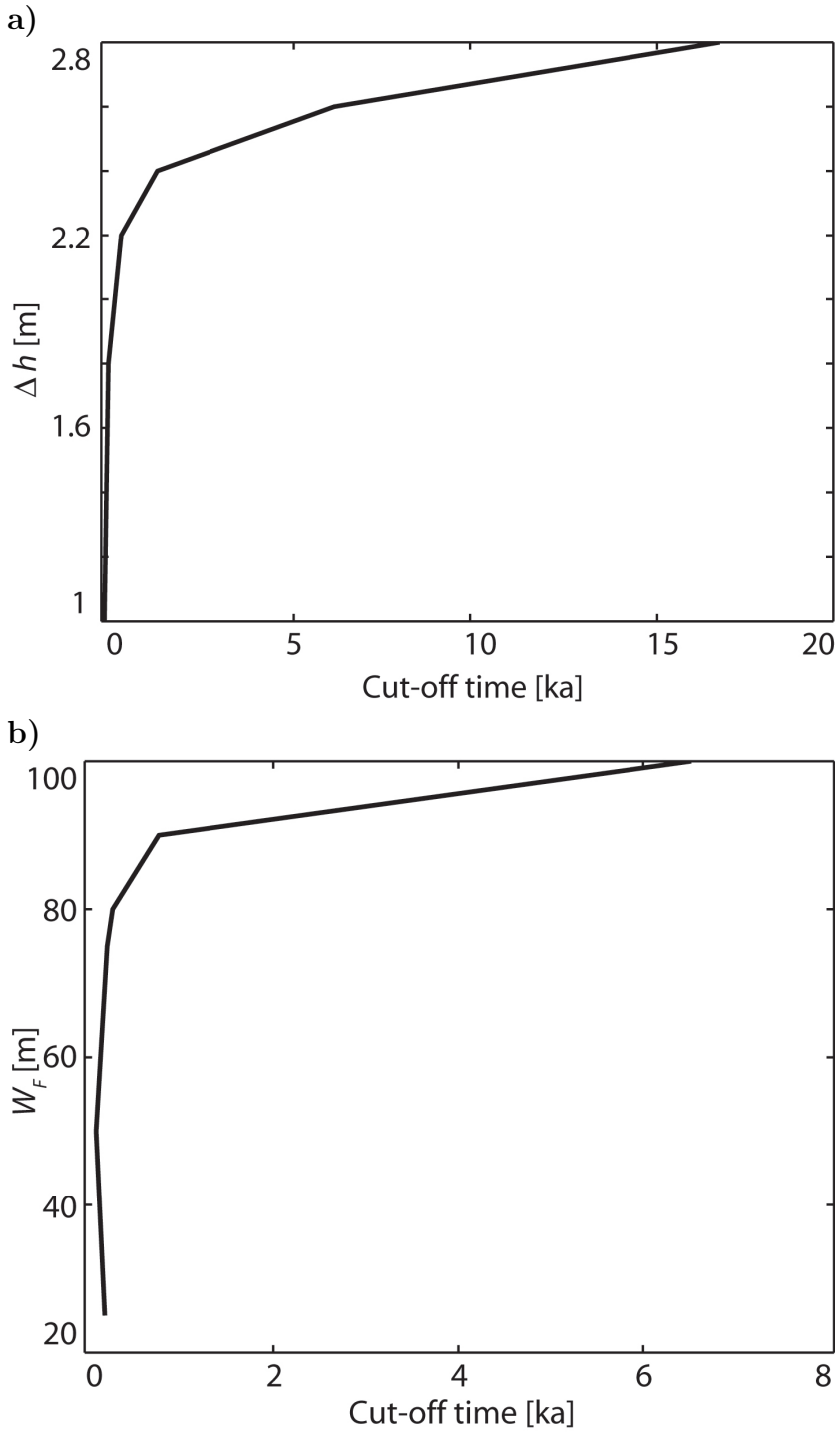

Figure 5.7: Sensitivity study for the model in which permeability structure is homogeneous. a) Cut-off timing for different head scenarios and b) fault widths W_F. a) is run with a fault width of 100 m and b) with a Δh of 2.6 m.

glacier surface can lead to a fast cut-off of glacier fed springs surrounded by permafrost (*Haldorsen et al.*, 2010; *DeFoor et al.*, 2011; *Iverson and Person*, 2012). In contrast, glacier thickening, or ice advance, increases the hydraulic head gradient and thus the flow. The response of the flow rate of the spring may be different if the morphology of the bedrock was not flat as we assume, or if subglacial lakes were present. A temporal variation in hydraulic head gradient has not been considered here.

The distribution of subglacial springs as modelled here is uncertain. The site at Borup Fiord Pass provides a unique view of these systems as after emerging from bedrock, the spring water discharges through the overlying glacial ice as a discrete spring. Typically, it would be expected that such springs would discharge into the proglacial area as part of basal discharge, where the spring water would be mixed with, and be indistinguishable from, subglacial meltwater.

Observed spring discharge at Borup Fiord Pass ranged from 8 l/min at some locations to diffuse seeps at other locations (*Gleeson et al.*, 2010). The volumetric rates of outflow in the fault zone over the top boundary of the model vary as function of the imposed head gradient as 0.06 l/min (Δh=1 m) and 0.17 l/min (Δh=2.8 m) for a homogeneous permeability structure, and between $4 \cdot 10^{-3}$ l/min (Δh=1 m) and $9 \cdot 10^{-3}$ l/min (Δh=2.8 m) for a heterogeneous permeability structure. These calculated discharges imply that a model thickness of several to several tens to hundred (homogeneous permeability structure) and up to a thousand meters (heterogeneous permeability structure) is required to reach discharges as observed in the field. The rate of discharge of groundwater in springs can be very site specific and are strongly dependent on local circumstances. The total volume of discharge is focused from a hinterland; here the wet-based part of an ice sheet, into a spring outlet. The size of the recharge area or the ice-sheet englacial conditions is unknown which control the volume of water available to emerge as spring discharge. These unknown boundary conditions of the system make a direct comparison complicated between model outputs and patterns observed in the field. Additionally, in this study we considered solely a deep groundwater source, as suggested by the high concentration of total dissolved solids of the emerging spring water (*Grasby et al.*, 2003). Potentially, shallow groundwater flow in the active layer can also contribute to the spring discharge seasonally (*Ge et al.*, 2011); however, summer field observations at Borup Fiord Pass suggest that the active layer is very shallow ($\sim$1 m), and we believe, considering only a deep groundwater source is a valid assumption.

Deep glacial groundwater systems modelled here point to much more active hydrogeological environment in Polar latitudes than previously recognised. Observations and numerical modelling strongly support the occurrence of groundwater discharge on Mars (*McEwen et al.*, 2011; *Goldspiel and Squyres*, 2011). Our study on a glacial driven groundwater system in regions of thick permafrost may provide a potential mechanism to drive such spring systems in Polar regions of Mars. A deep groundwater systems equivalent to the one found at Borup Fiord pass could form an important refuge for extraterrestrial life (*Grasby and Londry*, 2007).

Chapter 6

Impacts of glacially recharged groundwater flow systems on talik evolution [1]

Abstract

Most currently, permafrost covered landscapes underwent fundamental shifts in the hydrogeological and the thermal regime as a result of deglaciation after the Last Glacial Maximum (LGM). The transient effects of heat and fluid flow associated with retreating ice sheets are important to consider for the present-day hydrogeology of these regions. In this paper, we use numerical models to consider the evolution of taliks underneath proglacial lakes during deglaciation. In our models, the hydrological and thermal boundary conditions at the lake site are constraint by the hydrogeological impacts of ice sheet dynamics since the LGM. During the LGM, the ground surface was insulated from the air temperatures and as a result there was no permafrost underneath the wet-based ice. Subsequently, ice sheet retreat led to an exposure of a proglacial area to subzero air temperatures and the formation of permafrost. Where proglacial lakes form, inflow from deeper groundwater becomes focused. In this scenario, subpermafrost groundwater flow is driven by a combination of direct subglacial recharge, or by elevated hydraulic heads

[1] This chapter consists of a paper published in the Journal of Geophysical Research - Earth Surface, with the same title as this chapter (*Scheidegger and Bense*, 2014). The chapter is unchanged from the paper apart from the the model description which has been shortened to avoid repetition from Chapter 2, and the layout of the figures. JMS was responsible for the majority of the work under supervision of Victor Bense who provided scientific input and helped revise the manuscript for publication. In addition, comments by Sylvi Haldorsen and three anonymous reviewers helped to improve the quality of the manuscript.

preserved in that part of the aquifer. Advective heat flow can delay or prevent through taliks from freezing as function of aquifer properties. The presence and evolution of through taliks in thick permafrost can create complex and transient hydrogeological phenomena.

6.1 Introduction

Taliks, unfrozen zones within the confining permafrost, are important features to consider in permafrost hydrogeology, because they connect subpermafrost aquifers to the surface hydrology system. Classically, taliks are believed to occur underneath sufficiently large surface water bodies, where thermal surface isolation is sufficient for a through talik to develop (e.g. *Sloan and Van Everdingen*, 1988; *Burn*, 2002), here referred to as a 'conductive talik' (Figure 6.1a). The combination of heat transport through heat conduction and heat advection can result in the occurrence of 'conductive-advective taliks', where heat advection thermally erodes permafrost and can prevent or delay taliks from freezing (Figure 6.1b).

In permafrost covered regions, recharge and discharge can only occur through unfrozen zones, which can either be found under insulating surface water bodies, or under wet-based ice (e.g. *Andersen et al.*, 2002; *Haldorsen et al.*, 2010). *Bense et al.* (2012) suggest that recharge in a thawing permafrost environment is not sufficient for advective heat flow to have a significant impact on permafrost degradation in a nested groundwater flow system. In contrast, advective heat flow can influence transient taliks, where geothermal heat flow anomalies occur, where flow is strongly focused, or where the recharge is not limited by effective rainfall, such as glacial recharge (*Bense et al.*, 2012; *Scheidegger et al.*, 2012).

Proglacial areas in front of a wet-based glacier or an ice sheet could be influenced by groundwater, where the subpermafrost groundwater flow is driven by high hydraulic head gradients at the base of the ice sheet. Subglacial recharged groundwater flow paths can extend into the proglacial area, where upwelling to the surface can potentially occur via localized high permeability zones (*Boulton et al.*, 1993; *Piotrowski*, 2006; *Grasby et al.*, 2012), as observed in springs found in Svalbard (*Haldorsen et al.*, 2010), or on Ellesmere Island in the Canadian High Arctic (*Grasby et al.*, 2012; *Scheidegger et al.*, 2012). The presence of an ice sheet and the ice sheet history influences the hydrogeology, the thermal regime, and isostatic rebound. As a

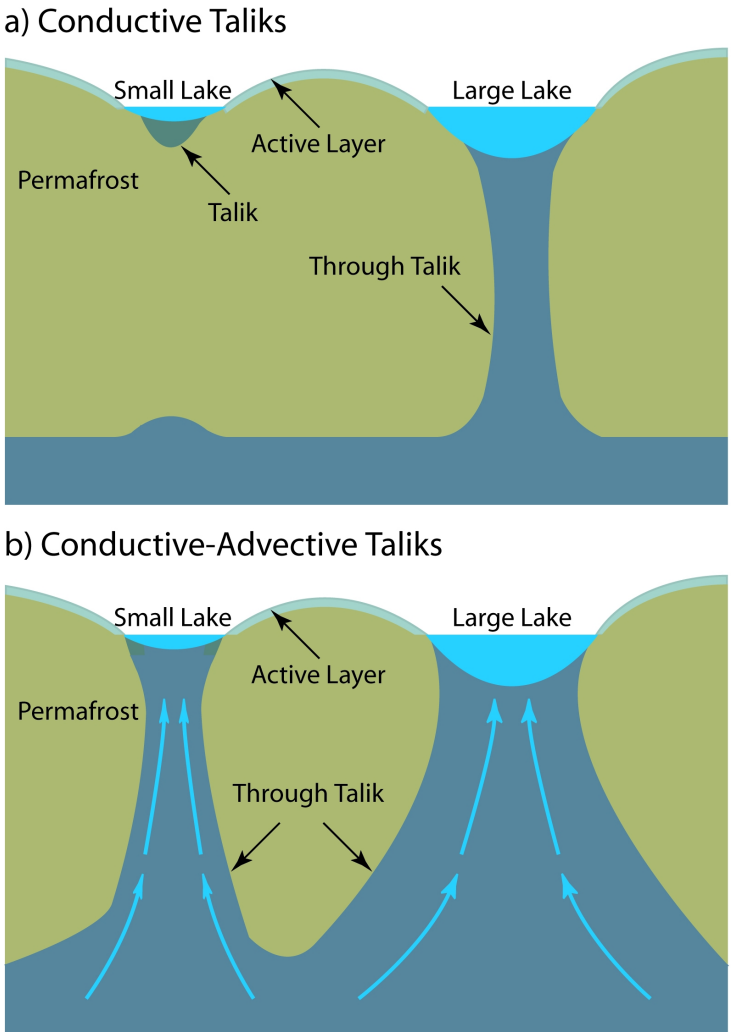

Figure 6.1: a) 'Conductive taliks' are formed through surface insulation alone. b) A combination of surface insulation and heat advection of groundwater flow forms 'conductive-advective taliks'.

result of ice sheet driven change in hydraulic head gradients, permafrost distribution and isostatic rebound, the groundwater flow field is in a transient state over millennia, (*Bense and Person*, 2008; *Lemieux et al.*, 2008a,b,c).

The evolution of taliks underneath proglacial lakes near an ice margin might not be fully understood with either a heat conduction only model (*Ling*, 2003) or a local scale model including heat and fluid flow (*Rowland et al.*, 2011; *Grenier et al.*, 2013). The latter two studies use a local scale model domain with a topography-controlled hydraulic gradient across the model domain, driving groundwater flow either into or out of a lake. Modelling results show a large impact of advective heat flow on talik evolution; for a warming scenario advective heat flow accelerates permafrost degradation (*Rowland et al.*, 2011) and for a cooling scenario, talik closure is delayed (*Grenier et al.*, 2013).

In order to improve our understanding of talik evolution and groundwater movement in proglacial areas, we carried out a modelling study that considers coupled heat and fluid flow including ice/water phase changes, where the local boundary conditions are derived from the larger scale dynamics of a moving ice sheet. This combines the approaches used by *Bense and Person* (2008) and *Lemieux et al.* (2008b), with those of *Rowland et al.* (2011) and *Grenier et al.* (2013), where a regional scale model of a retreating ice sheet provides the boundary conditions for the transient hydraulic head and temperature distribution for simulating the thermal regime and hydrogeology in a talik beneath a proglacial lake. Thus, the modelling approach of combining a large scale model with a local talik model considerably expands on those models in which a steady hydraulic head gradient is used to drive fluid flow as presented by *Rowland et al.* (2011) and *Scheidegger et al.* (2012). This model allows the investigation of the role of transient advective heat flow on talik evolution.

6.2 Numerical model

The numerical model as described in Chapter 2 is used, with the addition of hydraulic conductivity decrease with depth. Hydraulic conductivity decreases with depth and results in a weakened regional flow and an increase in penetration depth of local flow systems of a nested groundwater flow system (*Jiang et al.*, 2009; *Cardenas and Jiang*, 2010). An exponential decay model, assuming locally isotropic conditions, is used to calculate a spatially variable hydraulic conductivity $K(x, z)$ [m s^{-1}]:

$$K(x, z) = K_0 \, exp[-B(h_s(x) - z)] \tag{6.1}$$

where K_0 is the hydraulic conductivity at the surface, B is a decay component which indicates the decrease rate of K with depth, h_s the surface elevation and z is the depth (*Jiang et al.*, 2009; *Cardenas and Jiang*, 2010). Here, a value of B=0.001 m^{-1} is used, which is within the range of 0 to 0.01 m^{-1} as suggested by *Cardenas and Jiang* (2010). Applying the value for the decay component (B=0.001 m^{-1}) in equation 6.1 results in a slight increase in penetration depth of local groundwater flow as compared to models not considering a decline of permeability with depth. This value seems appropriate for a basin with a depth of about 1000 m (*Cardenas and Jiang*, 2010), such as the one considered here. The effects of assuming a declining permeability with depth are discussed in more detail for a generic basin in *Jiang*

et al. (2009) and *Cardenas and Jiang* (2010). An increase in penetration depth will potentially influence the amount of advective heat transport by sub-permafrost groundwater.

6.3 Boundary conditions

The models described in this chapter aim to be a generic and heuristic description of taliks under proglacial lakes surrounded by permafrost. However, the boundary conditions on taliks under lakes are loosely inspired by data from West Greenland near Kangerlussuaq (Figure 6.2), as the area is well studied (e.g. *Scholz and Grottenthaler*, 1988; *Willemse*, 2002; *Dietrich et al.*, 2005; *SKB*, 2011).

6.3.1 Glaciation history and ice-sheet geometry

The history of ice-sheet build up and collapse, and the topography of the ice-sheet surface are the primary drivers of the hydraulic and thermal boundary conditions applied to the surface boundary representing hydrogeological forcing by the ice sheet. The history of ice-sheet extent and thickness we apply here are comes from inferred trends based upon field observations from West Greenland as reported by Greenland (*Fleming and Lambeck*, 2004). The ice thickness (H [m]) is calculated using: (*Paterson*, 1994):

$$H = AL^{0.5}, \tag{6.2}$$

in which A [-] is a scaling factor and L [m] is the distance from the ice margin. A ranges between 1 (for warm based, soft-bedded ice) and 4.7 (for cold ice, resting on a solid bed) (*Paterson*, 1994). For present-day ice topography in West Greenland, A is estimated to be equal to ∼3.5 which is the value we use in our modelling. In our model simulations, we assume that A is not variable in time.

After the LGM (at ∼15,000 years BP), the West Greenland ice sheet margin retreated eastwards by 175-200 km, interrupted by small re-advances, and reached the present-day position at around 6000 a BP. Between 6000 years BP and 4000 years BP, the ice margin was East of the present-day position, with the ice sheet minimum occurring at around 4000 years BP around 60 km East of the present margin. This was followed by a re-advance to the present-day position (*van Tatenhove et al.*, 1996; *Scholz and Grottenthaler*, 1988; *Willemse*, 2002; *Dietrich et al.*, 2005). We have included a simplified

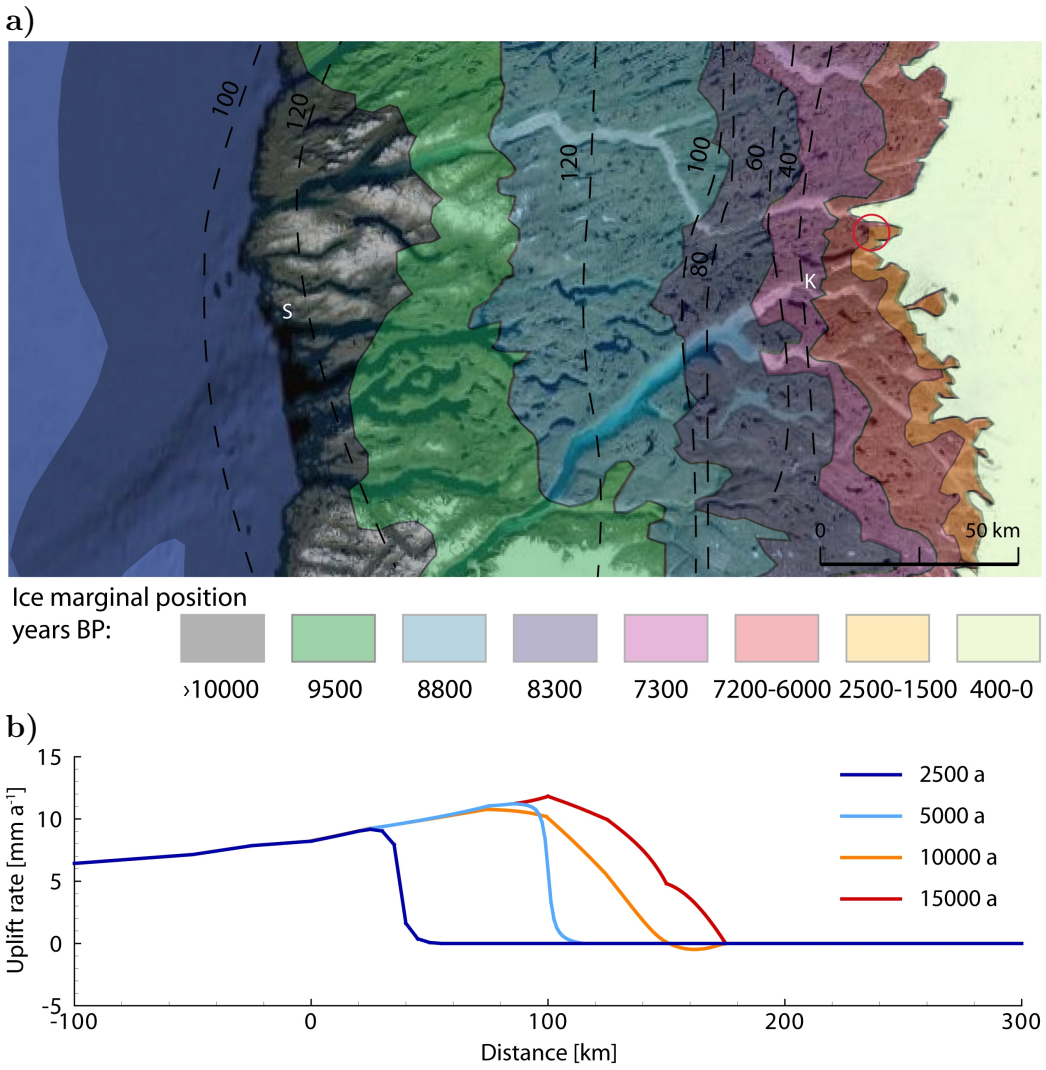

Figure 6.2: a) Recession of the inland ice and postglacial uplift between Sisimut (S) and Kangerlussuaq (K) with ice position and isostatic uplift after *Scholz and Grottenthaler* (1988). Note that between 6000 and 4000 years BP, the ice margin was behind its present position, followed by a re-advance period. b) Uplift-rates for different times implemented into model B with time given in simulation time. The ice sheet is retreating before 11,000 years simulation time and advancing between 12,000 and 14,000 years simulation time, and stagnant there after. The origin on the horizontal axis represents the location of the present coastline.

version of this glacial history in our model scenario build-up and retreat, as follows. The ice sheet boundary in the model is set to retreat steadily from 15000 years BP to 5000 years BP, when the ice sheet retreated 50 km behind the present-day margin where it stays steady between 5000 years BP and 4000 years BP, and readvances between 4000 years BP and 2000 years BP. Thereafter, the ice location is kept constant and the model is run for an additional 4000 years (Figure 6.2 after *Scholz and Grottenthaler* (1988)). The model is started at 16,000 years BP and spun up for 1000 years to 15,000 years BP, and run for a total of 20,000 years to 4000 years AP.

Uplift as a result of isostatic movement due to ice-sheet retreat in the proglacial areas of the West Greenland ice sheet near Kangerlussuaq is roughly -3.1 mm a^{-1}, whilst closer towards the coast this rate is declining to a small subsidence of $\sim$1 mm a^{-1} (*Dietrich et al.*, 2005). The complexity of the ice-sheet history in this area, and the impact of this on present and past isostatic adjustments make it impossible to simply take the unloading rate of the last ice retreat to model current uplift rates as was for example assumed by (*Bense and Person*, 2008).

No sea level changes due to isostatic and eustatic processes are considered, as in the model the location of the sea is just representing a permafrost free boundary. The investigation of the hydrogeological impacts of sea level changes goes beyond this study and is subject to further research.

In addition, no mechanical ice-sheet loading is considered, because crystalline rocks used for the study described here, have a very low compressibility and is thus neglected (*Domenico and Schwarz*, 1998; *Vidstrand et al.*, 2012).

6.3.2 Fluid flow

Subglacial meltwater can recharge an aquifer when the glacier bed is wet-based. For West Greenland, subglacial temperatures at pressure melting have been suggested by models from *Huybrechts* (1996) and *Brinkerhoff et al.* (2011). Subglacial water can either originate from in situ melt, or during the melt season draining from the surface to the ice base, through crevasses, moulins or englacial drainage structures (*Zwally et al.*, 2002). Subglacial meltwater is generated by frictional heating between the glacier and the substratum or through ice movement, and can result in a substantial amount of meltwater at the base of thermal parts of the glacier (*Boulton et al.*, 1993; *Piotrowski*, 2006). Subglacial water leaves the glacier system through a combination of Darcian flow through the till, laminar flow through a water film at the ice bed interface, and through turbulent flow through conduits at the

ice bed interface. Water discharges at the bed are generally too large to be discharged by groundwater flow only (*Iverson and Person*, 2012). However, it has been suggested that if the ice sheet is underlain by a high permeability bedrock, such as carbonates, all meltwater can be drained through the bedrock. In contrast, if the glacier is underlain by a low permeability bedrock, efficient drainage through the bedrock is inhibited and high subglacial water pressures can build (*Grasby and Chen*, 2005). This can then lead to channel flow and the formation of eskers (*Boulton et al.*, 1993). Alternatively, meltwater exceeding the drainage capacity of the bedrock has been suggested to drain as a water film (*Breemer et al.*, 2002). Hydraulic heads can be near flotation where the ice is underlain by a subglacial till with low permeability. The high water pressure and subglacial melting results in much larger groundwater recharge under thermal ice than that of present, ice free conditions (*Provost et al.*, 2012). For a crystalline glacier bed, fracture systems, often associated with fault zones, can provide the permeability required for substantial subglacial recharge.

To model the exchange of groundwater between the glacier bed and underlying aquifers, a flux boundary or a head boundary can be applied. A flux boundary condition based on estimated rates of basal melting may have an error of several orders of magnitudes, whereas setting the hydraulic head to the flotation value provides probably only a mild overestimate of actual heads at the bed surface (*Iverson and Person*, 2012). Potentiometric head from paleo-porewater pressures are estimated as 72 % of the ice thickness and have been inferred from the stress characteristics of the fine-grained sediments (*Piotrowski*, 1997). *Lemieux et al.* (2008a) argue that all meltwater reaching the glacier bed in excess of the flotation level of the ice sheet thickness should be treated as overland flow, and leave the glacier through channelized flow; because otherwise the ice sheet would become unstable.

To account for the uncertainties in the hydraulic head value at the base of the ice sheet, two hydraulic head scenarios are considered here; a maximum hydraulic head value at ice flotation level and half the flotation level, following the ice sheet thickness by a factor of 0.9 and 0.45.

6.3.3 Heat flow

The temperature distribution in the model is driven by the ground surface temperature at the top of the model domain, the basal heat flux at the base of the model and heat advection due to groundwater movement (Equation 2.12). The mean annual air temperature (MAAT) for Kangerlussuaq during

the period 1942-1992 was -5.2 ± 0.2°C (*van Tatenhove et al.*, 1996). However, ground surface temperatures differ from air temperatures due to the influence of slope, aspect, vegetation, soil type, and duration, thickness and properties of the snow cover. Borehole temperature profiles from DH-GAP03, approximately 1 km in front of the ice margin, suggest a mean annual ground surface temperature (MAGST) of -4.4°C before recent warming (*SKB*, 2011).

Lake water temperatures have been postulated to have been primarily driven by air temperature in the Kangerlussuaq area (*D'Andrea et al.*, 2011). A sensitivity analysis of the ground surface temperature is carried out with ground surface temperatures set to -6, -4 and -2°C and a lake bottom temperature scenario to 0, 2 and 4°C to evaluate the thermal influence of driving surface temperatures on the existence of a talik under a lake.

The temperature at the base of the wet-based ice sheet is set to 0°C, thus ignoring any pressure effects on the melting temperature, which is in the order of 1.3°C under 2000 m of ice. The impact of supercooled water could be important to include in future research, as this might decrease the advective heat flow in the proglacial area. The temperature at the sea is set to 1°C to mimic a permafrost free area.

In the model, surface temperatures are driven depending on the location of the ice margin with ground surface temperatures (GSTs) in the proglacial area and 0°C under the ice. Comparison of radiocarbon dates of shallow lake sediments and dating of moraines suggests lake development that coincides with the retreat of the ice-sheet margin (*Willemse*, 2002). Hence, lake formation in the Kangerlussuaq area is assumed to occur shortly after the local ice retreat. Thus, at the lake location the temperature is changed from surface temperature to lake bottom temperature (LBT) as soon as the ice has retreated locally.

The effects of variable density and viscosity in the calculated fluid flow field as a function of temperature and / or salinity are not taken into account. The effects of fluid properties on the regional flow field in this setting are not the primary focus of this study, and inclusion of these would require a different modelling approach. The chemical effects on freezing point depression could have an influence on the permafrost distribution, as found in cryopegs, where supercooled brine water are found within the permafrost (*Sloan and Van Everdingen*, 1988).

Parameter	Symbol	Value	Units
Average matrix porosity	n	0.0048	-
Hydraulic conductivity in bedrock	K_0	10^{-8}	m s^{-1}
Specific storage of the aquifer	S_s	10^{-6}/ $1.626 \cdot 10^{-4}$	m^{-1}
Volumetric heat capacity of water	C_w	$4220 \cdot 10^3$	J m^{-3} K^{-1}
Volumetric heat capacity of ice	C_i	$1835 \cdot 10^3$	J m^{-3} K^{-1}
Volumetric heat capacity of bedrock	C_s	$1875 \cdot 10^3$	J $m^{-3}K^{-1}$
Volumetric latent heat of fusion	L_i	$3.03 \cdot 10^8$	J m^{-3}
Heat flow density	q_{heat}	$34.8 \cdot 10^{-3}$	W m^{-2}
Gravitational acceleration	g	9.81	m s^{-2}

Table 6.1: Hydraulic and thermal properties of modelled bedrock. n, K_r, and q_{heat} are measured in a borehole nearby (DH-GAP01) taken from (*SKB*, 2011).

6.3.4 Hydraulic and thermal properties of bedrock

The possible impacts of the occurrence of till, lake sediments and soil over bedrock have not been taken into account, and the properties of the model domain have been simplified to homogeneous bedrock. The thermal and hydraulic properties of bedrock are based on those for fractured crystalline rock (Table 6.1). Folded or sheared zones of Precambrian crystalline metamorphic rock have been estimated to have a hydraulic conductivity in the order of 10^{-8} [m s^{-1}] (*SKB*, 2011). A thermal conductivity of 2.7 [W m^{-1} K^{-1}] is used to match the permafrost thickness of 335 m (*SKB*, 2011) for a steady state, conduction scenario. This value is in accordance with other measured thermal conductivities (*Kukkonen et al.*, 2011). The volumetric heat capacity of bedrock is not given in this report, but a medium value for gneiss of $2.2{\cdot}10^6$ [J m^{-3} K^{-1}] is applied (*Clauser*, 2011).

6.3.5 Initial conditions and model set-up

The model domain is 2D with depth of 1000 m and a with of 400 km; 100 km of fiord/sea and 300 km of ice, retreating 200 km since the LGM. To model heat flow, the sides of the model are non-flow and the base has a heat flux, q_{heat}. The sides and the base are no-flow boundaries for fluid flow (Figure 6.3).

The initial conditions are set during the LGM when the ice sheet terminated in the sea. The ground surface was insulated from the air temperatures and there was no permafrost, as a wet-based ice sheet is assumed. When the ice retreats and the front terminates above sea level, the ground surface gets exposed to sub-zero air temperatures and permafrost forms in the proglacial

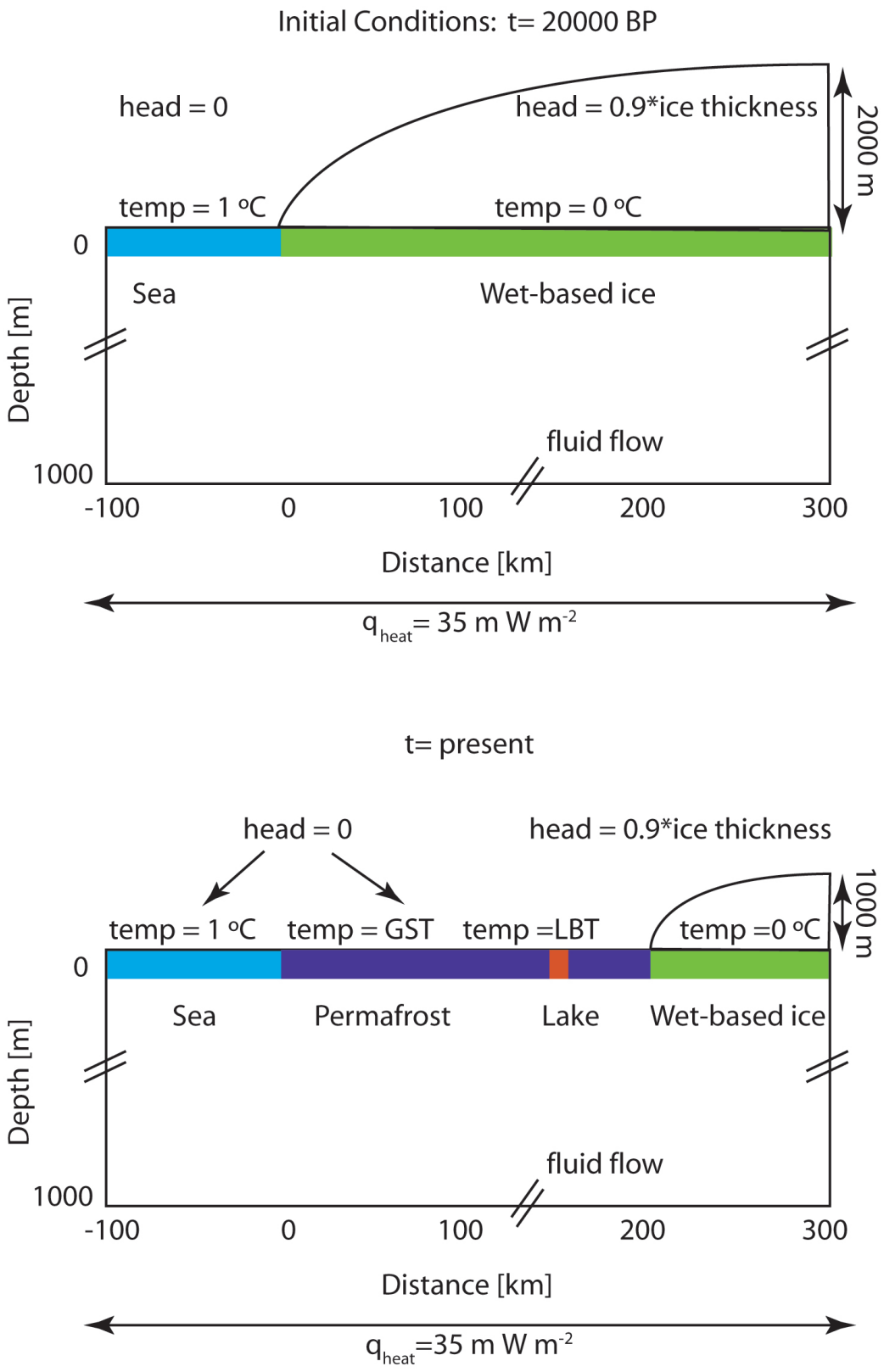

Figure 6.3: Initial- and boundary conditions for hydraulic head and temperature. GST is ground surface temperature and LBT is lake bottom temperature.

area.

Two sets of models are developed. Model A includes one lake and does not include isostatic rebound (Figure 6.3). This model is used to assess the relative importance of input parameters, and variations of model A are referred to as models A0 to A3. A conduction only scenario is considered in models A0 and A1, where model A0 is a steady-state model and A1 a transient model. Models A2 and A3 also consider heat advection, where the hydraulic head follows the ice sheet boundary by a factor of 0.45 and a factor of 0.9, respectively (Table 6.2). Models A2 and A3 are run for two scenarios for aquifer specific storage; a lower value of 10^{-6} m^{-1} typical for crystalline bedrock (e.g. *Domenico and Mifflin*, 1965) (models A2-1 and A3-1), and a higher value of $1.6 \cdot 10^{-4}$ m^{-1}, measured near Kangerlussuaq (*SKB*, 2011) (models A2-2 and A3-2), however this value is large for crystalline rock. Model A3-1-3 includes three lakes, but is otherwise identical to model A3-1. Model B includes isostatic rebound after glacier retreat and includes Tóthian topography (*Tóth*, 1963). The uplift rates are approximated from observed uplift, based on estimates (Figure 6.2a after *Scholz and Grottenthaler* (1988)), and implemented as described in Figure 6.2b.

6.4 Results

This section presents model results showing talik evolution under a proglacial lake for a steady state conduction model (A0), and near a retreating ice sheet for a transient conduction model (A1), a transient conduction and advection model for different aquifer properties (A2 & A3) considering one lake and three lakes, and a transient conduction and advection model including isostatic uplift (B). Results are given in simulation time.

6.4.1 Steady-state, heat conduction only model (A0)

In Figure 6.4, the permafrost distribution is presented for a lake with 100 m diameter for a steady state situation. Different temperature boundary values are used for the lake bottom temperature (LBT) ranging from 0°C to 4°C and with a ground surface temperature (GST) of -4°C. The boundary between permafrost and no-permafrost is defined as an ice saturation [-] of 0.95, whereas the ice saturation [-] ($p_i = \theta_i / n$) is defined as the ice content θ_i [-] divided by the porosity n [-]. When there is no thermal disturbance at the surface by the presence of a lake (black line), the permafrost thickness does not vary laterally. By introducing a 100 m wide lake with a LBT between

Model	Type	S_s [m^{-1}]
A0	steady state, heat conduction only	–
A1	transient, heat conduction only	–
A2−1	transient, coupled heat and fluid flow, $head = 0.45 \cdot H$	10^{-6}
A2−2	transient, coupled heat and fluid flow, $head = 0.45 \cdot H$	$1.626 \cdot 10^{-4}$
A3−1	transient, coupled heat and fluid flow, $head = 0.9 \cdot H$	10^{-6}
A3−2	transient, coupled heat and fluid flow, $head = 0.9 \cdot H$	$1.626 \cdot 10^{-4}$
A3−1−3	transient, coupled heat and fluid flow, $head = 0.9 \cdot H$, 3 lakes	10^{-6}
B	transient, coupled heat and fluid flow, $head = 0.9 \cdot H$, isostatic adjustment	10^{-6}

Table 6.2: Description of model scenarios used. H denotes ice surface height.

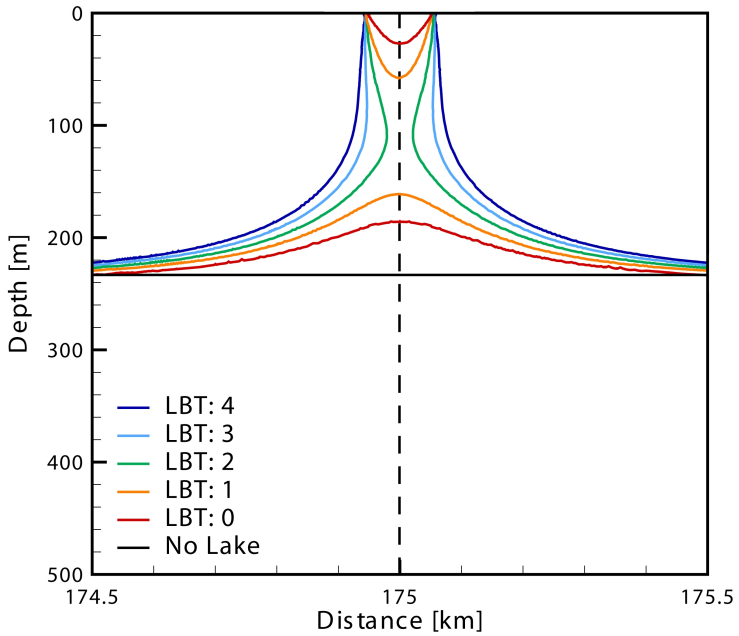

Figure 6.4: Permafrost distribution under a lake with different lake bottom temperatures (LBT) for a ground surface temperature (GST) of -4 °C for a steady state, conduction only model (A0).

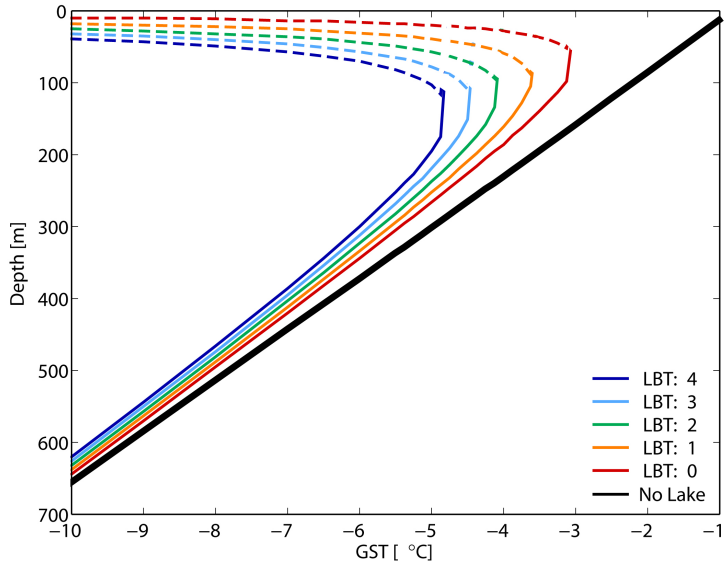

Figure 6.5: Depth of the permafrost base (solid line) and permafrost table (dashed line) under the centre of a lake of 100 m diameter for a steady state, conduction only permafrost model (A0). The black line represent the permafrost thickness with no thermal disturbance of a lake.

4°C and 0°C to the steady state model, the ground is insulated from air temperature and a talik forms under the lake.

Figure 6.5 presents the depth of the permafrost table and the permafrost base for different GST and LBT along a depth profile under the middle of the lake. In the absence of a lake (black line), permafrost depth for a

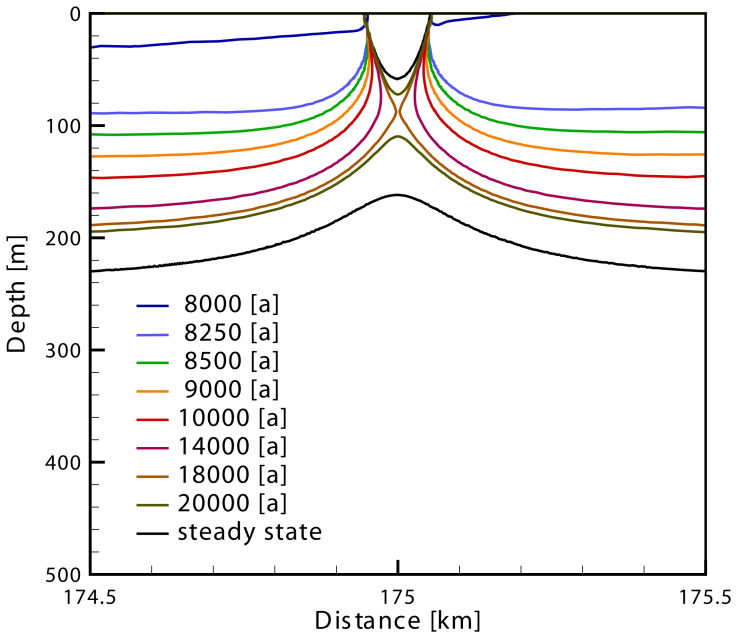

Figure 6.6: Permafrost formation over time under a lake with a lake bottom temperatures of 1 °C and a ground surface temperature of -4 °C for a transient, conduction only model (A1).

steady state model ranges from 656 m to 130 m for GST of -10°C and -2°C, respectively. The presence, or absence, of permafrost underneath the lake is the crucial factor here, as this disables or enables a subpermafrost groundwater to surface water connection.

6.4.2 Transient, heat conduction model (A1)

Modelled permafrost formation under a 100 m wide lake after ice retreat for one temperature scenario with a LBT of 1°C and a GST of -4°C is presented in Figure 6.6. Permafrost forms shortly after ice retreat at 8000 years of modelling time, which is when the ice retreats at the lake location. During the first years of the ground being exposed to subzero surface temperatures, permafrost forms at a larger rate than for subsequent years, which is evident from the permafrost thickness of $\sim$ 85 m after the exposure to GST for 250 years, and which is only doubled in 6000 years. The permafrost state under the lake centre takes millennia to reach a steady state; 10,000 years since local ice retreat, permafrost is forming under the lake and 12,000 years since local ice retreat, a steady state has not been reached yet with permafrost being approximately 30 m thinner than it should be for a steady state.

6.4.3 Transient conduction and advection model (A2 and A3)

Figure 6.7 presents model output of the ice sheet position, the discharge at the surface, the hydraulic head and the temperature distribution for four different time steps for model A3. Groundwater is initially recharged under the ice sheet (Figure 6.7a, t = 1000 years). With ice retreat, groundwater discharges underneath the ice near the ice margin, as newly formed permafrost is inhibiting groundwater-surface water interaction in the proglacial area, except through taliks under lakes. For transient conduction and advection models (A2 and A3), permafrost formation follows the retreating ice and its thickness decreases gradually near the ice margin when the ice sheet is retreating (Figure 6.7b, t = 10,000 years). However, when the ice is advancing, the thickness of the permafrost increases steeply, as advective heat flow is largest near the ice margin and thermally erodes the permafrost (Figure 6.7c, t = 15,000 years).

Due to the very strong hydraulic head gradient near the ice margin, a vigorous local flow cell develops (Figure 6.7). However, this local groundwater flow system does not impact the discharge into the talik lake, which is driven by a regional scale groundwater system. The magnitude of discharge into the lake decreases over time during ice sheet retreat and stagnation, implying that the system has not yet reached steady state (Figure 6.7, and Figure 6.11 k-n). When the ice sheet readvances, the regional hydraulic head gradient is forced by the position of the ice sheet, leading to an increase of discharge into the lake for models with relatively low aquifer specific storage (A2-1 and A3-1), but this is not seen in models with a higher aquifer specific storage (A2-2 and A3-2) (Figure 6.11). An open talik also results in a reversal of the groundwater flow direction near the lake, and groundwater flow closer to the sea is reversed and discharges into the talik (Figure 6.7b).

Once the talik has closed, the regional scale groundwater flow direction is still reversed near the lake (Figure 6.7c). The zone where the groundwater flow lines converge shifts seawards until the location meets the groundwater divide, from which time all groundwater will flow towards the sea again (Figure 6.7d).

A more detailed distribution of the depth of the permafrost base, hydraulic head field and flow vectors at the location of the lake is shown in Figure 6.8. When the lake is formed, the lake is subject to a low hydraulic head as defined by the land surface elevation, whereas a higher hydraulic head persists under the permafrost (Figure 6.8a). When the ground beneath

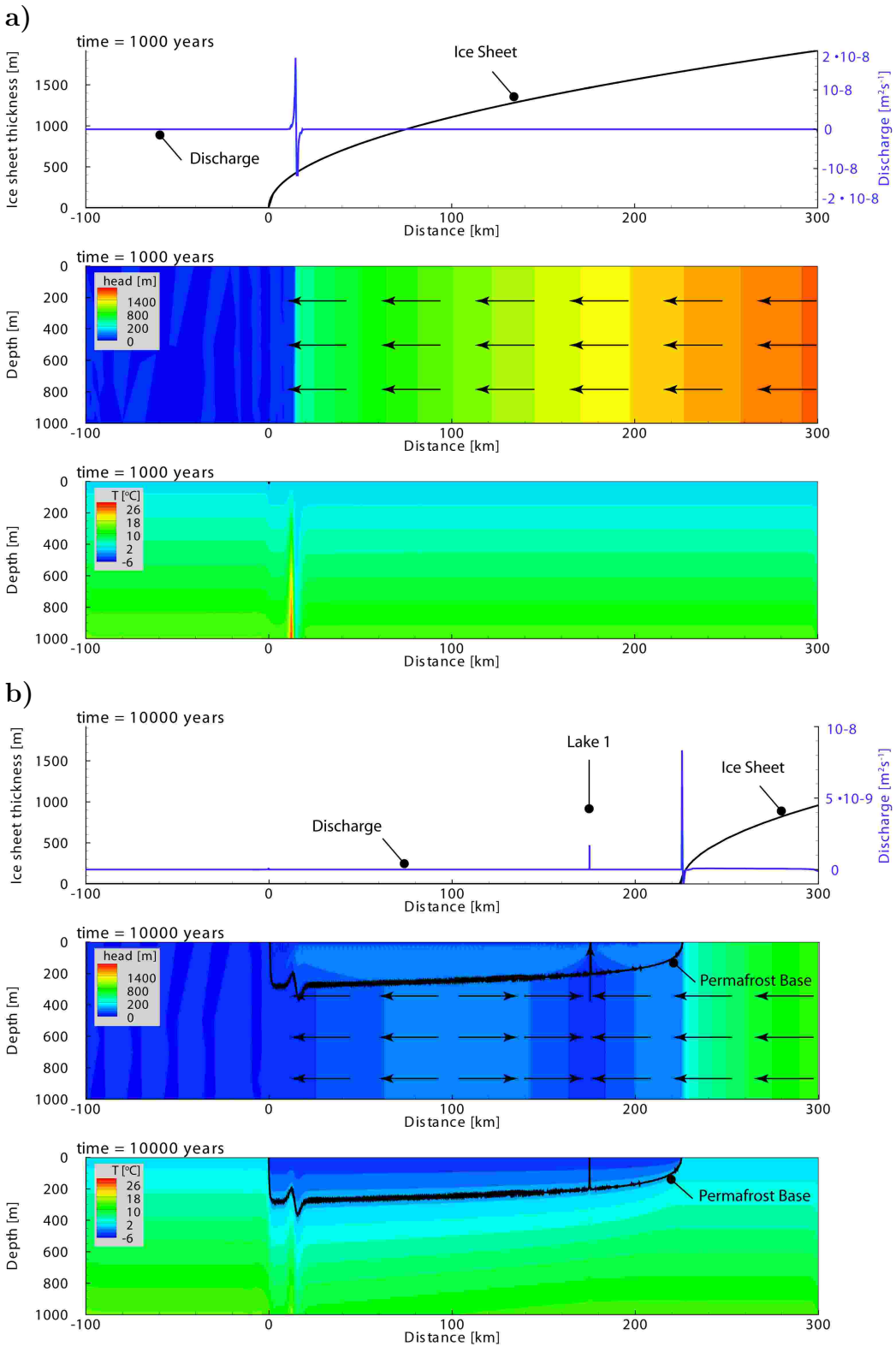

Figure 6.7: Modelled results for a transient conduction and advection scenario (model A3-1) with one lake of 100 m diameter. The first row presents the ice sheet location (black) and discharge to the surface (blue). The second row shows the hydraulic head field and flow vectors. The third row presents the temperature field and the permafrost base (black line). Result are presented for a) 1000 years, b) 10,000 years, c) 12,500 years and d) 20,000 years simulation time. Models are run for a GST of -6°C and LBT of 4°C. The flow vectors are not to scale. The vertical exaggeration is 1:100.

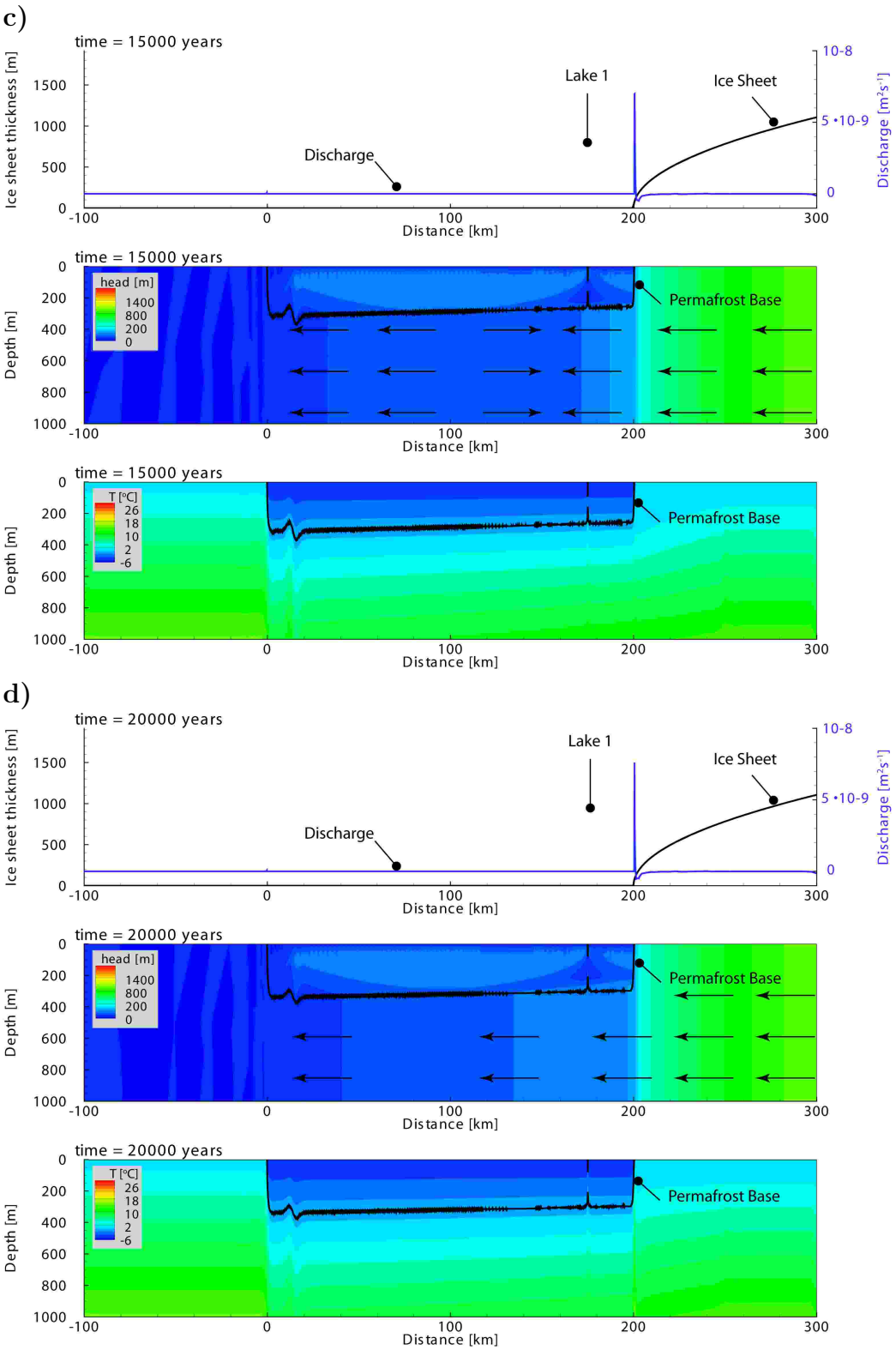

Figure 6.7: continued.

the lake centre is unfrozen, hydraulic head increases radially from the lake surface with exception of the surrounding permafrost, resulting in groundwater discharge into the lake. In the permafrost, the hydraulic heads are high, because the high hydraulic head values are preserved in the permafrost during permafrost formation from where they only very slowly dissipate. This, however, does not influence groundwater flow, as the hydraulic conductivity in the permafrost is eight orders of magnitude lower than in the unfrozen ground. Over time, the low hydraulic heads imposed at the lake location propagate radially into the subsurface resulting in a decrease of the hydraulic head gradient underneath the lake, and thus a decrease in discharge into the lake. With decreasing discharge, the advective heat flow cooling the talik, decreases and when upward advective heat flow becomes less than the lateral conductive heat flow, the talik starts to freeze. Once the through talik has started to close, the groundwater convergence will shift in the direction of the talik. When the ground underneath the lake becomes partially frozen, the hydraulic head difference between the surface water and the subpermafrost aquifer in a depth profile under the lake increases by several tens of meters (Figure 6.8b), controlled by larger scale dynamics of the ice sheet position. However, as the hydraulic conductivity decreases with ice saturation, discharge into the lake decreases overall. Once the through talik has frozen through and the discharge into the lake has ceased, hydraulic heads underneath the permafrost increase (Figure 6.8c and d).

Figure 6.9 presents a depth profile under the lake centre and 5 km away from the lake location, where the influence on hydraulic head and temperature of the lake should be negligible. Temperature (Figure 6.9a), ice saturation (Figure 6.9b), hydraulic head (Figure 6.9c) and vertical flow (Figure 6.9d) are presented for three different time steps of model A3-1 and the conduction only steady state. Transient processes of heat storage of the bedrock, release and uptake of latent heat, and elastic release of groundwater with decreasing hydraulic heads, result in heat flow large enough for a through talik to remain under the lake. In contrast, for a steady state situation considering only heat conduction, there is no through talik (Figure 6.9a & b). Hydraulic head is driven by the surface elevation and increases with depth, where the hydraulic head is influenced by the historic and current hydraulic head distribution near the ice margin. Hydraulic head differences in and under the permafrost are around twice as high as those under an open talik (Figure 6.9c); however this does not influence the groundwater flow, as hydraulic conductivities are several orders of magnitudes lower in

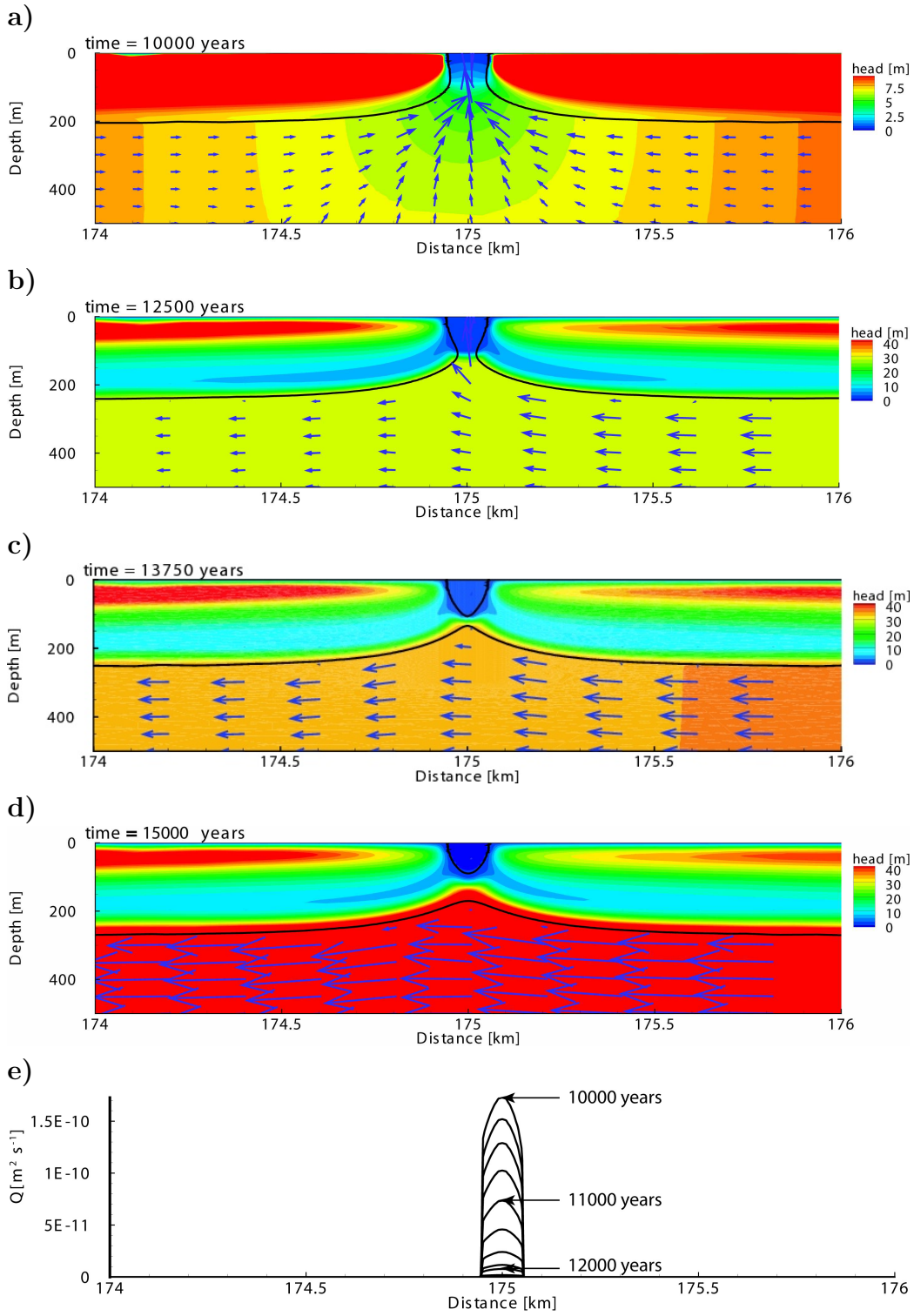

Figure 6.8: Detail of Figure 6.7 showing hydraulic head distribution, groundwater flow vectors and permafrost base under a lake of 100 m diameter for a transient, conduction and advection model (A3-1). Results are presented for a) 10,000 years, b) 12,500 years, c) 13,750 years, d) 15,000 years simulation time, and e) discharge into the lake for a 250 year interval. Models are run for a GST of -6°C and LBT of 4°C. Note different hydraulic head scales and that the flow vectors are not to scale.

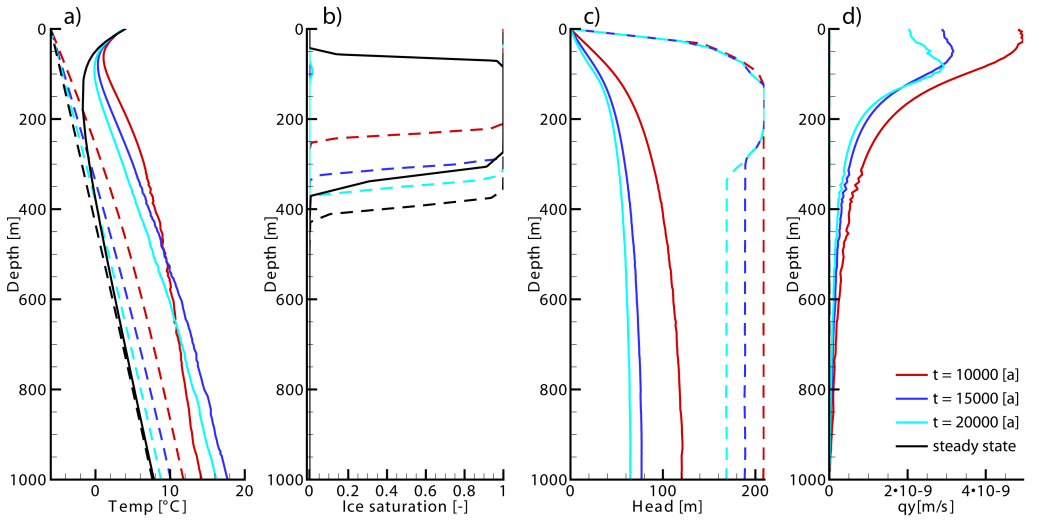

Figure 6.9: Profiles for a) temperature, b) ice saturation, c) hydraulic head, and d) vertical flow (q_y). The solid lines are for values under the middle of the talik and the dotted lines are for values 5 km next to the talik. Data shown are for a model run with GST of -6°C and a LBT of 4°C for model A3-1, and a steady state, model A0.

the permafrost than in the unfrozen material. The hydraulic head difference in the open talik between the surface and at depth decreases over time which results in a decrease in vertical groundwater flow over time (Figure 6.9d).

The influence of advective heat transport on talik closure is demonstrated by comparing the conduction only model (A1) with conduction and advection models (A2 and A3), for different aquifer properties, and is shown in Figure 6.10 for a GST of -6°C and LBT of 4°C (see Figure 6.11 for all model runs). For a lower specific aquifer storage of 10^{-6} m^{-1}, the influence of advective heat flow is relatively small. In this case the talik closure compared to the conduction only scenario gets delayed by 350 years where the hydraulic head follows the ice sheet thickness by a factor of 0.45 (model A2-1), and 700 years for the scenario where the hydraulic head follows the ice sheet thickness by a factor of 0.9 (model A3-1). For a scenario of larger aquifer specific storage of $1.6 \cdot 10^{-4}$ m^{-1}, the talik closure gets delayed compared to heat conduction by 4100 years for model A2-2, and does not freeze within the modelled time frame for model A3-2.

Figure 6.11 presents the complete sensitivity study for permafrost depth, ice saturation and discharge for a conduction only scenario (model A1), and for conduction and advection scenarios for different hydraulic boundaries and aquifer properties as described in Table 6.2. Ground surface temperatures (GSTs) of -6°C, -4°C, and -2°C and lake bottom temperatures (LBTs) of 4°C, 2°C, and 0°C are used.

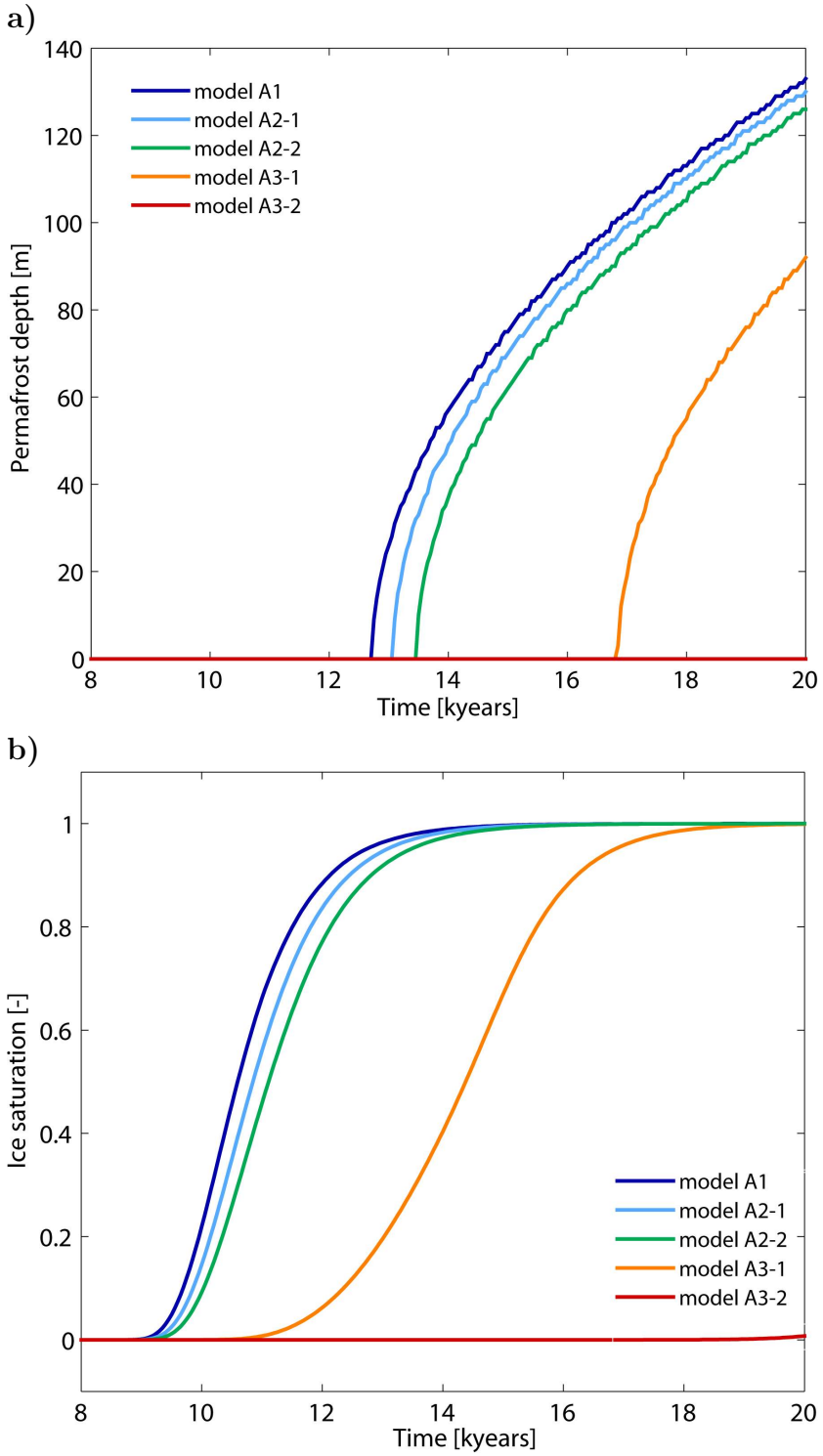

Figure 6.10: Comparison of a) permafrost depth and b) ice saturation of a talik of GST -6 °C and LBT of 4 °C for models with different hydraulic boundaries and aquifer properties as described in Table **??**. Advective heat flow is larger for a higher aquifer specific storage and higher hydraulic head gradients (model A3-2). Time is given in simulation time.

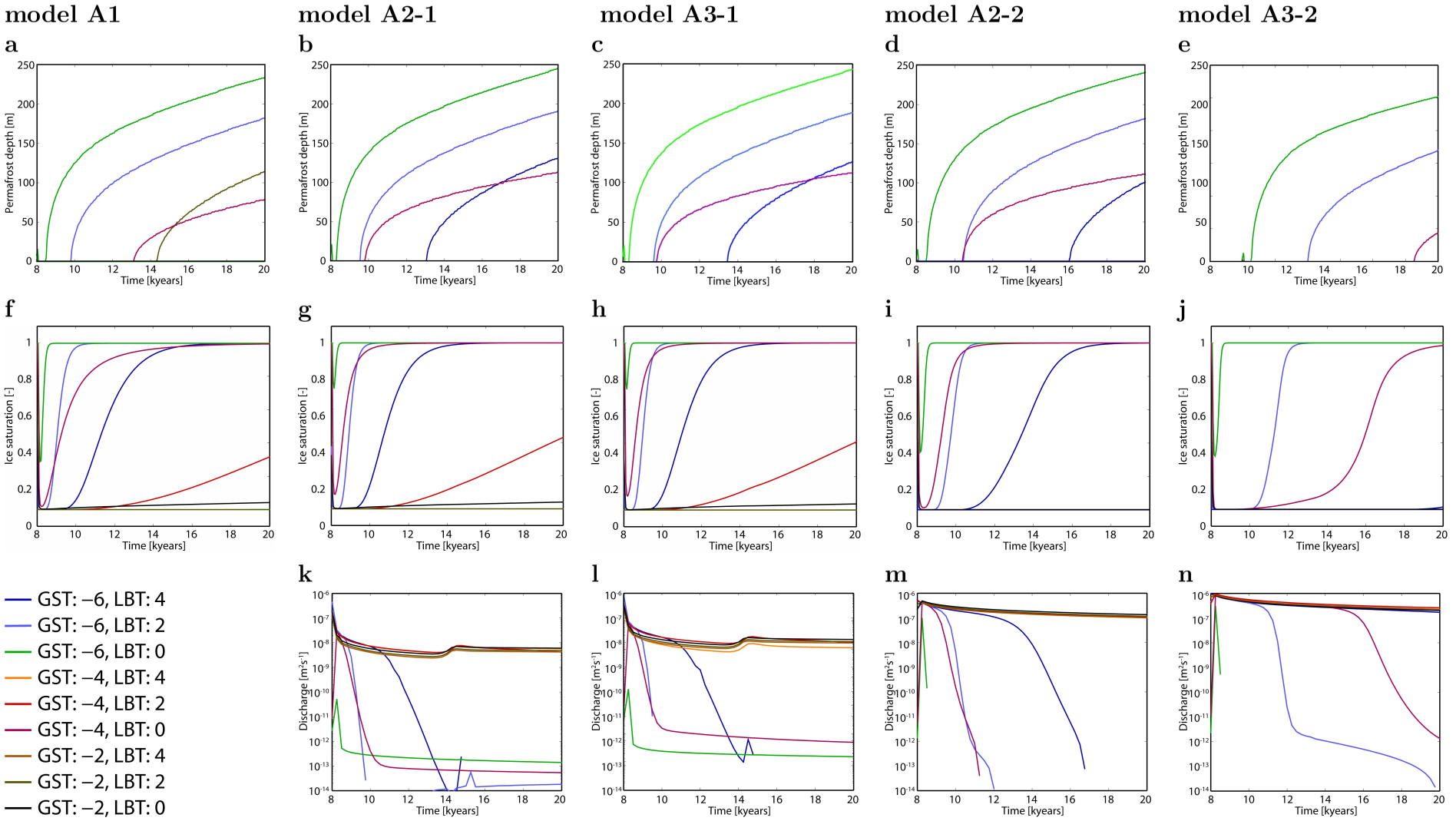

Figure 6.11: a - e) Permafrost depth under a lake of 100 m diameter. f - j) Maximum ice saturation under a lake of 100 m diameter. k - n) Discharge into the lake. Permafrost is defined as 95% ice saturation. GST is ground surface temperature and LBT is lake bottom temperature. All models are for a transient conduction only (model A1) and transient conduction and advection model (model A2 & A3) for a lower specific aquifer (S_s=10^{-6} [m^{-1}]) storage and a higher specific aquifer storage (S_s=$1.6 \cdot 10^{-4}$ [m^{-1}]).

Modelling permafrost formation under a 100 m wide lake after ice retreat for different lake bottom temperatures and ground surface temperatures considering heat conduction only, shows that for a GST of < -6°C all taliks freeze through between a few hundred years (LBT of 0°C) and up to 6000 a (LBT of 4°C) after ice retreat. For a GST of -4°C, only the talik with a LBT of 0°C freezes through (Figure 6.11 a). The freezing process of the taliks occurs over different time spans, depending on the LBT's; for a low LBT the talik freezes through quickly (hundred years) and for a higher LBT, the freezing process occurs over several thousand years. For two cases, lakes with a GST of -4°C and LBT of 2°C, as well as -2°C and 0°C, respectively are partially frozen and have not reached steady state during the modelling time (Figure 6.11 f).

Permafrost depth, ice saturation and discharge under a lake of 100 m diameter over time for GST ranging from -2°C to -6°C, LBT from 0°C to 4°C and for a hydraulic head boundary following the ice thickness by a factor of 0.45 (model A2) and 0.9 (model A3) are presented in Figure 6.11 (b-e, g-n). Discharge generally decreases over time, but peaks when the ice sheet readvances, responding to the regional hydraulic head gradients forced by the position of the ice sheet. The magnitude of discharge first decreases then the maximum ice saturation increases. When the ice saturation increases, discharge is decreasing at a faster rate and ceases. The permafrost formation under these lakes differs for model A2 and model A3; a higher head delays the freezing process. Using larger specific aquifer storage has the largest influence on the timing of permafrost formation.

6.4.4 Effects of several open taliks on the regional hydrogeology (model A3-1-3)

In addition to the influence of the ice sheet history, the occurrence of more than one lake further influences the hydraulic head distribution, and as a consequence the larger scale hydrogeology. As shown above, the existence of a through talik creates a hydraulic head minimum underneath an open talik, resulting in a reversal of the groundwater flow direction near the talik. Where there are several taliks adjacent to each other, the water divide occurs between two open taliks and convergences under each talik (Figure 6.12a). The high hydraulic head difference across the model domain under the permafrost decreases over time from up to tens of meters (Figure 6.12a) to meters (Figure 6.12b) and millimetres (Figure 6.12c).

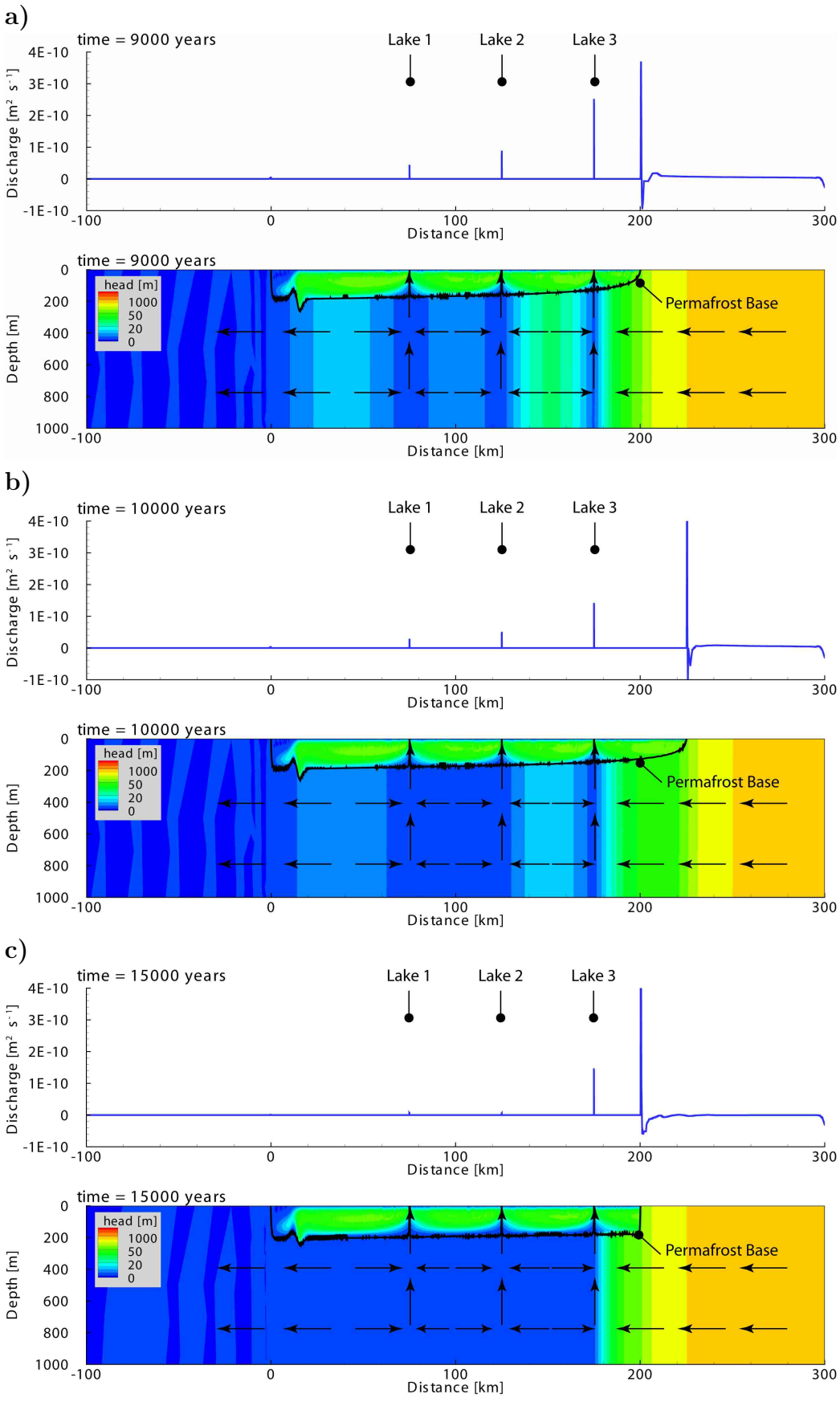

Figure 6.12: Surface discharge, hydraulic head and permafrost distribution with 3 lakes at 75, 125 and 175 km of the model domain (model A3-1-3) for a) 9000 years, b) 10,000 years and c) 15,000 years of simulation time. Models are run for a GST of -4°C and LBT of 4°C. The flow vectors are not to scale.

6.4.5 Effects of isostatic uplift and Tóthian topography on the regional hydrogeology (model B)

The effect of isostatic uplift further complicates the hydraulic head distribution, as the hydraulic head follows the surface elevation (Figure 6.13). With uplift, the higher hydraulic heads, as defined on the surface, propagate through the unfrozen ground and respond to the current surface elevations. The propagation of the higher heads from the surface into the aquifer results in the lakes acting as a groundwater recharge into the aquifer and not as a groundwater discharge as in the models A2 and A3. Different uplift rates over the model domain result in spatially different rates of change of the hydraulic head distribution. In addition, relative higher hydraulic heads from non-permafrost areas propagate underneath the permafrost, as can be observed at around distance = 80 km of the model domain (Figure 6.13).

The impact of the Tóthian topography (*Tóth*, 1963) as modelled here has a minor influence on the groundwater flow pattern.

6.5 Discussion and Conclusion

This chapter evaluates the influence of regional groundwater driven by ice sheet movement and associated advective heat transfer on the talik evolution of proglacial lakes since the LGM. This is done by comparison of simulated talik evolution under a proglacial lake for steady state and transient models including or excluding the effects of advective heat flow by groundwater flow.

The results from the models including advective heat flow demonstrate how local boundary conditions of a proglacial lake are controlled by larger scale processes of a retreating ice sheet by determining the hydraulic and thermal boundary conditions at the surface. Groundwater discharge into the lake is mainly driven by an elastic storage response, releasing water from the bedrock aquifer after deglaciation (Figure 6.14). During a glaciation, hydraulic heads underneath the wet-based ice sheet are driven by the hydrostatic pressure of the ice sheet (Figure 6.14a). Higher hydraulic heads at depth than at the surface are preserved underneath the newly formed permafrost after deglaciation. When a talik forms, lower hydraulic head from the surface penetrates into the subsurface, resulting in a decreasing hydraulic head gradient (Figure 6.14b-c). In addition, high subglacial heads can propagate into the proglacial area. The hydraulic head gradient drives relatively warm subpermafrost groundwater to discharge through the talik into the lake. As long as the upward advective heat flow is larger than the lateral

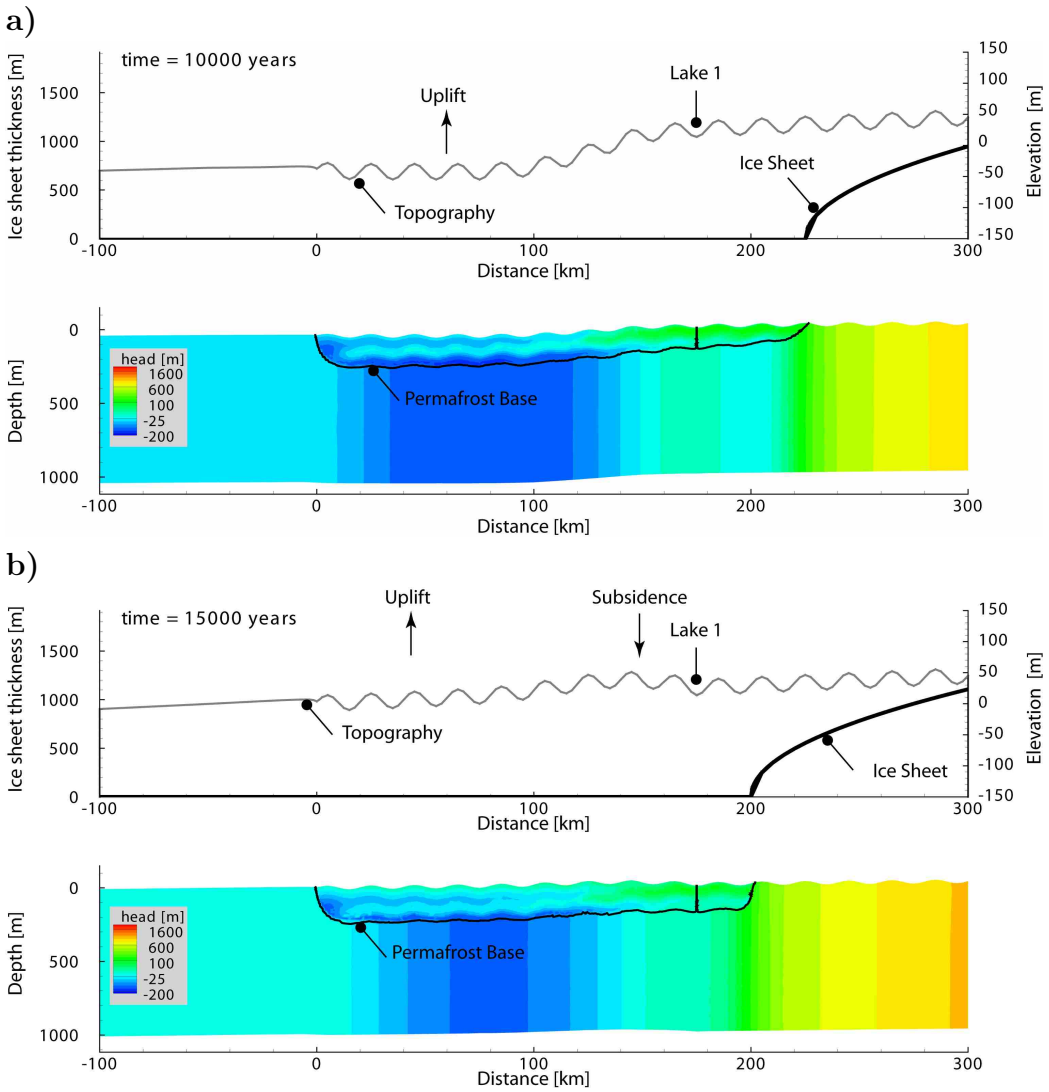

Figure 6.13: Permafrost depth, hydraulic head and groundwater flow direction for a transient, conduction and advection model including Tóthian topography and isostatic rebound (model B), for 10,000 years, and 15,000 years simulation time. Models are run for a GST of -4°C and LBT of 4°C.

conductive heat flow cooling the talik from the sides, the permafrost is thermally eroded and the talik gets enlarged. Hence, when the upward advective heat flow decreases, the size of the talik decreases and eventually disappears (Figure 6.14c).

We find that permafrost formation and change in hydraulic heads surrounding the talik interact, resulting in a complex pattern of hydraulic head gradients that changes over time. The models presented here considerably expand on the complexity of previous talik models under surface water bodies (*Rowland et al.*, 2011; *Grenier et al.*, 2013; *Wellman et al.*, 2013) which assume the hydraulic boundary conditions to be non-changing over time.

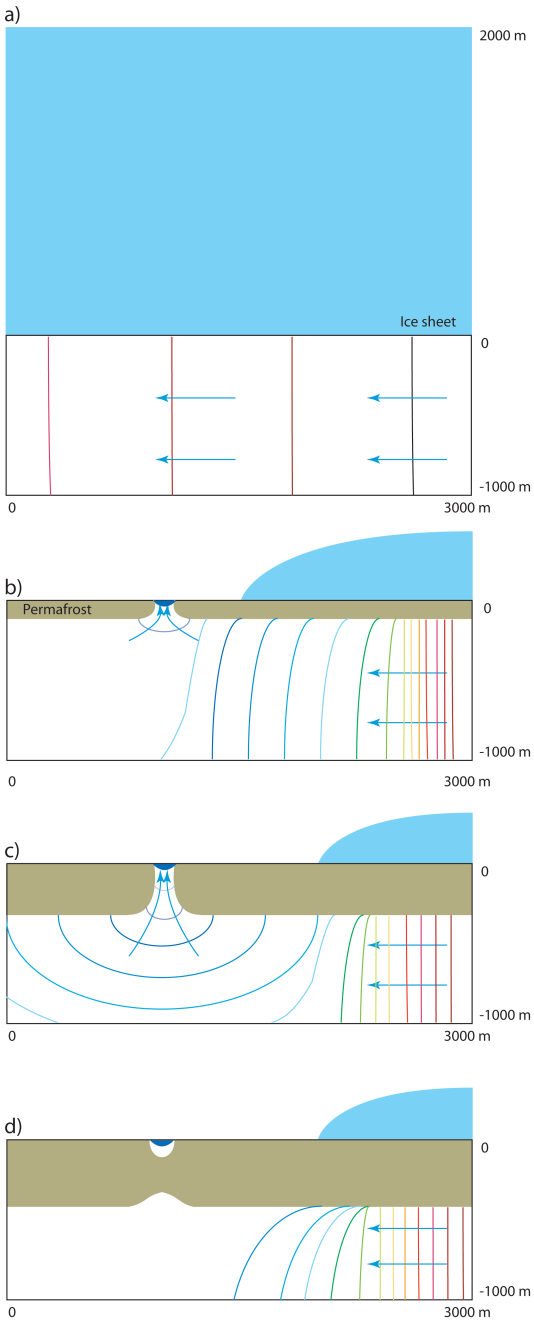

Figure 6.14: Conceptual model of the mechanism of groundwater discharge into a proglacial lake. The contours represent hydraulic head whereas blue is low and red a high value. a) During a glaciation, hydraulic heads underneath the wet based ice sheet are high and are driven by the hydrostatic pressure of the ice sheet. b-c) After ice retreat, the hydraulic heads at the surface have decreased by several 1000 m, however the hydraulic head underneath the permafrost remain high. Through an open talik, low hydraulic heads penetrate and force groundwater to discharge into the lake. In addition, subglacial hydraulic heads propagate into the proglacial area. The duration of this groundwater discharge into the lake depends on the amount of elastic storage of groundwater from the previously ice covered period. d) Once groundwater flow has decreased to a critical threshold, advective heat flow is not large enough and the through talik will close. After the through talik has closed, the hydraulic heads increase again underneath the former through talik.

The talik geometry is primarily controlled by the thermal boundary conditions (model A1). These constitute the lake radius, the lake bottom temperature (LBT), the temperature of the surrounding permafrost and the geothermal gradient govern the talik configuration. We did not vary lake size and geothermal gradient are not shown in this study, as we focus on ground surface temperature (GST) and LBT. However, for steady state models, an increase in LBT by 1°C can determine the presence or absence of ice of a depth profile under the lake centre. This would imply that for small lakes for which the LBT follows GST, climate change and associated increase in LBT may decrease the permafrost thickness underneath the lake, and may result in the formation of through taliks. However, comparing the transient conduction only scenario (model A1) with the steady state conduction only scenario (model A0) demonstrates that the permafrost formation under the lake has not yet reached a steady state for the transient models over a time scale of 12,000 years. Thus, this long response time to steady state conditions under lakes is an important factor to consider for larger scale models. Examples include models that estimate permafrost distribution with a steady state (e.g. TTOP model, *Henry and Smith*, 2001; *Juliussen and Humlum*, 2007) in regions with many lakes, or steady state models that estimate ground temperatures under lakes (*Mackay*, 1962; *Burn*, 2002). The latter type of models may seriously overestimate the permafrost thickness. Moreover, hydrogeological models that do not couple heat and fluid flow (*Bosson et al.*, 2012) may overestimate the permafrost distribution under surface water bodies.

In our model, the general groundwater flow direction is from the ice sheet towards the sea, however taliks can locally reverse the groundwater flow direction creating a groundwater flow divide and groundwater flow convergence at the talik. After talik closure, it will take several thousand years for the groundwater flow direction downstream of previous open taliks to reach its initial flow direction being from the ice sheet towards the sea (Figure 6.7). The larger scale hydrogeology is thus affected by the existence of through taliks, and the occurrence of several open taliks can result in a complex hydrogeological pattern for several open through taliks (Figure 6.12).

The flow direction through taliks gets further complicated by the influence of isostatic uplift on the hydraulic head distribution (model B). Changes of the deeper hydraulic heads lag behind those at the surface. Therefore, uplift with associated higher hydraulic heads at the surface results in down-welling of groundwater through the talik (Figure 6.13). However, the influence of uplift and undulating topography as used in model B has a minor influence

on the regional scale hydrogeology. Although not considered here, it could be expected that the surface topography of deeper lakes and fiords would have a larger impact.

In addition to the thermal boundaries, advective heat flow can have a large impact on the closure time of a talik. This has been confirmed with lake talik models using a set hydraulic boundary (*Rowland et al.*, 2011; *Grenier et al.*, 2013), and groundwater flow has been hypothesized to have an equally dominant control on talik evolution as climatic drivers (e.g. surface temperature) (*Wellman et al.*, 2013). However, here we find that the magnitude of advective heat flow is strongly dependent on the amount of groundwater flow, which in a transient system as described here is dependent on the aquifer specific storage and permeability. Depending on the aquifer properties, groundwater flow, and with it the associated advective heat flow component, has different response times to changing boundary conditions. An aquifer with a larger specific aquifer specific storage responds slower to changing boundary conditions. Paleo-effects of past ice sheet driven hydrogeology can influence the hydrogeology for millennia (*Bense and Person*, 2008), whereas an aquifer with a smaller aquifer specific storage is more sensitive to changing boundary conditions, and thus the model reacts faster to the moving ice sheet and reaches a steady state more quickly. This can be observed by the effect of the advancing ice sheet on discharge into the lake, which is only visible for a lower aquifer specific storage (10^{-6} m^{-1}), whereas for a higher aquifer specific storage ($1.6 \cdot 10^{-4}$ m^{-1}) no clear change can be seen (Appendix, Figure 6.11). This implies that for low porosity rock with a low aquifer specific storage the influence of advective heat flow is small and that the taliks are mainly 'conductive taliks'. However, for fissured and jointed rock as found in fault zones, advective heat flow is large and taliks are predominantly 'advective-conductive taliks'. Thus, a primary factor to consider for talik modelling is the aquifer specific storage of an aquifer, which can range over several orders of magnitudes for crystalline rock (*Domenico and Mifflin*, 1965). The importance of changing aquifer specific storage with permafrost degradation and hydraulic head increase has been confirmed with numerical modelling, and uptake of groundwater into elastic aquifer storage has been found to be most profound for low permeability and high specific storage aquifers (*Bense et al.*, 2012). In the models presented here, an elastic release of groundwater with decreasing hydraulic heads after ice retreat is found.

Comparison of the model output with field observations is difficult for

several reasons. First, field data enabling a direct comparison of permafrost occurrence are sparse and most temperature measurements are from boreholes (e.g. *SKB*, 2011). An exception is the surveying with airborne electromagnetic imaging under lakes and rivers that provides a 3D distribution of permafrost (*Minsley et al.*, 2012; *Jepsen et al.*, 2013). Geochemical analysis (e.g. *Clark et al.*, 2001; *Stotler et al.*, 2011; *Utting et al.*, 2012) can provide evidence for groundwater sources in surface water bodies. However, modelling input parameters, such as hydraulic head distribution, hydraulic conductivities and their spacial distribution are usually unknown.

Further to the uncertainties in model input parameters, uncertainties in processes covered and transfer functions describing ice saturation or permeability reduction over the freezing interval complicate a direct comparison (*Ireson et al.*, 2013). The timing of permafrost thaw or formation is also influenced by the definition of the temperature interval over which freeze/thaw occurs, with a wider freezing interval leading to later, and a narrower freezing interval leading to earlier talik closure (*McKenzie et al.*, 2007). In addition, the impacts of mechanical loading and unloading by the ice sheet are not included in this study, which impacts the fluid pressures in previously ice covered areas (*Bense and Person*, 2008). However, the compressibility values for crystalline rocks applied in this study are very low (*Domenico and Schwarz*, 1998; *Vidstrand et al.*, 2012), and were therefore neglected.

This model can be applied to regions of crystalline bedrock in front of a dynamic ice sheet that has been wet-based for the whole simulation period, which is valid for most of Greenland (*Huybrechts*, 1996). Where the glacier is polythermal (e.g. Arctic Canada and Svalbard), recharge only occurs in the wet-based parts of the glaciers and where there is no permafrost underlying the ice. For those regions, a model like the one used here will thus probably overestimate rates of subglacial recharge. The models described here are valid for a lake that formed immediately after ice retreat, which has been observed in West Greenland (*Willemse*, 2002).

Ongoing climate change can influence talik systems in several ways. First, ground surface temperature increase and increase of the lake bottom temperature will lead to the formation of more hydraulically conductive through taliks, enabling a groundwater surface water connection. These new through taliks may then shift the general groundwater flow direction near the talik to discharge into the lake. Second, with ice sheet dynamics, hydraulic head gradients will alter, and will thus affect the groundwater recharge and the hydraulic head distribution at near ice-marginal positions. Third, glacier

thinning may result in the glacier bed thermal regime becoming cold-based, inhibiting any further recharge. This has been observed at Ester Mine spring in Svalbard, where the spring discharge ceased after the recharging glacier had become cold based (*Haldorsen et al.*, 2010). Fourth, new regions will become ice free, enhancing the potential for more proglacial lakes to develop.

This study shows that permafrost regions in front of glaciers and ice sheets might be hydrogeologically active and that strong vertical fluxes through taliks under surface water bodies can occur. This enables the transport of pollutants from mining; as for example mines for rare Earth minerals and zinc are becoming increasingly popular in Greenland, and uranium-thorium mining is being considered (*GEUS and BMP*, 2011, 2013). In addition these types of models can be used for assessing the potential of groundwater movement around potential nuclear waste storage sites under future glaciation scenarios.

In summary, in this study we find that in glaciated regions near an ice margin the hydrogeology is complex and transient and cannot be modelled with a static hydraulic head boundary. In addition, advective heat flow can be large depending on the aquifer properties and through taliks can exist in areas where heat conduction only would not suggest a through talik.

Chapter 7

Summary and Conclusions

7.1 Summary

The principal aim of this thesis is to improve our understanding of the impacts of permafrost dynamics on Arctic groundwater flow systems. Despite the numerous recent studies of hydrogeology in permafrost covered areas, this topic still requires further research. This is because observed Arctic hydrological changes might be caused by a change in the hydrogeology of these areas and is suggested to response to a warming climate. The case studies presented in this thesis are summarised below and address the aims outlined in Chapter 1.

The first study aims to develop a model to estimate lake bottom temperatures for different climatic scenarios and lake sizes. In Chapter 3, a method to estimate the lake bottom temperature for different lake sizes and ground surface temperatures is developed. This model is compared to measured lake bottom temperatures from the literature, to which the modelled lake bottom temperatures agree well. Model results for a generic lake demonstrates that only shallow lakes (<2 m), or in environments with mean annual ground surface temperatures <10°C, are expected to be on average below freezing. Other lakes have a mean lake bottom temperature above freezing and develop a talik underneath. The modelled lake bottom temperatures are subsequently used in Chapter 4.

In Chapter 4, the aim is to estimate the response of the temperature regime underneath a lake with the influence of surface temperature warming, considering different hydraulic scenarios. The model developed in Chapter 3 is applied as a boundary condition to model talik evolution under a surface warming scenario or a lake growing scenario in Chapter 4. Results presented this chapter show that as a lake forms, it behaves in a purely conductive

manner, as long as permafrost impedes a groundwater surface water connection. However, as soon as a talik develops, the system changes from a purely conductive system to an advective-conductive system. This pattern is similar for a lake, where no through talik is found under the initial temperature distribution, but under a lake warming scenario, a through talik gets formed. The groundwater flow direction determines whether permafrost gets migrated, eroded or aggregated at a certain location. In addition, we find that hydraulic head gradients need to be large in order for advective heat flow to be sufficient to alter the permafrost distribution from the conduction only scenario. Furthermore, in a region that is subject to permafrost dynamics, the onset of the influence of advective heat flow is strongly influenced by the choice of function of hydraulic conductivity decrease over the freezing process. As this function is highly variable on the ground studied, more research is needed to estimate this function, in order to make the models used more site specific.

As noted in Chapter 4, groundwater recharge is likely to be a limiting factor for advective heat flow to significantly influence permafrost distribution. Groundwater flow is not likely to be a limiting factor where groundwater flow is not primarily driven by precipitation, is strongly focussed, or where there are heat flow anomalies. In Chapters 5 and 6 two different case studies of glacial recharged groundwater flow systems are studied. The aim in Chapter 5 is to better understand the dynamics of a spring system that is fed by a glacial meltwater source. A supraglacial spring system as found at Borup Fiord Pass, Ellesmere Island, Canadian High Arctic is modelled. This site suggests that the High Arctic might be more hydrogeologically active than previously recognised. The model results presented in Chapter 5 suggest that spring systems surrounded by permafrost cannot be explained as a steady state phenomenon, but have to be explained as a transient feature that can persist for millennia after freezing from the top has started. The lifetime of a spring system as modelled in Chapter 5 relates nonlinearly to the hydraulic head differential and to the width of the high permeable spring channel.

Chapter 6 improves our understanding of talik evolution and groundwater movement in front of a dynamic, wet-based ice sheet. Proglacial lakes found in front of a dynamic ice sheet and the influence of advective heat flow on talik evolution are both evaluated, and also the influence of the existence of a through talik on the regional scale hydrogeology. This chapter expands the models presented in Chapters 4 and 5 by considering a changing hydraulic boundary condition over time, and by using a larger scale model to

set the local boundary conditions surrounding a lake. Results show that the hydrogeology of a proglacial lake in front of a dynamic wet-based ice sheet is controlled by larger scale processes and is strongly affected by the paleo-hydrogeology. Advective heat flow can have a strong influence on the talik evolution under proglacial lakes. However, the magnitude of this influence is strongly dependent on the aquifer properties, especially aquifer storage. Under glaciated conditions, groundwater is uptaken into elastic aquifer storage and released after the ice has retreated locally. In addition to the influence of groundwater flow on the talik evolution, the groundwater flow direction is influenced by the existence of through taliks. The initial groundwater flow direction downstream of open taiks gets reversed after a talik has opened. Even after talik closure, reversed groundwater flow direction can persist for several thousand years. Thus the existence or previous occurrence of through taliks can influence the larger scale hydrogeological pattern.

7.2 Conclusions

This thesis demonstrates that mathematical modelling of conceptual models can be used as a powerful tool to investigate the dynamics of coupled permafrost and hydrogeologic systems, and allows the study of the relative importance of different input factors.

The systems modelled in this thesis are transient and non-linear. Results of a model estimating lake bed temperatures demonstrates that only shallow lakes (< 2 m), or in environments with mean annual ground surface temperatures < 10°C, are expected to be on average below freezing. Other lakes have a mean lake bottom temperature above freezing and develop a talik underneath (Chapter 3). A talik underneath a surface water body can take several hundred to thousands of years to respond to changing surface boundary conditions, such as climate warming, or evolution and growth of a lake. In addition, when sufficient groundwater flow is present, transient processes of aquifer storage and heat storage affect the permafrost dynamics by the means of latent heat and advective heat flow. Heat advection by groundwater flow can influence the permafrost distribution by permafrost erosion and aggregation. However, this effect depends on the permafrost-permeability-reduction function and further research in the quantification of this function for different ground types are needed (Chapter 4). In lowland regions (Chapter 4), the magnitude of groundwater flow is likely a limiting factor to influence the permafrost distribution, which contrast areas of high

hydraulic head gradients or strongly focused flow. An example dominated by advective heat flow is a local system of the evolution of a proglacial spring surrounded by permafrost, for which modelling suggest that these systems are transient and non-linear (Chapter 5). Chapter 6 up-scales the model from Chapters 4&5 and studies glacially recharged groundwater of a dynamic ice sheet, discharging into proglacial taliks. Results show that when hydraulic head changes over time are large, as in previously glaciated regions, groundwater flow from elastic storage has the potential to dominate the heat flow by advective heat transport over millennia. Thus, the proglacial hydrogeology is strongly driven by larger scale processes and paleohydrogeology (Chapter 6).

7.3 Wider impact

The main benefit of this thesis is to advance the study of first principles of permafrost hydrogeology. This thesis also contributes to technical advances in numerical modelling of coupled heat- and fluid-flow in permafrost. In addition, findings from this thesis have benefits to industry in the assessment of potential sites of waste storage in the Arctic or for future glaciation scenarios.

7.3.1 Academic progress

Academic contribution is achieved in technical advances and in the understanding of permafrost hydrogeology of glacial recharged groundwater. This thesis carries out research of the first principles in the application of conceptual models of permafrost hydrogeology to different talik settings.

7.3.1.1 Technical advances

The following technical advances have been undertaken in hydrogeological modelling permafrost regions. In Chapter 3, a method is presented in which a modelled system can be switched easily between a conduction dominated system and an advection dominated system. This method is applied to model the lake bottom temperature in a ice covered lake during the winter season. The method can be used to estimate the lake bottom temperature of any small lakes that are fully mixed during the summer and are ice covered during the winter.

The second part of Chapter 4 compares talik models using different permafrost-permeability-reduction functions. The result that the choice of the freezing interval can have a profound impact on whether a through talik

develops under a lake is of high importance. Therefore, especially when modelling partially frozen soil, the permafrost-permeability-reduction functions is highly sensitive to the amount of groundwater flow, and hence to advective heat transport eroding permafrost under a surface water body. More field and laboratory experiments are required to estimate functions of hydraulic conductivity with ice saturation or temperature for different materials.

In Chapter 6, a large scale (400 km) model is used to set the boundary conditions for a small scale model (100 m) by model scaling. This has not been previously done in hydrogeological modelling in permafrost regions. This approach allows a model of a local system to be dependent on larger scale processes, and is applied to a talik in front of a dynamic ice sheet, whose thickness and extent set the hydraulic head boundaries of the model domain over time.

7.3.1.2 Advance in system understanding

In Chapters 4-6 there was an emphasis on the importance of transient processes to explain the permafrost distribution and the hydrogeology in Arctic systems. With a change in the boundary conditions; either a temperature change at the surface due to climate change or change of a lake size, or a change in the hydraulic head boundary conditions due to e.g. glacier dynamics; the system can take hundreds to thousand years (Chapter 4) or up to several 10,000 years (Chapters 5 and 6) to respond to the new boundary conditions. Therefore, the transient processes of aquifer storage effects and heat storage effects can affect the occurrence of a through talik by the effect of latent heat and advective heat flow. Thus the present day or future distribution of through taliks might be driven by past boundary conditions. This is seen when a system is advection driven, there is a non-linear relationship between flow and the cut-off time of the groundwater surface water connection, as seen in Chapter 5.

There is a feedback between groundwater flow and the existence of through taliks; first advective heat flow through groundwater flow can determine the existence of through taliks. Also, the occurrence of through taliks can influence the groundwater flow direction in a larger scale setting and locally reverse the groundwater flow direction, as in Chapter 6.

7.3.2 Benefit to industry and society

This thesis demonstrates that permafrost covered regions might be hydrogeologically active, despite thick permafrost coverage that is seen as impermeable. This is particularly important in ice-marginal locations, as discussed in Chapters 5 and 6, where strong vertical groundwater fluxes along fault zones or under surface water bodies can occur, that have been recharged from underneath an ice sheet. Over longer time scales transport of pollutants from mining or from nuclear waste disposal sites might still be possible (*Iverson and Person*, 2012; *GEUS and BMP*, 2013). In addition, of great importance to the climate system and and ecosystem are increased nutrient and carbon release from organic matter and transport through the freshwater network, caused by a increased baseflow contribution to surface water bodies (*O'Donnell et al.*, 2012).

7.4 Questions and further research

This thesis has investigated hydrogeologic change under changing surface temperature and/or glaciation scenarios by the means of numerical modelling. Verifying and comparing these models is difficult, as only limited field data and laboratory experiments are available. Therefore, a crucial expansion of hydrogeologic studies in permafrost is by the means of field studies and laboratory experiments. Some ideas for further research are outlined below.

7.4.1 Field studies

Field studies that are related to Chapter 6 would allow us to quantify the hydrogeological activity in a proglacial area. Chapter 6 demonstrates with numerical modelling that proglacial areas in front of an ice sheet may be hydrogeolocial active, that groundwater surface water connections can exist underneath small lakes, and that the larger scale hydrogeology may be influenced by the existence of open taliks. Quantifying permafrost distribution around proglacial lakes, groundwater discharge or recharge in a proglacial lake and the characterisation of hydraulic head gradients would expand and validate the study from Chapter 6. Possible research questions include:

Imaging of the permafrost distribution around lakes. The distribution of permafrost and taliks is crucial in order to assess a potential groundwater surface-water connection. For example using airborne electromagnetic imaging, as used in the Yukon river basin (*Minsley et al.*, 2012). Another approach to characterise the permafrofrost characteristics is with a combination of Electrical Resistivity Tomography (ERT) and refraction seismic, for which a 4-phase model allows us to differentiate between the ice content, the water content and the air content (*Hauck et al.*, 2011). With Vertical Electrical Sounding (VES), the thickness of permafrost up to several hundred meters can be measured (*Borzotta and Trombotto*, 2004).

Characterisation of seepage in river and lake beds. Measurement of groundwater discharge can be quantified with heat as a tracer. For example, groundwater seepage into surface water bodies can be detected by infrared photography (*Pandey et al.*, 2013) or through airborne infrared imaging (*Wirth et al.*, 2012). In addition, the fibre-optic based Distributed Temperature Sensing (DTS) can be used to measure a high spatial and temporal resolution of temperatures at a stream bed or lake bed (*Selker et al.*, 2006). A time series of temperature distributions across a lake bed can be a tracer for groundwater fluxes into the lake that have a different temperature to the lake water temperature. It is expected that during summer months, the inflowing groundwater is cooler than the lake water, and during winter months the groundwater is warmer than the lake water.

Characterisation of hydraulic heads in the subsurface. The hydraulic head distribution near surface water bodies and their dynamics associated with permafrost dynamics would be an interesting subject of research. A seasonal variation in hydraulic head has been measured in a thermokarst pond (*Yoshikawa and Hinzman*, 2003). With the models applied in this thesis, very high hydraulic head gradients are predicted when a through talik is opening. It would be interesting to investigate how the hydraulic head distribution changes with permafrost dynamics both spatially and temporally.

7.4.2 Laboratory experiments

Experimental quantification of freezing functions (Θ_w) and permafrost-permeability-reduction functions (k_{rw}). As discussed in Chapter 4, the function describing the phase change from water to ice and the function of hydraulic conductivity decrease with temperature around the freezing point

are dependent on the properties of the specified ground. There are numerous measurements for soil, however, there is no experimental data for the hydraulic conductivity decrease function for consolidated rock.

Experimental quantification of hydraulic head change over freezing and thawing. As discussed above, the variation in hydraulic head gradient in as a function of dynamic permafrost is unknown and could be quantified with laboratory experiments.

7.4.3 Model development

The model applied in this thesis models groundwater flow in permafrost for fully saturated conditions. The following changes to the model could be made:

Model the LBT for a lake that is stratified under unfrozen conditions. The model developed in Chapter 3 to model LBT for a fully mixed lake under ice free conditions could be adapted to measure the temperature distribution along a lake bed for a stratified lake, by including density driven overturning.

Modelling of shallow groundwater flow contribution to lakes. In Chapter 4, the model could be expanded to model shallow groundwater flow through the active layer. This could either be done by using fully saturated conditions, as applied for the rest of the thesis, or by modifying the code to unsaturated fluid flow. For the latter however, a different FE solver would be required, because a cluster would be required due to the greater model complexity.

Site-specific modelling of a spring system. In Chapter 5, the modelled spring discharge underestimates the observed spring discharge by one to two orders of magnitudes. This discrepancy between observed and modelled discharge is due to parameter uncertainty and unknown hydraulic head gradients. A larger hydraulic head gradient, higher hydraulic conductivity, a larger fault zone or groundwater that is released from aquifer storage would contribute to a higher spring discharge. In addition, using a 3D model could increase the flow rate by focusing the spring flow to a single point, resulting in higher local discharges. In the scenario, where hydraulic conductivity is heterogeneous, a different distribution in log-normally distributed

hydraulic conductivity alters the location and the magnitude of the peak discharge. More model realisations altering the hydraulic conductivity distribution could represent the observed discharges more closely than the single realisation presented in Chapter 5.

Modelling of springs on Mars. In Chapter 5 the transient evolution of spring systems that are driven by hydraulic head gradients from the base to the top of the model domain, as found in front of glaciers or ice sheets, is studied. In the discussion of this chapter, it is mentioned that this mechanism could provide a groundwater-surface water connection for springs on Mars. In order to expand on this hypothesis, modelling of a spring system, as presented in Chapter 5, could be carried out and adapted to parameters that are valid for a Martian environment (e.g. gravity, freezing point, surface temperature).

Further development of the ice sheet driven groundwater model. In Chapter 6, the taliks are forced by imposing a positive lake bottom temperature at the top boundary of the model. These taliks will enable a groundwater-surface water connection by a combination of heat conduction from the surface and heat advection by groundwater flow. Alternatively, heat advection could be the only driving force, similar to the spring system modelled in Chapter 5. Instead of imposing the location of the talik by setting the surface temperature to a sub-zero value, subsurface heterogeneity could be added, representing high-permeability fracture and fault zones. In addition, groundwater can discharge at the permafrost boundary near the ice margin without the added subsurface heterogeneity or temperature surface boundary. Discharge here is larger than into the taliks, as the hydraulic gradients at the ice margin are very large.

The model presented in Chapter 6 is held as simple as possible; however complexity could be added step-wise. Step-wise added complexity already presented in Chapter 6 include the occurrence of several open taliks, and the effect of isostatic uplift with an undulating topography. For the latter, the effect of isostatic uplift is found to be dominant, changing the groundwater flow direction into the talik. More simulations investigating the effect of isostatic uplift on a similar system would expand the presented work. For a site-specific realisation, the effect of topography and subsurface heterogeneity could be included. By using a spatially more complex model, a 3D realisation could help to model lake taliks more realistically. For example, the conceptualisation of circular lakes in 2D is difficult, as lakes in 2D are represented as

infinitely long lakes, or rivers. In addition, topographic heterogeneity could be represented as non-parallel. A further addition to the existing model is the inclusion of seasonal variation, in order to include a seasonal shallow groundwater flow component into the lake. However, for most of the above mentioned possible model extensions, it would be necessary to run the model on a more powerful computer or cluster.

References

Abbott, M., and J. Refsgaard (Eds.), *Distributed hydrological modelling*, Springer, 1996.

Allen, M., I. Herrera, and P. G.F., *Numerical Modeling in Science and Engineering*, John Wiley, 1988.

Amon, R., et al., Dissolved organic matter sources in large Arctic rivers, *Geochimica et Cosmochimica Acta*, *94*, 217–237, doi:10.1016/j.gca.2012.07.015, 2012.

Andersen, D., W. Pollard, and C. McKay, The Perennial Springs of Axel Heiberg Island as an Analogue for Groundwtater Discharge on Mars, in *Ninth International Conference on Permafrost*, vol. 1, edited by D. Kane and K. Hinkel, pp. 43–48, 2008.

Andersen, D. T., W. H. Pollard, C. P. McKay, and J. Heldmann, Cold springs in permafrost on Earth and Mars, *Journal of Geophysical Research E: Planets*, *107*(E3), doi:10.1029/2000JE001436, 2002.

Andersen, D. T., C. P. McKay, W. H. Pollard, and J. Heldmann, Cold springs in permafrost on Earth and Mars (vol 107, pg 5015, 2002), *Journal of Geophysical Research E: Planets*, *110*(E4), E04,007, doi:10.1029/2004JE002384, 2005.

Arctic Portal, Interactive data map, 2013.

Azmatch, T., D. C. Sego, L. U. Arenson, and K. Biggar, Using soil freezing characteristic curve to estimate the hydraulic condcutivity function of partially frozen sioils, *Cold Regions Science and Technology*, *83–84*, 103–109, doi:10.1016/j.coldregions.2012.07.002, 2012.

Bense, V. F., and M. A. Person, Transient hydrodynamics within intercratonic sedimentary basins during glacial cycles, *Journal of Geophysical Research F: Earth Surface*, *113*(F4), doi:10.1029/2007JF000969, 2008.

Bense, V. F., G. Ferguson, and H. Kooi, Evolution of shallow groundwater flow systems in areas of degrading permafrost, *Geophysical Research Letters*, *36*, doi:10.1029/2009GL039225, 2009.

Bense, V. F., H. Kooi, G. Ferguson, and T. Read, Permafrost degradation as a control on hydrogeological regime shifts in a warming climate,

Journal of Geophysical Research F: Earth Surface, *117*, F03,036, doi: 10.1029/2011JF002143, 2012.

Borzotta, E., and D. Trombotto, Correlation between frozen ground thickness measured in Antarctica and permafrost thickness estimated on the basis of the heat flow obtained from magnetotelluric soundings, *Cold Regions Science and Technology*, *40*(1-2), 81–96, doi:10.1016/j.coldregions.2004.06.002, 2004.

Bosson, E., U. Sabel, L. Gustafsson, M. Sassner, and G. Destouni, Influences of shifts in climate, landscape, and permafrost on terrestrial hydrology, *Journal of Geophysical Research D: Atmospheres*, *117*(5), doi: 10.1029/2011JD016429, 2012.

Boulton, G. S., and P. Caban, Groundwater-flow beneath ice sheets: Part ii - its impact on glacier tectonic structures and moraine formation, *Quaternary Science Reviews*, *14*(6), 563–587, 1995.

Boulton, G. S., T. Slot, K. Blessing, P. Glasbergen, T. Leijnse, and K. Vangijssel, Deep circulation of groundwater in overpressured subglacial aquifers and its geological consequences, *Quaternary Science Reviews*, *12*(9), 739–745, doi:10.1016/0277-3791(93)90014-D, 1993.

Brabets, T., and M. Walvoord, Trends in streamflow in the Yukon River Basin from 1944 to 2005 and the influence of the Pacific Decadal Oscillation, *Journal of Hydrology*, *371*(1-4), 108–119, doi:10.1016/j.jhydrol.2009.03.018, 2009.

Breemer, C., P. Clark, and R. Haggerty, Modeling the subglacial hydrology of the late Pleistocene Lake Michigan Lobe, Laurentide Ice Sheet, *GSA Bulletin*, *114*(6), 665–674, doi:10.1130/0016-7606(2002)114⟨0665:MTSHOT⟩2.0.CO;2, 2002.

Brinkerhoff, D. J., T. W. Meierbachtol, J. V. Johnson, and J. T. Harper, Sensitivity of the frozen/melted basal boundary to perturbations of basal traction and geothermal heat flux: Isunnguata Sermia, western Greenland, *Annals of Glaciology*, *52*(59), 43–50, doi:10.3189/172756411799096330, 2011.

Brutsaert, W., and T. Hiyama, The determination of permafrost thawing trends from long-term streamflow measurements with an application in eastern Siberia, *Journal of Geophysical Research D: Atmospheres*, *117*(22), doi:10.1029/2012JD018344, 2012.

Burn, C., and M. Smith, Development of Thermokarst Lakes During the Holocene at Sites Near Mayo, Yukon Territory, *Permafrost and Periglacial Processes*, *1*, 161–176, 1990.

Burn, C. R., Tundra lakes and permafrost, Richards Island, western Arctic coast, Canada, *Canadian Journal of Earth Sciences*, *39*(8), 1281–1298, doi:10.1139/E02-035, 2002.

Burn, C. R., Lake-bottom thermal regimes, western Arctic Coast, Canada, *Permafrost and Periglacial Processes*, *16*(4), 355–367, doi:10.1002/PPP.542, 2005.

Burt, T. P., and P. J. Williams, Hydraulic conductivity in frozen soils, *Earth Surface Processes and Landforms*, *1*(4), 349–360, 1976.

Caine, J., J. Evans, and C. Forster, Fault zone architecture and permeability structure, *Geology*, *24*(11), 1025–1028, 1996.

Cardenas, M. B., and X.-W. Jiang, Groundwater flow, transport, and residence times through topography-driven basins with exponentially decreasing permeability and porosity, *Water Resources Research*, *46*, W11,538, doi:10.1029/2010WR009370, 2010.

Clark, I., B. Lauriol, L. Harwood, and M. Marschner, Groundwater Contributions to Discharge in a Permafrost Setting, Big Fish River, NWT, Canada, *Arctic, Antarctic, and Alpine Research*, *33*, 62–69, doi:10.2307/1552278, 2001.

Clauser, C., Encyclopedia of solid earth geophysics, chap. Thermal storage and transport Properties of Rocks, I: Heat Capacity and Latent Heat, Springer, 2011.

Cutler, P. M., D. R. MacAyeal, D. M. Mickelson, B. R. Parizek, and P. M. Colgan, A numerical investigation of ice-lobe-permafrost interaction around the southern Laurentide ice sheet, *Journal of Glaciology*, *46*(153), 311–325, doi:10.3189/172756500781832800, 2000.

D'Andrea, W. J., Y. Huang, S. C. Fritz, and N. J. Anderson, Abrupt Holocene climate change as an important factor for human migration in West Greenland, *Proceedings of the National Academy of Sciences of the United States of America*, *108*, 9765–9769, doi:10.1073/pnas.1101708108, 2011.

Dardis, O., and J. McCloskey, Permeability porosity relationships from numerical simulations of fluid flow, *Geophyical Research Letters*, *25*, 1471–1474, 1998.

De Cogan, D., and A. De Cogan, *Applied Numerical Modelling for Engineers*, Oxford University Press, 1997.

DeFoor, W., M. Person, H. C. Larsen, D. Lizarralde, D. Cohen, and B. Dugan, Ice sheet-derived submarine groundwater discharge on Greenland's continental shelf, *Water Resources Research*, *47*, W07,549, doi:10.1029/2011WR010536, 2011.

Dietrich, R., A. Rulke, and M. Scheinert, Present-day vertical crustal deformations in West Greenland from repeated GPS observations, *Geophysical Journal International*, *163*(3), 865–874, doi:10.1111/j.1365-246X.2005.02766.x, 2005.

Domenico, P., and F. Schwarz, *Physical and Chemical Hydrogeology*, John Wiley, 1998.

Domenico, P. A., and M. Mifflin, Water from low-permeability sediments and land subsidenc, *Water Resources Research*, *1*(4), 563–576, 1965.

Dugan, H., T. Gleeson, S. Lamoureux, and K. Novakowski, Tracing groundwater discharge in a high arctic lake using radon-222, *Environmental Earth Sciences*, *66*(5), 1385–1392, doi:10.1007/s12665-011-1348-6, 2012.

Fairley, J., Modeling fluid flow in a heterogeneous, fault-controlled hydrothermal system, *Geofluids*, *9*, 153–166, doi: 10.1111/j.1468-8123.2008.00236.x, 2009.

Fleming, K., and K. Lambeck, Constraints on the Greenland Ice Sheet since the Last Glacial Maximum from sea-level observations and glacial-rebound models, *Quaternary Science Reviews*, *23*(9-10), 1053–1077, doi:10.1016/j.quascirev.2003.11.001, 2004.

Frampton, A., S. Painter, S. Lyon, and G. Destouni, Non-isothermal, three-phase simulations of near-surface flows in a model permafrost system under seasonal variability and climate change, *Journal of Hydrology*, *403*, 352–359, doi:10.1016/j.jhydrol.2011.04.010, 2011.

Frampton, A., S. Painter, and G. Destouni, Permafrost degradation and subsurface-flow changes caused by surface warming trends, *Hydrogeology Journal*, *21*, 271–280, doi:10.1007/s10040-012-0938-z, 2013.

Frappart, F., G. Ramillien, and J. S. Famiglietti, Water balance of the arctic drainage system using grace gravimetry products, *International Journal of Remote Sensing*, *32*(2), 431–453, doi:10.1080/01431160903474954, 2011.

Freeze, R. A., and J. A. Cherry, *Groundwater*, 1st ed., Prentice-Hall, Inc., London, 1979.

French, H. M., *The Periglacial Environment*, Wiley-Blackwell, 2007.

Frey, K. E., and J. W. McClelland, Impacts of permafrost degradation on arctic river biogeochemistry, *Hydrological Processes*, *23*(1), 169–182, doi:10.1002/hyp.7196, 2009.

Frey, K. E., D. I. Siegel, and L. C. Smith, Geochemistry of west siberian streams and their potential response to permafrost degradation, *Water Resources Research*, *43*(3), doi:10.1029/2006WR004902, 2007.

Frohn, R., K. Hinkel, and W. Eisner, Satellite remote sensing classification of thaw lakes and drained thaw lake basins on the North Slope of Alaska, *Remote Sensing of Environment*, *97*(1), 116–126, doi:10.1016/j.rse.2005.04.022, 2005.

Gardaz, J.-M., Distribution of mountain permafrost, Frontanesses Basin, Valaisian Alps, Switzerland, *Permafrost and Periglacial Processes*, *8*(1), 101–105, 1997.

Ge, S., J. McKenzie, C. Voss, and Q. Wu, Exchange of groundwater and surface-water mediated by permafrost response to seasonal and long term air temperature variation, *Geophysical Research Letters*, *38*, L14,402, doi: 10.1029/2011GL047911, 2011.

GEUS, and BMP, MINEX, Greenland Mineral Exploration Newsletter, *MINEX*, *40*, 1–8, 2011.

GEUS, and BMP, MINEX, Greenland Mineral Exploration Newsletter, *MINEX*, *43*, 1–8, 2013.

Gleeson, D. F., et al., Characterization of a sulfur-rich Arctic spring site and field analog to Europa using hyperspectral data, *Remote Sensing of Environment*, *114*(6), 1297–1311, doi:10.1016/j.rse.2010.01.011, 2010.

Goldspiel, J. M., and S. W. Squyres, Groundwater discharge and gully formation on martian slopes, *Icarus*, *211*(1), 238–258, doi:10.1016/j.icarus.2010.10.008, 2011.

Gooseff, M., J. E. Barrett, and J. Levy, Shallow groundwater systems in a polar desert, McMurdo Dry Valleys, Antarctica, *Hydrogeology Journal*, *21*, 171–183, doi:10.1007/s10040-012-0926-3, 2013.

Grasby, S., and Z. Chen, Subglacial recharge into the Western Canada Sedimentary Basin - Impact of Pleistocene glaciation on basin hydrodynamics, *GSA Bulletin*, *117*(3/4), 500–514, doi:10.1130/B25571.1, 2005.

Grasby, S., and K. Londry, Biogeochemistry of hypersaline springs supporting a mid continent marine ecosystem: An analogue for Martian Springs?, *Astrobiology*, *7*, 662–683, doi:10.1089/ast.2006.0029, 2007.

Grasby, S. E., C. C. Allen, T. G. Longazo, J. T. Lisle, D. W. Griffin, and B. Beauchamp, Supraglacial sulfur springs and associated biological activity in the Canadian high arctic - Signs of life beneath the ice, *Astrobiology*, *3*(3), 583–596, doi:10.1089/153110703322610672, 2003.

Grasby, S. E., B. Beauchamp, and V. Bense, Sulfuric Acid Speleogenesis Associated with a Glacially Driven Groundwater System-Paleo-spring "Pipes" at Borup Fiord Pass, Nunavut, *Astrobiology*, *12*(1), 19–28, doi: 10.1089/ast.2011.0700, 2012.

Grenier, C., D. Régner, E. Mouche, H. Benabderrahmane, F. Costard, and P. Davy, Impact of permafrost development on groundwater flow patterns: a numerical study considering freezing cycles on a two-dimensional vertical cut through a generic river-plain system, *Hydrogeology Journal*, *21*(1), 257–270, doi:10.1007/s10040-012-0909-4, 2013.

Grosse, G., and B. M. Jones, Spatial distribution of pingos in northern Asia, *Cryosphere*, *5*(1), 13–33, doi:10.5194/tc-5-13-2011, 2011.

Gurney, S. D., Aspects of the genesis and geomorphology of pingos: perennial permafrost mounds, *Progress In Physical Geography*, *22*(3), 307–324, 1998.

Haldorsen, S., and M. Heim, An Arctic groundwater system and its dependence upon climatic change: An example from Svalbard, *Permafrost and Periglacial Processes*, *10*(2), 137–149, 1999.

Haldorsen, S., M. Heim, B. Dale, J. Y. Landvik, M. van der Ploeg, A. Leijnse, O. Salvigsen, J. Hagen, and D. Banks, Sensitivity to long-term climate change of subpermafrost groundwater systems in Svalbard, *Quaternary Research*, *73*(2), 393–402, doi:10.1016/j.yqres.2009.11.002, 2010.

Hansson, K., J. Simunek, M. Mizoguchi, L. Lundin, and M. T. Genuchten, Water flow and heat transport in frozen soil: Numerical solution and freeze - thaw applications applied, *Vadose Zone Journal*, *3*, 693–704, doi:10.2113/3.2.693., 2004.

Harris, S., Causes and consequences of rapid thermokarst development in permafrost and glacial terrain, *Permafrost and Periglacial Processes*, *13*, 237–242, doi:10.1002/ppp.419, 2002.

Hauck, C., . Bttcher, M, and H. Maurer, A new model for estimating subsurface ice content based on combined electrical and seismic data sets, *Cryosphere*, *5*(2), 453–468, doi:10.5194/tc-5-453-2011, 2011.

Heikenfeld, M., M. Langer, and S. Westermann, SnowPI 3.0, Snow-Permafrost Interaction Soil Model, 2012.

Henry, K., and M. Smith, A model-based map of ground temperatures for the permafrost regions of Canada, *Permafrost and Periglacial Processes*, *12*(4), 389–398, doi:10.1002/ppp.399, 2001.

Huybrechts, P., Basal temperature conditions of the Greenland ice sheet during the glacial cycles, *Annals of Glaciology*, *23*, 226–236, 1996.

Ireson, A., G. van der Kamp, a. N. U. Ferguson, G., and H. Wheater, Hydrogeological processes in seasonally frozen northern lattitudes: understanding gaps and challenges, *Hydrogeology Journal*, *21*, 53–66, doi:10.007/s10040-012-0916-5, 2013.

Irvine-Fynn, T. D. L., A. J. Hodson, B. J. Moorman, G. Vatne, and A. L. Hubbard, Polythermal glacier hydrology: A review, *Reviews of Geophysics*, *49*, RG4002, doi:10.1029/2010RG000350, 2011.

Iverson, N., and M. Person, Glacier-bed geomorphic processes and hydrologic conditions relevant to nuclear waste disposal, *Geofluids*, *12*(1), 38–57, doi:10.1111/j.1468-8123.2011.00355.x, 2012.

Jepsen, S. M., C. I. Voss, M. A. Walvoord, B. J. Minsley, and J. Rover, Linkages between lake shrinkage/expansion and sublacustrine permafrost distribution determined from remote sensing of interior Alaska, USA, *Geophysical Research Letters*, doi:10.1002/grl.50187, 2013.

Jiang, X.-W., L. Wan, X.-S. Wang, S. Ge, and J. Liu, Effect of exponential decay in hydraulic conductivity with depth on regional groundwater flow, *Geophysical Research Letters*, *36*, L24,402, doi:10.1029/2009GL041251, 2009.

Jorgenson, M., V. Romanovsky, J. Harden, Y. Shur, J. O'Donnell, E. A. G. Schuur, M. Kanevskiy, and S. S. Marchenko, Resilience and vulnerability of permafrost to climate change, *Canadian Journal of Forest Research*, *40*(7), 1219 –1236, doi:10.1139/x10-060, 2010.

Juliussen, H., and O. Humlum, Towards a TTOP Ground Temperature Model for Mountainous Terrain in Central-Eastern Norway, *184*, 161–184, doi:10.1002/ppp, 2007.

Kane, D., K. Yoshikawa, and J. McNamara, Regional groundwater flow in an area mapped as continuous permafrost, NE Alaska (USA), *Hydrogeology Journal*, *21*, 41–52, doi:10.1007/s10040-012-0937-0, 2013.

Karra, S., S. L. Painter, and P. C. Lichtner, Three-phase numerical model for subsurface hydrology in permafrost-affected regions, *The Cryosphere Discussions*, *8*(1), 149–185, doi:10.5194/tcd-8-149-2014, 2014.

Keller, F., Automated Mapping of Mountain Permafrost Using the Program PERMAKART within the Geographical Information System ARC/INFO, *Permafrost and Periglacial Processes*, *3*, 133–138, 1992.

Kleinberg, R. L., and D. D. Griffin, NMR measurements of permafrost: unfrozen water assay, pore-scale distribution of ice, and hydraulic permeability of sediments, *Cold Regions Science and Technology*, *42*(1), 63–77, doi:10.1016/j.coldregions.2004.12.002, 2005.

Kleinberg, R. L., C. Flaum, D. D. Griffin, P. Brewer, G. Malby, and E. Pelzer, Deep sea NMR: Methane hydrate growth habit in porous media and its relationship to hydraulic permeability, deposit accumulation, and submarine slope stability, *Journal of Geophysical Research B: Solid Earth*, *108*(B10), 2508, 2003.

Konikow, L., W. Sanford, and P. Campbell, Constant-concentration boundary condition: Lessons from the hydrocoin variable-density groundwater benchmark problem, *Water Resources Research*, *33*(10), 2253–2261, 1997.

Kraemer, T., and T. Brabets, Uranium isotopes (234U/ 238U) in rivers of the Yukon Basin (Alaska and Canada) as an aid in identifying water sources, with implications for monitoring hydrologic change in arctic regions, *Hydrogeology Journal*, *20*(3), 469–481, doi:10.1007/s10040-012-0829-3, 2012.

Kreyszig, E., H. Kreyszig, and E. J. Norminton, *Advanced Engineering Mathematics*, 10 ed., John Wiley & Sons, Inc, 2011.

Kukkonen, I., L. Kivekäs, S. Vuoriainen, and M. Kääriä, Thermal Properties of Rocks in Olkiluoto: Results of Laboratory Measurements 1994–2010, *Tech. Rep. WR 2011–17*, Geological Survey of Finland, 2011.

Kurylyk, B., and K. Watanabe, Review: The mathematical representation of freezing and thawing processes in variably saturated, non-deformable soils, *Advances In Water Resources*, doi:10.1016/j.advwatres.2013.07.016, 2013.

Lachenbruch, A. H., J. H. Sass, B. V. Marshall, and T. H. Moses, Permafrost, Heat-flow, and the Geothermal Regime At Prudhoe Bay, Alaska, *Journal of Geophysical Research*, *87*(NB11), 9301–9316, 1982.

Lauritzen, S. E., and S. Bottrell, Microbiological Activity In Thermoglacial Karst Springs, South Spitsbergen, *Geomicrobiology Journal*, *12*(3), 161–173, 1994.

Lawrence, D., A. Slater, and S. Swenson, Simulation of present-day and future permafrost and seasonally frozen ground conditions in CCSM4, *Journal of Climate*, *25*(7), 2207–2225, doi:10.1175/JCLI-D-11-00334.1, 2012.

Lemieux, J. . M., E. A. Sudicky, W. R. Peltier, and L. Tarasov, Dynamics of groundwater recharge and seepage over the Canadian landscape during the Wisconsinian glaciation, *Journal of Geophysical Research F: Earth Surface*, *113*(F1), F01,011, doi:10.1029/2007JF000838, 2008a.

Lemieux, J. . M., E. A. Sudicky, W. R. Peltier, and L. Tarasov, Simulating the impact of glaciations on continental groundwater flow systems: 1. Relevant processes and model formulation, *Journal of Geophysical Research F: Earth Surface*, *113*(F3), F03,017, doi:10.1029/2007JF000928, 2008b.

Lemieux, J. . M., E. A. Sudicky, W. R. Peltier, and L. Tarasov, Simulating the impact of glaciations on continental groundwater flow systems: 2. Model application to the Wisconsinian glaciation over the Canadian landscape, *Journal of Geophysical Research F: Earth Surface*, *113*(F3), F03,018, doi:10.1029/2007JF000929, 2008c.

Ling, F., Numerical simulation of permafrost thermal regime and talik development under shallow thaw lakes on the Alaskan Arctic Coastal Plain, *Journal of Geophysical Research D: Atmospheres*, *108*(D16), doi:10.1029/2002JD003014, 2003.

Ling, F., and T. J. Zhang, Modeling study of talik freeze-up and permafrost response under drained thaw lakes on the Alaskan Arctic Coastal Plain, *Journal of Geophysical Research D: Atmospheres*, *109*(D1), doi:10.1029/2003JD003886, 2004.

Ling, F., Q. Wu, T. Zhang, and F. Niu, Modelling open-talik formation and permafrost lateral thaw under a thermokarst lake, Beiluhe Basin, Qinghai-Tibet Plateau, *Permafrost and Periglacial Processes*, *23*, 312–321, 2012.

Loch, J., Thermodynamic equilibrium between ice and water in porous media, *Soil Science*, *126*, 77–80, doi:10.1097/00010694-197808000-00002, 1978.

Lunardini, V., Freezing of soil with phase change occurring over a finite temperature difference, in *Proceedings of the 4th international offshore mechanics and arctic engineering symposium*, 1985.

Mackay, J. R., Pingos of the Pleistocene Mackenzie delta area, *Geographical Bulletin*, *18*, 21–63, 1962.

Mackay, J. R., Pingo growth and collapse, Tuktoyaktuk Peninsula Area, Western Arctic Coast, Canada: A long-term field study, *Geographie Physique Et Quaternaire*, *52*(3), 271–323, 1998.

Marsh, P., and M. Woo, The Water Balance of a Small Pond in the High Arctic, *Arctic*, *30*, 109–117, 1977.

Marsh, P., M. Russell, S. Pohl, H. Haywood, and C. Onclin, Changes in thaw lake drainage in the Western Canadian Arctic from 1950 to 2000, *Hydrological Processes*, *23*(1), 145–158, doi:10.1002/hyp.7179, 2009.

Matell, N., R. S. Anderson, I. Overeem, C. Wobus, F. E. Urban, and G. D. Clow, Modeling the subsurface thermal impact of Arctic thaw lakes in a warming climate, *Computers and Geosciences*, *53*, 69–79, doi:10.1016/j.cageo.2011.08.028, 2013.

McClelland, J. W., S. J. Dery, B. J. Peterson, R. M. Holmes, and E. F. Wood, A pan-arctic evaluation of changes in river discharge during the latter half of the 20th century, *Geophysical Research Letters*, *33*(6), doi:10.1029/2006GL025753, 2006.

McEwen, A. S., et al., Seasonal flows on warm Martian slopes, *Science*, *333*(6043), 740–743, doi:10.1126/science.1204816, 2011.

McIntosh, J. C., M. Schlegel, and M. Person, Glacial impacts on hydrologic processes in sedimentary basins: evidence from natural tracer studies, *Geofluids*, *1*(1), 7–21, doi:10.1111/j.1468-8123.2011.00344.x, 2012.

McKenzie, J. M., and C. I. Voss, Permafrost thaw in a nested groundwater-flow system, *Hydrogeology Journal*, *21*(1), 299–316, doi:10.1007/s10040-012-0942-3, 2013.

McKenzie, J. M., C. I. Voss, and D. I. Siegel, Groundwater flow with energy transport and water-ice phase change: Numerical simulations, benchmarks, and application to freezing in peat bogs, *Advances In Water Resources*, *30*(4), 966–983, doi:10.1016/j.advwatres.2006.08.008, 2007.

Minsley, B., et al., Airborne electromagnetic imaging of discontinuous permafrost, *Geophysical Research Letters*, *39*(2), doi:10.1029/2011GL050079, 2012.

Moorman, B., Glacier-permafrost hydrology interactions, Bylot Island, Canada, in *Permafrost, vols 1 and 2*, edited by Phillips, M and Springman, S.M. and Arenson, L.U., pp. 783–788, 8th international conference on permafrost, Zurich, Switzerland, Jul 21-25, 2003, 2003.

Moorman, B. J., Glacier-permafrost hydrology interactions, Bylot Island, Canada, *Permafrost*, *1 and 2*, 783–788, 2003.

Moorman, B. J., S. D. Robinson, and M. M. Burgess, Imaging periglacial conditions with ground-penetrating radar, *Permafrost and Periglacial Processes*, *14*(4), 319–329, doi:10.1002/ppp.463, 2003.

Mualem, Y., New model for predicting hydraulic conductivity of unsaturated porous-media, *Water Resources Research*, *12*(3), 513–522, 1976.

Muskett, R., and V. Romanovsky, Alaskan permafrost groundwater storage changes derived from grace and ground measurements, *Remote Sensing*, *3*(2), 378–397, 2011.

Muskett, R. R., and V. E. Romanovsky, Groundwater storage changes in arctic permafrost watersheds from GRACE and in situ measurements, *Environmental Research Letters*, *4*(4), doi:10.1088/1748-9326/4/4/045009, 2009.

Narasimhan, T., and P. Witherspoon, An integrated finite difference method for analyzing fluid flow in porous media, *Water Resourdes Research*, *12*(1), 57–64, 1976.

Neuzil, C., Hydromechanical effect of continental glaciation on groundwater systems, *Geofluids*, *12*(1), 22–37, doi:10.1111/j.1468-8123.2011.00347.x, 2012.

O'Donnell, J., G. Aiken, M. Walvoord, and K. Butler, Dissolved organic matter composition of winter flow in the Yukon River basin: Implications of permafrost thaw and increased groundwater discharge, *Global Biogeochemical Cycles*, *26*(4), doi:10.1029/2012GB004341, 2012.

Overeem, I., and J. P. M. Syvitski, Shifting discharge peaks in arctic rivers, 1977-2007, *Geografiska Annaler Series A-physical Geography*, *92A*(2), 285–296, doi:10.1111/j.1468-0459.2010.00395.x, 2010.

Painter, S., Three-phase numerical model of water migration in partially frozen geological media: model formulation, validation, and applications, *Computational Geosciences*, *15*, 69–85, doi:10.1007/s10596-010-9197-z, 2011.

Painter, S., J. Moulton, and C. Wilson, Modeling challenges for predicting hydrologic response to degrading permafrost, *Hydrogeology Journal*, *21*, 221–224, doi:10.1007/s10040-012-0917-4, 2013.

Pandey, P., T. Gleeson, and . M. Baraer, Toward quantifying discrete groundwater discharge from frozen seepage faces using thermal infrared images, *Geophyical Research Letters*, *40*, 123–127, doi:10.1029/2012GL054315, 2013.

Paterson, W. S. B., *The Physics of Glaciers*, Third Edition ed., Butterworth-Heinemann, 1994.

PDE Solutions, *FlexPDE v.5.10*, http://www. pdesolutions.com, 2006.

Peiró, J., and S. Sherwin, Finite difference, finite element and finite volume methods for partial differential equations, in *Handbook of Materials Modeling*, Springer, 2005.

Peng, G., L. Leslie, and Y. Shao (Eds.), *Environmental Modelling and Prediction*, Springer, 2002.

Person, B. V. C. D. B. A., M.a, Models of ice-sheet hydrogeologic interactions: A review, *Geofluids*, *12*(1), 58–78, cited By (since 1996) 2, 2012.

Piotrowski, J., *Glacier Science and Environmental Change*, chap. Groound-water under ice sheets and glaciers, pp. 50–59, Blackwell Publishing, 2006.

Piotrowski, J. A., Subglacial hydrology in north-western Germany during the last glaciation: Groundwater flow, tunnel valleys and hydrological cycles, *Quaternary Science Reviews*, *16*(2), 169–185, doi:10.1016/S0277-3791(96)00046-7, 1997.

Plug, L. J., and J. J. West, Thaw lake expansion in a two-dimensional coupled model of heat transfer, thaw subsidence, and mass movement, *Journal of Geophysical Research F: Earth Surface*, *114*, doi:10.1029/2006JF000740, 2009.

Provost, A. M., C. I. Voss, and C. E. Neuzil, Glaciation and regional groundwater flow in the Fennoscandian shield, *Geofluids*, *12*, 79–96, doi:10.1111/j.1468-8123.2012.00361.x, 2012.

Riseborough, D. W., Discussion of cr burn's 'lake-bottom thermal regimes, western arctic coast, canada', *Permafrost and Periglacial Processes*, *17*(1), 87–89, doi:10.1002/ppp.534, 2006.

Romanovsky, V., S. Smith, and H. Christiansen, Permafrost thermal state in the polar northern hemisphere during the international polar year 2007-2009: A synthesis, *Permafrost and Periglacial Processes*, *21*(2), 106–116, doi:10.1002/ppp.689, 2010a.

Romanovsky, V. E., et al., Thermal state of permafrost in russia, *Permafrost and Periglacial Processes*, *21*, 136–155, doi:10.1002/ppp.683, 2010b.

Rowland, J. C., B. J. Travis, and C. J. Wilson, The role of advective heat transport in talik development beneath lakes and ponds in discontinuous permafrost, *Geophysical Research Letters*, *38*, L17,504, doi:10.1029/2011GL048497, 2011.

Scheidegger, J. M., and V. F. Bense, Impacts of glacially recharged groundwater flow systems on talik evolution, *Journal of Geophysical Research: Earth Surface*, doi:10.1002/2013JF002894, 2014.

Scheidegger, J. M., V. F. Bense, and S. E. Grasby, Transient nature of Arctic spring systems driven by subglacial meltwater, *Geophysical Research Letters*, *39*, L12,405, doi:10.1029/2012GL051445, 2012.

Scholz, H., and W. Grottenthaler, Beiträge zur jungholozänen Deglaziationsgeschichte im mittleren Westgrönland, *Polarforschung*, *58*(1), 25–40, 1988.

Sebok, E., C. Duque, J. Kazmierczak, P. Engesgaard, B. Nilsson, S. Karan, and M. Frandsen, High-resolution Distributed Temperature Sensing to detect seasonal groundwater discharge into Lake Væng, Denmark, *Water Resources Research*, *49*(9), 5355–5368, doi:10.1002/wrcr.20436, 2013.

Selker, J. S., et al., Distributed fiber-optic temperature sensing for hydrologic systems, *Water Resources Research*, *42*, W12,202, doi:10.1029/2006WR005326, 2006.

Sjöberg, Y., A. Frampton, and S. Lyon, Using streamflow characteristics to explore permafrost thawing in northern Swedish catchments, *Hydrogeology Journal*, *21*, 121–131, doi:10.1007/s10040-012-0932-5, 2013.

SKB, The Greenland Analogue Project Yearly Report 2010, *Tech. Rep. R-11-23*, SKB, 2011.

Sloan, C., and R. Van Everdingen, Region 28, Permafrost region, in *Hydrogeology*, pp. 263–270, Geological Society of America, 1988.

Smith, L. C., Y. Sheng, G. M. MacDonald, and L. D. Hinzman, Disappearing Arctic lakes, *Science*, *308*(5727), 1429–1429, doi:10.1126/science.1108142, 2005.

Smith, L. C., T. M. Pavelsky, G. M. MacDonald, A. I. Shiklomanov, and R. B. Lammers, Rising minimum daily flows in northern Eurasian rivers: A growing influence of groundwater in the high-latitude hydrologic cycle, *Journal of Geophysical Research G: Biogeosciences*, *112*(G4), doi:10.1029/2006JG000327, 2007.

Smith, S., V. Romanovsky, C. Lewkowicz, A.G.and Burn, M. Allard, G. Clow, K. Yoshikawa, and J. Throop, Thermal state of permafrost in North America: A contribution to the international polar year, *Permafrost and Periglacial Processes*, *21*(2), 117–135, 2010.

St Jacques, J. M., and D. J. Sauchyn, Increasing winter baseflow and mean annual streamflow from possible permafrost thawing in the Northwest Territories, Canada, *Geophysical Research Letters*, *36*, doi:10.1029/2008GL035822, 2009.

Stotler, R., S. Frape, B. Freifeld, B. Holden, T. Onstott, T. Ruskeeniemi, and E. Chan, Hydrogeology, chemical and microbial activity measurement through deep permafrost, *Ground Water*, *49*(3), 348–364, doi:10.1111/j.1745-6584.2010.00724.x, 2011.

Taylor, A. E., S. R. Dallimore, and J. F. Wright, Thermal Impact of Holocene Lakes on a Permafrost Landscpae, Mackenzie Delta, Canada, in *Ninth International Conference on Permafrost Fairbanks, Alasa USA June 29 – July 3, 2008*, 2008.

Tóth, L., A theoretical analysis of groundwater flow in small drainage basins, *Journal of Geophysical Research*, *68*(16), 4795–4812, 1963.

Utting, N., I. Clark, B. Lauriol, M. Wieser, and W. Aeschbach-Hertig, Origin and Flow Dynamics of Perennial Groundwater in Continuous Permafrost Terrain using Isotopes and Noble Gases: Case Study of the Fishing Branch River, Northern Yukon, Canada, *Permafrost and Periglacial Processes*, *23*(2), 91–106, doi:10.1002/ppp.1732, 2012.

van Genuchten, M. T., A closed-form equation for predicting the hydraulic conductivity of unsaturated soils, *Soil Science Societyof America Journal*, *44*, 892–898, 1980.

van Tatenhove, F., A. Fabre, R. Greve, and P. Huybrechts, Modelled ice-sheet margins of three Greenland ice-sheet models compared with a geological record from ice-marginal deposits in central West Greeland, *Annals of Glaciology*, *23*, 52–58, 1996.

Vidstrand, P., S. Follin, J.-O. Selroos, J.-O. Näslund, and I. Rhén, Modeling of groundwater flow at depth in crystalline rock beneath a moving ice-sheet margin, exemplified by the Fennoscandian Shield, Sweden, *Hydrogeology Journal*, doi:10.1007/s10040-012-0921-8, 2012.

Wainstein, P., M. B.J., and K. Whitehead, Importance of glacier-permafrost interactions in the prservation of a proglacial icing: Fountain glacier, bylot island, canada, in *Ninth International Conference on Permafrost*, edited by D. Kane and K. Hinkel, 2008.

Wainwright, J., *Environmental Modelling: finding Simplicity in Complexity*, John Wiley & Sons, Ltd, 2004.

Walsh, J. E., *Arctic Climate Impact Assessment*, chap. Cryosphere and Hydrology, pp. 184–242, Cambridge University Press, 2005.

Walter, K., S. Zimov, J. Chanton, D. Verbyla, and F. Chapin, Methane bubbling from Siberian thaw lakes as a positive feedback to climate warming, *Nature*, *443*, 71–75, doi:10.1038/nature05040, 2006.

Walvoord, M. A., and R. G. Striegl, Increased groundwater to stream discharge from permafrost thawing in the Yukon River basin: Potential impacts on lateral export of carbon and nitrogen, *Geophysical Research Letters*, *34*(12), doi:10.1029/2007GL030216, 2007.

Wang, H., and M. P. Anderson, *Introduction to groundwater modeling : finite difference and finite element methods*, Academic Press, 1982.

Wang, J., Y. Sheng, K. Hinkel, and E. Lyons, Drained thaw lake basin recovery on the western Arctic Coastal Plain of Alaska using high-resolution digital elevation models and remote sensing imagery, *Remote Sensing of Environment*, *119*, 325–336, 2012.

Watanabe, K., and M. Flury, Capillary bundle model of hydraulic conductivity in frozen soil, *Water Resources Research*, *44*, W12,402, doi: 10.1029/2008WR007012, 2008.

Watson, V., H. Kooi, and V. Bense, Potential controls on cold-season river flow behavior in subarctic river basins of Siberia, *Journal of Hydrology*, *489*, 214–226, doi:10.1016/j.jhydrol.2013.03.011, 2013.

Wellman, T. P., C. I. Voss, and M. Walvoord, Impacts of climate, lake size, and supra- and sub-permafrost groundwater flow on lake-talik evolution, Yukon Flats, Alaska (USA), *Hydrogeology Journal*, doi:10.1007/ s10040-012-0941-4, 2013.

Westermann, S., J. Boike, M. Langer, T. Schuler, and B. Etzelmüller, Modeling the impact of wintertime rain events on the thermal regime of permafrost, *The Cryosphere*, *5*, 945–959, doi:10.5194/tc-5-945-2011, 2011.

White, M., Theory and numerical application of subsurface flow and trasnport for trasnient freezing conditions, in *Fifteenth Annual "Hydrology Days" Conference*, 1995.

White, M., and M. Oostrom, *STOMP, Subsurface Transport Over Multiple Phases*, Pacific Northwest National Laboratory, Department of Energy, Richland, Washington, pNNL-15782, 2006.

Willemse, N., Holocene Sedimentation History of the Shallow Kangerlussuaq Lakes, West Greenland, *Meddellelser om Grønland, Geoscience*, *41*, 2002.

Williams, J., Ground water in the permafrost regions of alaska, *Tech. rep.*, Geological Survey Professional Paper 696, 1970.

Williams, P., and M. Smith, *The Frozen Earth, Fundamentals of Geocryology*, Cambridge University Press, 1989.

Wirth, L., A. Rosenberger, A. Prakash, R. Gens, J. Margraf, and T. Hamazak, A remote-sensing, gis-based approach to identify, characterize, and model spawning habitat for fall-run chum salmon in a sub-arctic, glacially fed River, *Transactions of the American Fisheries Society*, *141*(5), 1349–1363, doi:10.1080/00028487.2012.692348, 2012.

Woo, G. X., M.-K., Hydrological connectivity and seasonal storage change of tundra ponds in a polar oasis environment, Canadian High Arctic, *Permafrost and Periglacial Processes*, *17*(4), 309–323, doi:10.1002/ppp.565, 2006.

Woo, M.-K., *Permafrost Hydrology*, Springer, Heidelberg, 2012.

Wu, Z. H., P. J. Barosh, D. G. Hu, Z. H. Wu, P. S. Ye, Q. S. Liu, and C. J. Zhou, Migrating pingos in the permafrost region of the Tibetan Plateau, China and their hazard along the Golmud-Lhasa railway, *Engineering Geology*, *79*(3-4), 267–287, doi:10.1016/j.enggeo.2005.02.003, 2005.

Yoshikawa, K., and L. D. Hinzman, Shrinking thermokarst ponds and groundwater dynamics in discontinuous permafrost near Council, Alaska, *Permafrost and Periglacial Processes*, *14*(2), 151–160, doi:10.1002/ppp.451, 2003.

Yoshikawa, K., L. D. Hinzman, and D. L. Kane, Spring and aufeis (icing) hydrology in brooks range, alaska, *Journal of Geophysical Research G: Biogeosciences*, *112*(G4), doi:10.1029/2006JG000294, 2007.

Zektser, I., and A. Dzyuba, Submarine discharge into the seas of the Arctic Ocean from the European Russia territory, *Water Resources*, *37*(6), 745–751, doi:10.1134/S0097807810060011, 2010.

Zwally, H. J., W. Abdalati, T. Herring, K. Larson, J. Saba, and K. Steffen, Surface melt-induced acceleration of Greenland ice-sheet flow, *Science*, *297*, 218–222, doi:10.1126/science.1072708, 2002.